Direct conversion of root primordium into shoot meristem relies on timing of stem cell niche development

Olga Rosspopoff[1, 2+]
Liudmila Chelysheva[1+]
Julie Saffar[1, 3]
Lena Lecorgne[2]
Delphine Gey[4]
Erwann Caillieux[5]
Vincent Colot[5]
François Roudier[5]
Pierre Hilson[1*]
Richard Berthomé[6, 7]
Marco Da Costa[1,2*++]
Philippe Rech[1,2*++]

[1] Institut Jean-Pierre Bourgin, INRA, AgroParisTech, CNRS, Université Paris-Saclay, 78000 Versailles, France.
[2] Sorbonne Universités, UPMC Univ. Paris 06, UFR927, 4 Place Jussieu, F-75252, Paris, France.
[3] Université Paris-Diderot, Sorbonne Paris Cité, 75205 Paris Cedex 13, France
[4] Muséum d'Histoire Naturelle, UMS 2700, OMSI, Paris, France.
[5] Institut de Biologie de l'Ecole Normale Supérieure, CNRS UMR8197, INSERM U1024, F-75005, Paris, France.
[6] INRA, Laboratoire des Interactions Plantes-Microorganismes (LIPM), UMR441 INRA CNRS Castanet-Tolosan 31326, France; CNRS, Laboratoire des Interactions Plantes-Microorganismes, UMR2594, Castanet-Tolosan 31326, France.
[7] Plant Genomics Research Unit, UMR INRA 1165 - CNRS 8114 - UEVE, 2, Gaston Crémieux St., CP5708, 91057 Evry Cedex, France.

[+] co first authors
[++] co senior authors
Corresponding authors:
Marco Da Costa, Pierre Hilson, Philippe Rech

Development • Advance article

*Correspondence: marco.da-costa@inra.fr, pierre.hilson@inra.fr, philippe.rech@inra.fr

Keywords: Transdifferentiation, Arabidopsis, Regeneration, Root to shoot conversion, Stem cell niche, Totipotency

One sentence summary:

Stem cell niche reprogramming underlies direct root-to-shoot transdifferentiation.

Abstract

To understand how the identity of an organ can be switched, we studied the transformation of lateral root primordia (LRP) into shoot meristems in Arabidopsis root segments. In this system, the cytokinin-induced conversion does not involve the formation of callus-like structures. Detailed analysis showed that the conversion sequence starts with a mitotic pause and is concomitant with the differential expression of regulators of root and shoot development. The conversion requires the presence of apical stem cells and only LRP at stages VI or VII can be switched. It is engaged as soon as cell divisions resume because their position and orientation differ in the converting organ compared to the undisturbed emerging LRP. By alternating auxin and cytokinin treatments, we showed that the root and shoot organogenetic programs are remarkably plastic because the status of the same plant stem cell niche can be reversed repeatedly within a set developmental window. Thus, the networks at play in the meristem of a root can morph in the span of a couple cell division cycles into those of a shoot, and back, through transdifferentiation.

Introduction

Since the 1950s, *in vitro* culture methods have contributed to the study of plant cell totipotency and enabled the propagation of plant materials for research or commercial purposes. A large body of work illustrates the complexity of the mechanisms at play during organogenesis. While plants can be regenerated from a wide variety of tissues, their *in vitro* response largely depends on cell types, species and genotypes (Cary et al., 2002; Ikeuchi et al., 2016; Motte et al., 2014; Pulianmackal et al., 2014; Skoog and Miller, 1957).

In Arabidopsis, organogenesis can be induced in explants prepared from root, or hypocotyl (Atta et al., 2009; Che et al., 2006; Gordon et al., 2007; Valvekens et al., 1988). In two-step protocols, cell proliferation is first enhanced in explants placed on a callus-inducing medium (CIM) characterized by a high auxin/cytokinin ratio. After a few days, the resulting calli can be transferred on a root-inducing medium (RIM) that only contains auxin or on a shoot-inducing medium (SIM) with a high cytokinin/auxin ratio, and some founder cells then initiate the formation of one or the other type of organs (Che et al., 2006). The balance between exogenously applied auxin and cytokinin thus directs the development of new organs.

The genetic control of *in vitro* plant regeneration occurs at multiple levels of regulation (Motte et al., 2014; Xu and Huang, 2014). Among the transcription factors involved, *WUSCHEL* (*WUS*) plays a key role in the initiation of shoot organogenesis (Chatfield et al., 2013; Gallois et al., 2004; Gordon et al., 2007; Su et al., 2015). *SHOOT MERISTEMLESS* (*STM*) is another transcription factor required for shoot regeneration *in vitro* (Barton and Poethig, 1993; Endrizzi et al., 1996; Hibara et al., 2003) and linked to the establishment of meristems in response to cytokinin (Brand et al., 2002; Scofield et al., 2013). Both *WUS* and *STM* transcripts over-accumulate in explants incubated on SIM (Chatfield et al., 2013; Gordon et al., 2007). In addition, specific histone methylation marks have been linked to shoot regeneration (He et al., 2012) and *WUS* induction is controlled in part through DNA demethylation in Arabidopsis calli on SIM (Li et al., 2011), indicating that epigenome reprogramming takes place during cell fate transitions.

Shoot-producing calli derived from various Arabidopsis explants seem to originate from perivascular cells, similar to the xylem-pole pericycle cells that are the

founders of lateral roots (LR). Converging evidence suggests that explants compatible with *de novo* organogenesis do not undergo dedifferentiation and resemble LR primordia (LRP) because regenerative calli express genes associated with LR initiation and have transcript profiles reminiscent of root apical meristem (RAM), rather than shoot apical meristem (SAM) or globular embryo (Atta et al., 2009; Che et al., 2007; Sugimoto et al., 2010). Furthermore, LRPs may eventually develop into roots or shoots, whether the root segments that produce them are placed on auxin- or cytokinin-rich medium, respectively (Atta et al., 2009; Cary et al., 2002; Che et al., 2007; Sugiyama, 1999), and the ability to regenerate shoot progenitor cells is controlled through a hormone-dependent pathway by root stem cell regulators (Kareem et al., 2015).

The stem cells at the core of plant apical meristems drive development and produce all post-embryonic organs in response to diverse cues (Heidstra and Sabatini, 2014; Scheres, 2007). The production of organs from *in vitro* cultured tissues implies cell fate switches for the initiation of novel meristematic structures. While such transitions are often assumed to involve a dedifferentiation phase, the *de novo* organogenesis observed in CIM/SIM systems is thought to be a transdifferentiation process, whereby a cell is directly transformed into another cell type without dedifferentiation (Sugimoto et al., 2011). The conversion of root meristems into shoot ones, or vice versa is a very rare phenomenon. But it has been observed in the dominant negative *tpl-1* mutant or through overexpression of a root master regulator in the embryo shoot pole and inversely (Smith and Long, 2010).

The successive phases of tissue regeneration are difficult to comprehend because they rely on the coordinated action of multiple factors. In particular, the early events leading to shoot formation in CIM/SIM protocols are difficult to capture because regenerating explants produce massive amount of proliferating tissues that do not participate in *de novo* organogenesis. Hence, the molecular mechanisms as well as the cells involved in the very first steps of organ initiation remain poorly characterized.

To understand how the identity of an organ can be switched, we studied the direct conversion of an LRP into a shoot meristem (SM) (LRP/SM) combining cytological, molecular and genomic approaches. Our results show that the development of a root primordium can be diverted to yield a growing shoot in as little as four days following cytokinin treatment, without any proliferating callus being

formed. The detailed analysis of the LRP/SM conversion proved that it is a transdifferentiation process concomitant with the differential expression of regulators of root and shoot development, dynamic hormonal crosstalks, and coordinated mitotic activity. The conversion is only possible within a narrow window during the development of the initial LRP and requires the presence of apical stem cells. However, within that window, the root and shoot organogenetic programs are remarkably plastic and the status of the stem cell niche can be reversed repeatedly, as previously observed in animal developmental processes.

Results

Root-to-shoot conversion is restricted to specific stages of lateral root development

Arabidopsis primary roots may produce shoots that develop from LRPs when treated with an exogenous cytokinin (Atta et al., 2009; Chatfield et al., 2013; Kareem et al., 2015). We noticed that LRs follow distinct organogenetic paths depending on their developmental stage when treated with the cytokinin 2-isopentenyladenine (2-iP): young root primordia rapidly terminate development, intermediate LRPs convert into shoots, and emerged LRs remain as such (Fig. 1). To investigate the determinants of root-to-shoot conversion, LR formation was primed with the application of the auxin 1-naphthaleneacetic acid (NAA) on primary roots segments, after confirming that induced LRPs had the same structure as spontaneous ones (Malamy and Benfey, 1997). The response to cytokinin according to LRP developmental stages was measured based on 4453 LRPs (in 210 root segments) of which 1072 switched into SMs (see Supplemental Experimental Procedures for details). When transferred on 2-iP medium at stage V or younger, almost all LRPs terminate growth as green bulges (Fig. 2, A, E, I and J), with very few converted shoots originating from such early stages (0.7% of all SMs). These arrested organs grow in size mainly through the enlargement of outer cell layers, with some aberrant cell divisions taking place shortly after transfer. Most shoots develop from LRPs at stage VI or VII upon transfer (90.2%) (Fig. 2, B, C, F, G). These new shoots have an actively dividing central zone and form leaf primordia as early as four days after 2-iP application (Fig. 2K). LRPs at

stage VIII or older when transferred either sustain growth with no change in organ identity, or stop developing and turn green, in similar numbers (Fig. 2, L and M). But few of the converted shoots originate from these later stages (9.1%).

In conclusion, exogenous cytokinin can induce the conversion of an LRP into a functional SM, but only within a very narrow developmental window, corresponding to stages VI and VII in Col-0 primary root segments. LRs at either of these stages are referred to as competent LRs (CLRs) hereafter.

Cell division repatterning initiates meristem conversion

Next, we studied the evolving structure of CLRs across the conversion sequence to understand the cytological features enabling the transformation of a root primordium into a functional shoot meristem. Based on the analysis of cell boundaries in fixed tissues, very little morphological changes occur after the first 24 h of 2-iP treatment, indicating that mitotic activity rapidly decreases upon transfer from NAA to 2-iP medium (Fig. 3, A and B). This mitotic pause was confirmed with two mitotic markers in lines that express either the KNOLLE-GFP fusion protein labeling preferentially the position of the newly formed cell wall during cytokinesis (Fig. 3, G to K) (Boutté et al., 2010) or the Destruction Box-GUS fusion protein under the *CYCB1;1* promoter marking the G2-M transition (Fig. 3, L to P) (González-García et al., 2011). Both markers showed that cell divisions are frequent throughout the CLR before the transfer from NAA to 2-iP, but rare shortly after (paused CLR, pCLR ; Fig. 3, H, M and Q).

The organ resumes growth gradually during the second and third day of 2-iP treatment with the production of smaller cells indicative of mitotic activity in the provasculature and in the upper half of the dome (converting organ, CO; Fig. 3, C, I, N and Q). In the stele, the procambial cells differentiate into vascular tissues. At the top of the CO, divisions result in a round shape after three days of 2-iP treatment (early Shoot Promeristem, eSP; Fig. 3, D, J, and O) and in a flattened structure distinct from a root after four days (late Shoot Promeristem, lSP; Fig. 3E) and that portends the leaf primordia bulging out after four to five days (Shoot Meristem, SM; Fig. 3, F, K, and P). Whereas root meristems produce files of cells, cells in all layers of the converting organ divide according to multiple planes as shown by the orientation of the newly formed cell walls (Fig. 3, C to E, I and J). Only the epidermis

shows a simple pattern with almost exclusively anticlinal divisions. The leaf primordia always form on opposite flanks of the promeristem suggesting that the root-to-shoot conversion induced in our system does not involve the disorganized proliferation of cells into callus-like structures.

Thus, the developmental shift towards the shoot meristem appears to be engaged as soon as active cell divisions resume because their position and orientation differ in the converting organ compared to the emerging LR (Fig. 3R).

Remodeling of the hormone network during the root-to-shoot switch

As cytokinin and auxin provide cues to position and maintain stem cell niches (Schaller et al., 2015), we analyzed these hormonal responses in the converting CLR. Auxin fluctuations were investigated through the activity of the auxin-responsive *DR5* promoter (Ulmasov et al., 1997), the DII-VENUS fluorescent protein that is degraded in the presence of auxin (Brunoud et al., 2012), and the PIN-FORMED (PIN1) auxin transporter (Benková et al., 2003) (Fig. 4, A to O). As expected, cells in NAA-primed CLR have a strong *DR5* signal, no detectable DII-VENUS fluorescence, and a preferential localization of PIN1 in the basal plasma membrane, indicating that an auxin maximum is building up at the tip of the primordium where the new RAM should form (Fig. 4, A, F and K) (Benková et al., 2003; Kleine-Vehn et al., 2009). The transfer to 2-iP medium induces a sharp drop in auxin level and the clearing of PIN1 from the plasma membranes during the mitotic pause (Fig. 4, B, G and L). Auxin levels rise back in the first cells dividing at the tip of the converting organ (Fig. 4, C and H), while PIN1 strongly marks the L2 and L3 cell layers, then L4 (Fig. 4M). This zone overlaps with the central cell cluster that forms the QC in the CLR.

The transient auxin maximum together with the resurgence of a PIN1 domain (Fig. 4, C and M) suggests that *de novo* auxin synthesis occurs in the apical portion of the organ. In the late Shoot Promeristem (ISP), the central auxin maximum disappears and a maximum forms in the subepidermal zone of each incipient leaf primordium (Fig. 4, D and I), while the PIN1 domain extends in all dividing cell layers in the top half of the organ (Fig. 4N). In the fully structured shoot meristem, auxin maxima are restricted to the leaf primordia (Fig. 4, E and J) and the PIN1 protein is predominantly located in the L1 layer and in the provascular strands of the growing leaves (Fig. 4O) (Heisler et al., 2005; Reinhardt et al., 2003). No PIN1 protein or

auxin signal is detected in the bottom half of the converting organ where PIN1 is normally expressed during LR development (Benková et al., 2003).

Changes in cytokinin signaling were tracked with the *TCSn* reporter gene (Zürcher et al., 2013). No signal is detected in NAA-primed CLR (Fig. 4P), in agreement with previous reports (Bielach et al., 2012; Chang et al., 2013). Transfer on 2-iP medium strongly induces the *TCSn* signal in the stele (Fig. 4Q) and this signal decreases rapidly once cell divisions resume, without expanding into the transient auxin maximum of the CO (Fig. 4R). Finally, the *TCSn* signal is detected in the inner part of the late shoot promeristem and the shoot meristem (Fig. 4, S and T) consistent with the pattern observed in the SAM (Zürcher et al., 2013).

Thus, the auxin and cytokinin response domains rapidly evolve along the conversion process, from the patterns typical of an LRP to those of a SAM. Our data suggest that auxin and cytokinin shape partially complementary domains and act antagonistically to position the new shoot stem cell niche arising from the lateral root meristem.

Changes in gene expression profiles reflect the switch in organ identity

The expression of genes involved in the initiation and maintenance of root or shoot meristems was further analyzed across the conversion sequence with previously characterized reporter lines, *in situ* hybridization (ISH) and RT-qPCR. The selected genes code for transcription factors and a secreted peptide and are involved in the development of the stem cell niche, specifically in the root [*PLETHORA* (*PLT*), *SHORTROOT* (*SHR*), *WUSCHEL-RELATED HOMEOBOX 5* (*WOX5*), *SCARECROW* (*SCR*)] or in the shoot [*WUS*, *CLAVATA3* (*CLV3*), *STM*] (Heidstra and Sabatini, 2014).

Down-regulation of root genes. The *PLT1*, *SHR* and *SCR* genes are transcriptionally active in CLR tissues in domains similar to those observed in the primary root meristem (Aida et al., 2004; Helariutta et al., 2000; Terpstra and Heidstra, 2009). The expression of *PLT1* and *SHR* is rapidly turned off after transfer to 2-iP medium and is not detected in the converting organ when active divisions resume (Fig. S1).

Up-regulation of shoot genes. At the beginning of the conversion sequence, *CLV3*, *WUS* and *STM* are not expressed in the CLR (Fig. 5, A, B, C, E and F). Within 24 h

following transfer on 2-iP medium, thus during the mitotic pause (pCLR), all three genes are induced in cells located at the center of the organ, corresponding to the root QC, endodermis, pericycle and a part of the stele (Fig. 5, A, B, E and F). Once cell divisions resume (CO), the *CLV3, STM* and *WUS* domains are restricted to the apex (Fig. 5, A, B, E and F) where the STM protein is initially detected (Fig. 5C). At this stage, *CLV3*, *WUS* and *STM* are expressed in overlapping domains. As the promeristem is formed, the *CLV3* and *WUS* domains gradually narrow down to their typical organization in the SAM, with *CLV3* marking the central zone containing the stem cells (Fig. 5A) and *WUS* the organizing center (OC) (Fig. 5, B and E). Similar to the STM fusion protein, *STM* transcription is first restricted to the apical L2 cells layer, when divisions resume, then expands into the promeristem, and is eventually detected across the entire shoot meristem, at high level in the two peripheral zones where the first two leaf primordia bulge out (Fig. 5, C and F) (Heisler et al., 2005). The RT-qPCR profiles followed the patterns seen in the reporter lines (Fig. 5D).

The opposite root *vs.* shoot trends faithfully reported the dynamic remodeling that the converting organ operated through defined cell divisions. The transient expression of root and shoot specific genes in converting organs at the same developmental stage suggests that they may retain a dual identity during a short time window (Fig. 5 and Fig. S1). Alternatively, certain root and shoot markers may be mutually exclusive. But either hypothesis is difficult to prove because the comparative analysis of patterns is limited by the quality of the synchrony between separate objects and by the sensitivity of signal detection.

Direct conversion is a transdifferentiation process

To gain further insight into the root-to-shoot conversion molecular process, we analyzed the transcriptome signature of the early events involved in the transition phases between the two organogenetic developmental programs. To maximize specificity, the lateral organs were laser microdissected from the root segments and pooled according to four conversion stages: T_0, 42 h NAA-priming, competent lateral root (CLR); T_6, 6 h 2-iP treatment, paused CLR; T_{34}, 34 h 2-iP, converting organ (CO) resuming cell divisions; T_{58}, 58 h 2-iP, early shoot promeristem (eSP) (Fig. 5G, see Supplemental Experimental Procedures for details). Hereafter, a transcript profile change at a given time point refers to a pairwise comparison with the previous

time point. Accordingly, 748 genes were differentially expressed (DEGs) at T_6, 1806 at T_{34} and 527 at T_{58} (Fig. S2). Table S1 provides the list of all DEGs together with their functional classification and the p-value indicative of statistically significant differential expression. Table S2 presents a summary of the intersection between DEGs identified in this study (i) with genes associated with cell cycle (Vandepoele et al., 2002; Chatfield et al., 2013) or auxin and cytokinin metabolism or signaling (Nemhauser et al., 2006; Brenner and Schmülling, 2015), or (ii) with DEGs identified in other studies.

The transcriptome profiles were congruent with cytological and molecular observations. However the transcript level of some key regulators described above and expressed in specific cells or developmental stages (e.g. *CLV3*, *PLT1*, *PLT2, WUS*) could not be distinguished from background, despite microdissection tissue enrichment. Cell cycle and nucleosome components DEGs were down regulated at the T_6 paused CLR stage (*CYCB1;4*, *CYCB2;4*, *CYCD3;3*, 17 histone-encoding genes) while negative mitotic regulators were up (*KRP2*). Genes typically responsive to cytokinin were highly regulated in the conversion sequence. In comparison to the core set of 77 cytokinin-regulated genes deduced from multiple independent studies (Brenner and Schmülling, 2015), all 25 matching DEGs were up at T_6 ($p=8.64.10^{-18}$) and most were downregulated at T_{58} (Tables S1 and S2). Inversely, genes associated with auxin responses were mostly down at T_6 but up at T_{34} (Tables S1 and S2), suggesting that auxin production is rapidly tuned after 6 h of 2-iP treatment and contributes to the formation of the shoot promeristem. The down-regulation of genes controlling root meristem functions (e.g. *GLV5/RGF2*, *LBD16*, *SHR*, *WOX5*) and the induction of genes specific to shoot meristem development (e.g. *BLH8/PNF*, *CUC1*, *MYB37/RAX1*, *PHV*) were also confirmed, either during the mitotic pause (T_6) or after divisions resumed (T_{34}). Furthermore, the genes induced at T_6 indicated that the 2-iP treatment rapidly triggered anabolic processes and intense cellular activity as they are significantly enriched in functions involved in amino-acid, nucleotide, nitrogen and secondary metabolism, gluconeogenesis, and protein and transport pathways (Table S3).

We then compared our data with publicly available transcriptome datasets to examine the nature of the converting tissues. Che et al. (2006) profiled Arabidopsis explants after short or long auxin treatments, and producing shoots or roots depending on the medium they were transferred to. Explant undergoing direct

conversion (this study) match most closely shoot-forming calli, but have some DEGs in common with root-forming ones, possibly indicating their dual identity and highlighting that mechanisms linked to shoot commitment are already upregulated 6h after 2-iP treatment (Table S2). Additionally, we compared the most deregulated genes in the conversion sequence to genes expressed in different anatomical parts and classified as root, shoot or cell cultures (https://genevestigator.com/) (see Supplemental Experimental Procedures). Conversion DEGs are most similar to root and shoot gene sets, but are poorly related to genes associated to callus or cell culture/primary cell classes (Table S4, Fig. S3).

Collectively, these findings indicate that conversion is a transdifferentiation process because the transition from root to shoot operates without an intermediary step of tissue dedifferentiation.

Changes in DNA methylation occurring during conversion are not correlated with transcription modulation

Mutants resulting in the functional loss of DNA methylation showed earlier and more efficient *de novo* shoot regeneration that correlated with hypomethylated regions in the *WUS* locus, and with earlier and higher *WUS* transcription than in wild-type (Li et al., 2011; Shemer et al., 2015). We thus tested whether the large-scale changes in gene expression observed through the root-to-shoot conversion are linked with variations in DNA methylation across the nuclear genome.

We first compared the DEGs identified in this study with genes regulated by DNA methylation and possibly involved in shoot regeneration according to Li et al. (2011). These authors showed that over 300 genes differentially expressed in *met1-1* mutant calli incubated on CIM medium, compared to wild-type, were also differentially expressed in wild-type calli transferred from CIM to SIM, suggesting regulation through MET1-dependent DNA methylation. DEGs induced at T_{34} and T_{58} in our system are over-represented in this 300 genes subset (see Supplemental Experimental Procedures for details), pointing to the putative involvement of MET1-dependent transcriptional regulation in direct conversion (Table S2).

To explore this potential connection further, methylated regions were tracked via MeDIP-chip analysis in genomic DNA extracted from lateral organs whose development was synchronized by growing plantlets in the presence of NPA prior to

NAA priming (Fig. 1, Fig. 5G, Experimental Procedures). At the level of resolution afforded by MeDIP-chip, the methylome appears largely constant across the conversion sequence, with major root (*WOX5*, *PLT1*) and shoot (*WUS*, *STM*) development transcription factor genes remaining unmethylated across the series (data not shown). Nevertheless, 400 differentially methylated regions (DMRs) underwent significant albeit low-amplitude changes in methylation level (Fig. S4), of which only 10 coincided with nearby DEGs (Table S5). Whether or not these changes affect the three possible sequence contexts for DNA methylation, namely CG, CHG and CHH, remains to be investigated.

Competence for conversion is acquired with the apical stem cell niche

Most LRPs at stage V or earlier stall when transferred on 2-iP medium while LRPs at stages VI and VII can be converted into shoot meristems. To understand what determines the ability to convert, we examined the primordium morphology at stage VI and VII, compared to V. A central cluster of cells characterizes the later stages (red cells in Fig. 2F and G) (Malamy and Benfey, 1997). It is positioned between the incipient root cap and the provasculature, and flanked on both sides by the forming cortex and endodermis. The precise location and developmental fate of these central LRP cells were confirmed with the expression profile of *WOX5*, encoding a transcription factor that positively controls cell pluripotency in the QC of the primary root (Lavenus et al., 2013; Pi et al., 2015). Whole mount ISH revealed that *WOX5* transcripts are first detected in these cells at the transition between stages V and VI. The initial *WOX5* domain is wider than at stages VII and VIII, when only the third and fourth central cell layers remain labeled (Fig. S1A). Immediately following 2-iP exposure, the transcription of *WOX5* collapses (Fig. S1B). As soon as divisions resume in the converting organ, the same apical stem cells that formed the QC express the shoot meristem genes *WUS*, *CLV3*, and *STM* (Fig. 5, A, B, C, E and F).

In conclusion, LRPs at competent stages already contain a stem cell niche, the development of which appears to be required for conversion. These results agree with the earlier observation that shoot primordia only poorly regenerate in root segments of a *plt1/plt2* double mutant in which QC specification and maintenance are altered (Kareem et al., 2015). Upon 2-iP treatment, the same niche is reprogrammed to form a shoot, before cell divisions resume.

Root-to-shoot conversion is reversible, but only transiently

Last, we investigated whether the identity of the newly formed shoots is fixed or can also be reversed. As illustrated in Fig. 3, round-shaped early shoot primordia (eSP) are visible on root explants placed for 3 d on 2-iP medium, following an initial NPA/NAA synchronization (Fig. 6A). When treated further with NAA, most of these converting organs revert back to lateral root development (Fig. 6B).

The reversion rate was measured by comparing explants either kept on 2-iP medium for 6 d, or incubated for 3 d on 2-iP medium then transferred back on NAA medium. We estimate that 9 out of 10 of the organs at the early shoot primordium stage revert into emerged roots after the final NAA exposure in this experimental setup (see Supplemental Experimental Procedures for details).

Following NPA/NAA synchronization and 4 d on 2-iP medium, the later shoot promeristems (lSP) flatten with the bulging of paired leaf primordia (Fig. 6C). When transferred to NAA medium, these more mature meristems do not revert into roots and develop anthocyanin-colored leaflets (Fig. 6D).

WOX5 and *WUS* expression patterns corroborated the observed reversion constraints. As described above, 2-iP rapidly represses *WOX5* and gradually induces *WUS* in the converting organs (Fig. 6E). But the response to the subsequent 3-d NAA treatment depends on the duration of the prior 2-iP exposure. In all cases, *WOX5* transcript level is increased by NAA, but to a lesser extent after 4-d compared to 3-d 2-iP treatments. Concomitantly, *WUS* level is decreased by NAA, but is higher after 4-d than 3-d 2-iP exposure (Fig. 6F).

Whole mount ISH shows that, in CLRs, *WOX5* transcription is restricted to the QC (Fig. 6G) and *WUS* is not expressed (Fig. 6K). In early shoot promeristem, *WOX5* is turned off (Fig. 6H) and *WUS* transcripts define a large zone (Fig. 6L), in a pattern that prefigures the locked shoot meristem in which *WUS* expression is reduced to the OC (Fig. 6, I and M). However, in the early shoot promeristem exposed for 3 d to NAA, *WOX5* is expressed again (Fig. 6J), while *WUS* is off (Fig. 6N), thereby matching the morphological switch back to root development. The *WOX5* domain in reverted roots only includes a few cells, as observed in undisturbed LRPs from late stage VI onward (Fig. S1A), but it is positioned at least four layers away from the outer boundary of the enlarged organ formed following 2-iP treatment.

Presumably, the *WOX5*-labeled cells mark the new QC in the reverted roots that have other typical hallmarks, including two to three outer root cap layers, made of large cells containing amyloplasts, and radially organized endodermis- and pericycle-like layers surrounding the vascular cylinder (Fig. 6, J and N).

In summary, cells previously involved in the formation of the early shoot promeristem may be recruited back for the development of a new root meristem. However, the NAA-induced reversion is only possible during early shoot development, after a short exposure to cytokinin.

Discussion

We have shown that three successive phases can be distinguished during the direct conversion of a lateral root into a shoot meristem. The LR initiates the formation of an apical stem cell niche necessary for sustained organ development. Exogenous cytokinin transiently pauses cell division and induces the organ switch. The cells forming the incipient QC and the surrounding cell layers are recruited to form the novel shoot meristem through active and coordinated cell divisions. The molecular factors involved in the transitions are discussed here below.

Exogenous cytokinin rapidly changes lateral root meristem cell-type specificity

Genes involved in shoot development, including *STM*, *CLV3* and *WUS*, are turned on during the mitotic pause that immediately follows the cytokinin treatment. This early induction is most likely a key step triggering the conversion process (Gordon et al., 2007). It may be a direct cytokinin transcriptional response because the initial expression domain for these shoot genes is rather wide, encompassing the stele of the converting organ.

Concomitantly, genes involved in root development, including *SCR* and *WOX5*, are repressed, marking the loss of the QC (Zhang et al., 2013). Analysis of molecular reporters of auxin response and PIN1 protein localization showed that exogenous cytokinin also dramatically affects auxin fluxes and gradients necessary for the patterning of the root stem cell niche in the LRPs, reflecting the known

antagonism between auxin and cytokinin in the course of root development (Dello Ioio et al., 2008; Marhavý et al., 2011; Marhavý et al., 2014). These perturbations alter the maintenance of the lateral root meristem and result in a reduction of mitotic activity.

Auxin signaling participates to the conversion

At the onset of LRP/SM conversion, the apical zone of the organ where mitotic activity resumes strictly overlaps with the transient auxin maximum, in cells that accumulate the PIN1 protein in their plasma membrane. Therefore, auxin plays a key role in direct conversion, even though the switch of organ identity is induced by the replacement of an auxin by a cytokinin in the culture medium. This observation agrees with the demonstration that auxin action is required for the establishment of the stem cell organizing center and the SAM formation during somatic embryogenesis (Su et al., 2009; Su et al., 2015). Furthermore, the presence of shoot progenitor cells is correlated with auxin action (Gordon et al., 2007; Gordon et al., 2009; Kareem et al., 2015) and defects in auxin synthesis or transport dramatically disrupt shoot regeneration (Cheng et al., 2013; Kakani et al., 2009).

In the late phase of the shoot promeristem development, auxin maxima only mark the leaf primordia, in accordance with the observation that auxin response must be repressed for the proper homeostatic maintenance of the shoot meristem (de Reuille et al., 2006; Heisler et al., 2005; Roodbarkelari et al., 2015; Yadav et al., 2010). At these late stages, the central apical zone of the meristem is instead characterized by the cytokinin transcriptional response, as expected in an established shoot meristem (Gordon et al., 2009; Zürcher et al., 2013) and previously reported in shoots induced in CIM/SIM protocols (Che et al., 2002; Gordon et al., 2007).

Auxin and cytokinin define separate but complementary domains as the lateral root meristem is reprogrammed. Their spatial arrangement may position the new shoot stem cell niche and guide patterning, as observed during apical meristem initiation and maintenance or when an apical root meristem is regenerated after root tip excision (Efroni et al., 2016; Schaller et al., 2015).

Direct conversion occurs through transdifferentiation

The root-to-shoot conversion induced in our setup did not involve the disorganized proliferation of cells resulting in the formation of callus-like structures for several reasons. The detailed morphological analysis of the converting organ demonstrates that the root meristem cells were directly recruited for the formation of the shoot meristem whose shape rapidly conformed with that of a typical shoot apex, with no tearing or squashing of tissues. The SM central zone (CZ) was positioned at the apex of the lateral organ, its main axis was always perpendicular to that of the primary root segment, and the leaf primordia appeared on opposite sides of the CZ. Such robust patterns are not observed when SMs originate from calli.

Direct conversion is a developmental process that involves major transcriptional reprogramming. Approximately 3,000 genes were differentially expressed during the four early time points analyzed. Most genes were significantly up or down at only one time point, suggesting that the switch of organ identity occurs through a succession of rapidly evolving states. The transition relies on the regulatory action of transcription factors (TF), a class that is significantly overrepresented among the deregulated genes. For example, *MYB37* (AT5G23000), among the most highly induced TFs genes during the mitotic pause, regulates the formation of the axillary shoot meristem and is its earliest spatial marker, in agreement with a plausible role in root-to-shoot conversion (Keller et al., 2006).

Altogether, our data suggest that the conversion process does not involve cell dedifferentiation but, instead, a rapid switch in the fate of the cells involved, referred to as transdifferentiation.

How does a root meristem become a shoot meristem?

This report factually demonstrates that the networks at play in the meristem of a root can morph within a couple division cycles into those of a shoot. Comparative analysis of root and shoot meristem functions points to common features (Heidstra and Sabatini, 2014), including molecular regulatory modules that may be interchangeable, thus enabling a seamless transition between LRP and SM, and vice versa (Hobe et al., 2003; Perilli et al., 2012; Sarkar et al., 2007; Sebastian et al.,

2015; Zhou et al., 2015). For example, *WOX5* is replaced by *WUS* within hours at the onset of conversion, and reversely upon reversion, while they control pluripotency, in the root and shoot apex, respectively.

When divisions resume, cells within the incipient QC and adjacent layers are directly recruited to form the shoot meristem, through a coordinated process circumscribed to the central cell cluster. Such *de novo* specification implies that positional signals exchanged between stem cells and differentiating daughter cells – proteins, RNAs, phytohormones, secreted peptides – can be rapidly reconfigured (Reddy and Meyerowitz, 2005; Stuurman et al., 2002; van den Berg et al., 1995; Yadav et al., 2010).

In all developmental transitions we studied, *WOX5* and *WUS* are first expressed in a relatively wide domain when a new meristematic structure is initiated, then reach their narrower known positions in the established meristem. It was observed for *WOX5* in the first LRP stages. During conversion, the large initial *WUS* domain also narrows down to the organizing center of the new SM. A similar early confinement of *WUS* was reported during zygotic embryogenesis (Mayer et al., 1998) and after the laser ablation of the SAM or RAM organizing center (Haecker et al., 2004; Reinhardt et al., 2003; Xu et al., 2006). The *STM* transcript profile at first overlaps with *WUS*, but eventually marks the entire shoot promeristem and meristem. We reasoned that the dynamic process leading to the stereotypical organization of an apical meristem is driven by complex regulatory loops, some of which only kicking in after specific signals, thus explaining the sequential confinement observed during conversion.

However, the induction of *WUS* is not sufficient to operate the root-to-shoot conversion because it is also triggered by cytokinin in stage V LRPs that do not develop into shoots. In contrast to the pattern observed in converting organs, the *WUS* domain does not focus after 2-iP treatment in unconverted LRPs (Fig. S5). In this LRP/SM system as in others, the expression of shoot development genes is therefore not strictly correlated with shoot regeneration (Cary et al., 2002; Motte et al., 2011).

Finally, it remains unclear whether organ identity markers are mutually exclusive. Do cells expressing either *WOX5* or *WUS* coexist in the same converting organ? Can both genes be expressed simultaneously in the same cell? If such instances occur in the LRP/SM system, they must be short-lived. At the tissue level,

the superposition of cell identity markers has already been observed. For example, when a RAM regenerates after root tip excision, cells recruited from multiple tissues in the remaining stump first converge to a common mixed identity, before dividing to form the columella and QC in the new apex (Efroni et al., 2016).

Why is the stem cell niche necessary for conversion?

In the direct conversion system described herein, the lateral root primordium can be switched into a shoot only after the onset of *WOX5* expression and only for a few hours. Furthermore, the misspecification of the QC strongly affects conversion (Kareem et al., 2015). A simple interpretation of these results is that the developing organ must first acquire a functional stem cell niche before the application of exogenous cytokinin. Accordingly, the niche is able to withstand the hormonal shock and continues to provide cells to sustain organ growth, root or shoot, while a precocious cytokinin treatment results in the terminal differentiation of cells in the bulging primordium in the absence of a stem cell niche.

But the presence of a stem cell niche is not always required for organogenesis, suggesting that different regeneration mechanisms may occur in plants. Indeed, a new RAM can be formed after the excision of the root tip removing the apical stem cells, even in mutants (*plt1, plt2* and *scr*) in which the niche cannot be maintained in the adult root (Sena et al., 2009; Sena, 2014). In such excision experiments, the regeneration of the root apical meristem starts with an embryonic-like sequence and terminates with the formation of an active stem cell niche, with stem-cell-like divisions observed before the expression of cell identity markers (Efroni et al., 2016).

What locks organ identity?

Models of RAM and SAM functions describe how organ growth is shaped through complex interconnections between the constraints imposed by the encasing cell walls, the genetic programs driving cell expansion and cell division, and the signals exchanged between neighboring cells (Drisch and Stahl, 2015; Gaillochet et al., 2015). Logically, the RAM and SAM structural features may lock their identity. But our results highlight that organ identity remains undefined for several days after the initiation of shoot development or root reversion. Thus, the lock on organ identity

probably resides in the final pattern of the meristematic tissues. It may be encoded in the tensile stress networks that characterize different cell arrangements because mechanical forces regulate key meristem factors including *STM* (Landrein et al., 2015). Alternatively, the size and shape of the lateral organ may alter the distribution of morphogens or the penetration of exogenous cytokinin, as well as other compounds, that control meristem functions.

In addition to morphological constraints, epigenetic factors may prevent the organ switch because the expression of plant genes involved in cell differentiation or totipotency depends in part on changes in the chromatin landscape (Berdasco et al., 2008; Grafi, 2004; Grafi et al., 2007; He et al., 2012; Ikeuchi et al., 2015; Koukalova et al., 2005; Lafos et al., 2011; Zhang et al., 2011). Our data confirmed that, together with additional regulators of shoot development (e.g. *STM*), *WUS* is not methylated in the competent lateral root and remains in that state throughout the early stages of conversion. Since methylation is generally associated with gene repression, an unmethylated *WUS* locus may reflect that the developing LRP is open to a change in identity, in this case induced by cytokinin (Li et al., 2011; Shemer et al., 2015). The hypothesis that switchable organs have a chromatin state favorable to conversion is further supported by the identification of genes similarly regulated during direct conversion (this report) and in hypomethylated mutants prone to shoot organogenesis (Li et al., 2011). Thus, key regulators of shoot initiation that are actively repressed in the fully developed root would remain inducible until repression is established. But further analysis will be required to determine whether changes in chromatin marks, including DNA methylation but also histone modifications, occur earlier in LR development or later when organ identity is locked.

This study stresses that subtle differences in development timing may results in dramatically contrasted *in vitro* responses explaining why regeneration protocols must always be optimized locally. In our view, the precise and microscopic analysis of the cultured plant tissues is the best guide when test-proofing regeneration methods.

In conclusion, the mechanisms at play in direct organ conversion are complex and draw on functional modules involved in other developmental pathways. Their further study in the original and – now – well-controlled conversion program may help us distinguish the factors that determine cell totipotency in a generic plant apical meristem and that are involved in establishing and locking organ identity.

Experimental procedures

Plant materials and growth conditions

All plants were grown in climate-controlled growth chambers, at 24 °C, under 16 h day / 8 h night photoperiod (Philips 36W 840 neon, 110 $\mu E.m^{-2}.s^{-1}$). Sterilized *Arabidopsis thaliana* seeds were sown, stratified for one night at 4 °C, and grown for 6 d on solid medium. In explants prepared for morphological and marker line analysis, LR initiation was induced with NAA priming for 42 h. In explants sampled for RT-qPCR, transcriptomic and methylome studies, LR initiation was further synchronized by germinating and growing plantlets in the presence of NPA prior to NAA priming (see Supplemental Experimental Procedures for additional details, including composition of media, Arabidopsis reporter lines).

Explant imaging and analysis

Propidium iodide staining and confocal microscopy analysis were adapted from Truernit et al. (2008). Developing lateral organs were imaged as stacks of confocal optical sections and their organization was analyzed in the sagittal plane reconstructed for each object. Stacks were reoriented according to the primary root main axis to define transverse and sagittal planes across the LRP center by 3D multi-planar reconstruction with the OsiriX software. LRP developmental stages were identified based on epidermal cell numbers and stele cell organization, analyzed in reconstructed sagittal planes. To measure conversion and reversion rates according to LRP stages, samples were photographed across developmental series (Zeiss Axio zoom stereo-microscope) and each LRP of each explant was tracked with Image J. Whole-mount *in situ* hybridization was performed according to Morin et al. (in press). Additional details and GUS staining protocols are provided in Supplemental Experimental procedures.

Transcript profiling

For transcriptome analysis, lateral organs at each time point (T_0, T_6, T_{34}, T_{58}; Fig. 5G) were microdissected from fresh explants with the Zeiss Axiobserver PALM. Total RNA was extracted from pooled dissected organs with the RNeasy Plus Micro kit

(QIAGEN). RNA integrity was tested with the Agilent Bioanalyzer. Transcript profile analysis was performed on two independent biological experiments with the 25 K CATMA_v2.1 microarray bearing 24,576 gene specific tags. Details about quantitative real-time RT-PCR analysis and transcriptome data interpretation are available in Supplemental Experimental Procedures. All raw and normalized data available via CATdb (http://urgv.evry.inra.fr/CATdb/; Projects: Gnp07_Regeneome_transdifferenciation) and Gene Expression Omnibus (GEO; http://www.ncbi.nlm.nih.gov/geo/; super-series accession GSE30259).

Methylome profiling

Genome methylation marks were analyzed through MeDIP-chip analysis in two independent biological experiments at T_0, T_6, T_{34} and T_{58}, as described by Seifert et al. (2012). In these experiments, root segments were NPA-synchronized but not microdissected. Methylome patterns were compared to transcriptome datasets generated from the same explants. MeDIP-chip raw and processed data are available via Gene Expression Omnibus (GEO; http://www.ncbi.nlm.nih.gov/geo/; super-series accession GSE84415).

Acknowledgments:

This work was funded in part by the project Regeneome (ANR-07-GPLA-011) of the French *Agence Nationale de la Recherche* (ANR), coordinated by J.D. Faure. The authors thank the reviewers for their insightful comments, P. Laufs and B. Müller for their generous gift of reporter lines seeds, J.C Palauqui and K. Belcram for their help with microscope imaging and analyses, J.D. Faure, P. Laufs and J.C. Palauqui for their critical reading of the manuscript. The IJPB benefits from the support of the LabEx Saclay Plant Sciences-SPS (ANR-10-LABX-0040-SPS).

Competing interests:

The authors declare no competing or financial interests.

Author contributions:

V.C, F.R., M.D.C. and P.R. conceived and designed the research. O.R., L.C., J.S., L.L., E.C., F.R., D.G., M.D.C and P.R. performed the experiments. E.C., V.C, F.R., P.H., R.B., M.D.C. and P.R. analyzed the data. V.C, F.R., P.H., R.B., M.D.C. and P.R. wrote and revised the paper.

Funding information:

This work was funded in part by the project Regeneome (ANR-07-GPLA-011) of the French *Agence Nationale de la Recherche* (ANR). The IJPB benefits from the support of the LabEx Saclay Plant Sciences-SPS (ANR-10-LABX-0040-SPS).

References

Aida, M., Beis, D., Heidstra, R., Willemsen, V., Blilou, I., Galinha, C., Nussaume, L., Noh, Y.-S., Amasino, R. and Scheres, B. (2004). The *PLETHORA* genes mediate patterning of the Arabidopsis root stem cell niche. *Cell* **119**, 109–120.

Atta, R., Laurens, L., Boucheron-Dubuisson, E., Guivarc'h, A., Carnero, E., Giraudat-Pautot, V., Rech, P. and Chriqui, D. (2009). Pluripotency of Arabidopsis xylem pericycle underlies shoot regeneration from root and hypocotyl explants grown in vitro. *Plant J.* **57**, 626–644.

Barton, M. K. and Poethig, R. S. (1993). Formation of the shoot apical meristem in Arabidopsis thaliana: an analysis of development in the wild type and in the shoot meristemless mutant. *Development* **119**, 823–831.

Benková, E., Michniewicz, M., Sauer, M., Teichmann, T., Seifertová, D., Jürgens, G. and Friml, J. (2003). Local, efflux-dependent auxin gradients as a common module for plant organ formation. *Cell* **115**, 591–602.

Berdasco, M., Alcázar, R., García-Ortiz, M. V., Ballestar, E., Fernández, A. F., Roldán-Arjona, T., Tiburcio, A. F., Altabella, T., Buisine, N., Quesneville, H., et al. (2008). Promoter DNA hypermethylation and gene repression in undifferentiated Arabidopsis cells. *PloS One* **3**, e3306.

Bielach, A., Podlesáková, K., Marhavý, P., Duclercq, J., Cuesta, C., Müller, B., Grunewald, W., Tarkowski, P. and Benková, E. (2012). Spatiotemporal regulation of lateral root organogenesis in Arabidopsis by cytokinin. *Plant Cell* **24**, 3967–3981.

Boutté, Y., Frescatada-Rosa, M., Men, S., Chow, C.-M., Ebine, K., Gustavsson, A., Johansson, L., Ueda, T., Moore, I., Jürgens, G., et al. (2010). Endocytosis restricts Arabidopsis KNOLLE syntaxin to the cell division plane during late cytokinesis. *EMBO J.* **29**, 546–558.

Brand, U., Grünewald, M., Hobe, M. and Simon, R. (2002). Regulation of *CLV3* expression by two homeobox genes in Arabidopsis. *Plant Physiol.* **129**, 565–575.

Brenner, W. G. and Schmülling, T. (2015). Summarizing and exploring data of a decade of cytokinin-related transcriptomics. *Front. Plant Sci.* **6**, 29.

Brunoud, G., Wells, D. M., Oliva, M., Larrieu, A., Mirabet, V., Burrow, A. H., Beeckman, T., Kepinski, S., Traas, J., Bennett, M. J., et al. (2012). A novel sensor to map auxin response and distribution at high spatio-temporal resolution. *Nature* **482**, 103–106.

Cary, A. J., Che, P. and Howell, S. H. (2002). Developmental events and shoot apical meristem gene expression patterns during shoot development in *Arabidopsis thaliana*. *Plant J.* **32**, 867–877.

Chang, L., Ramireddy, E. and Schmülling, T. (2013). Lateral root formation and growth of Arabidopsis is redundantly regulated by cytokinin metabolism and signalling genes. *J. Exp. Bot.* **64**, 5021–5032.

Chatfield, S. P., Capron, R., Severino, A., Penttila, P.-A., Alfred, S., Nahal, H. and Provart, N. J. (2013). Incipient stem cell niche conversion in tissue culture: using a systems approach to probe early events in *WUSCHEL*-dependent conversion of lateral root primordia into shoot meristems. *Plant J.* **73**, 798–813.

Che, P., Gingerich, D. J., Lall, S. and Howell, S. H. (2002). Global and hormone-induced gene expression changes during shoot development in Arabidopsis. *Plant Cell* **14**, 2771–2785.

Che, P., Lall, S., Nettleton, D. and Howell, S. H. (2006). Gene expression programs during shoot, root, and callus development in Arabidopsis tissue culture. *Plant Physiol.* **141**, 620–637.

Che, P., Lall, S. and Howell, S. H. (2007). Developmental steps in acquiring competence for shoot development in Arabidopsis tissue culture. *Planta* **226**, 1183–1194.

Cheng, Z. J., Wang, L., Sun, W., Zhang, Y., Zhou, C., Su, Y. H., Li, W., Sun, T. T., Zhao, X. Y., Li, X. G., et al. (2013). Pattern of auxin and cytokinin responses for shoot meristem induction results from the regulation of cytokinin biosynthesis by AUXIN RESPONSE FACTOR3. *Plant Physiol.* **161**, 240–251.

Dello Ioio, R., Nakamura, K., Moubayidin, L., Perilli, S., Taniguchi, M., Morita, M. T., Aoyama, T., Costantino, P. and Sabatini, S. (2008). A genetic framework for the control of cell division and differentiation in the root meristem. *Science* **322**, 1380–1384.

de Reuille, P. B., Bohn-Courseau, I., Ljung, K., Morin, H., Carraro, N., Godin, C. and Traas, J. (2006). Computer simulations reveal properties of the cell-cell signaling network at the shoot apex in Arabidopsis. *Proc. Natl. Acad. Sci. U. S. A.* **103**, 1627–1632.

Drisch, R. C. and Stahl, Y. (2015). Function and regulation of transcription factors involved in root apical meristem and stem cell maintenance. *Front. Plant Sci.* **6**, 505.

Endrizzi, K., Moussian, B., Haecker, A., Levin, J. Z. and Laux, T. (1996). The SHOOT MERISTEMLESS gene is required for maintenance of undifferentiated cells in Arabidopsis shoot and floral meristems and acts at a different regulatory level than the meristem genes WUSCHEL and ZWILLE. *Plant J.* **10**, 967–979.

Efroni, I., Mello, A., Nawy, T., Ip, P.-L., Rahni, R., DelRose, N., Powers, A., Satija, R. and Birnbaum, K. D. (2016). Root Regeneration Triggers an Embryo-like Sequence Guided by Hormonal Interactions. *Cell* **165**, 1721–1733.

Gaillochet, C., Daum, G. and Lohmann, J. U. (2015). O cell, where art thou? The mechanisms of shoot meristem patterning. *Curr. Opin. Plant Biol.* **23**, 91–97.

Gallois, J.-L., Nora, F. R., Mizukami, Y. and Sablowski, R. (2004). WUSCHEL induces shoot stem cell activity and developmental plasticity in the root meristem. *Genes Dev.* **18**, 375–380.

González-García, M.-P., Vilarrasa-Blasi, J., Zhiponova, M., Divol, F., Mora-García, S., Russinova, E. and Caño-Delgado, A. I. (2011). Brassinosteroids control meristem size by promoting cell cycle progression in Arabidopsis roots. *Development* **138**, 849–859.

Gordon, S. P., Heisler, M. G., Reddy, G. V., Ohno, C., Das, P. and Meyerowitz, E. M. (2007). Pattern formation during de novo assembly of the Arabidopsis shoot meristem. *Development* **134**, 3539–3548.

Gordon, S. P., Chickarmane, V. S., Ohno, C. and Meyerowitz, E. M. (2009). Multiple feedback loops through cytokinin signaling control stem cell number within the Arabidopsis shoot meristem. *Proc. Natl. Acad. Sci. U. S. A.* **106**, 16529–16534.

Grafi, G. (2004). How cells dedifferentiate: a lesson from plants. *Dev. Biol.* **268**, 1–6.

Grafi, G., Ben-Meir, H., Avivi, Y., Moshe, M., Dahan, Y. and Zemach, A. (2007). Histone methylation controls telomerase-independent telomere lengthening in cells undergoing dedifferentiation. *Dev. Biol.* **306**, 838–846.

Haecker, A., Gross-Hardt, R., Geiges, B., Sarkar, A., Breuninger, H., Herrmann, M. and Laux, T. (2004). Expression dynamics of *WOX* genes mark cell fate decisions during early embryonic patterning in *Arabidopsis thaliana*. *Development* **131**, 657–668.

He, C., Chen, X., Huang, H. and Xu, L. (2012). Reprogramming of H3K27me3 is critical for acquisition of pluripotency from cultured Arabidopsis tissues. *PLoS Genet.* **8**, e1002911.

Heidstra, R. and Sabatini, S. (2014). Plant and animal stem cells: similar yet different. *Nat. Rev. Mol. Cell Biol.* **15**, 301–312.

Heisler, M. G., Ohno, C., Das, P., Sieber, P., Reddy, G. V., Long, J. A. and Meyerowitz, E. M. (2005). Patterns of auxin transport and gene expression during primordium development revealed by live imaging of the Arabidopsis inflorescence meristem. *Curr. Biol.* **15**, 1899–1911.

Helariutta, Y., Fukaki, H., Wysocka-Diller, J., Nakajima, K., Jung, J., Sena, G., Hauser, M. T. and Benfey, P. N. (2000). The SHORT-ROOT gene controls radial patterning of the Arabidopsis root through radial signaling. *Cell* **101**, 555–567.

Hibara, K., Takada, S. and Tasaka, M. (2003). CUC1 gene activates the expression of SAM-related genes to induce adventitious shoot formation. *Plant J.* **36**, 687–696.

Hobe, M., Müller, R., Grünewald, M., Brand, U. and Simon, R. (2003). Loss of CLE40, a protein functionally equivalent to the stem cell restricting signal CLV3, enhances root waving in Arabidopsis. *Dev. Genes Evol.* **213**, 371–381.

Ikeuchi, M., Iwase, A., Rymen, B., Harashima, H., Shibata, M., Ohnuma, M., Breuer, C., Morao, A. K., de Lucas, M., De Veylder, L., et al. (2015). PRC2 represses dedifferentiation of mature somatic cells in Arabidopsis. *Nat. Plants* **1**, 15089.

Ikeuchi, M., Ogawa, Y., Iwase, A. and Sugimoto, K. (2016). Plant regeneration: cellular origins and molecular mechanisms. *Development* **143**, 1442–1451.

Kakani, A., Li, G. and Peng, Z. (2009). Role of AUX1 in the control of organ identity during in vitro organogenesis and in mediating tissue specific auxin and cytokinin interaction in Arabidopsis. *Planta* **229**, 645–657.

Kareem, A., Durgaprasad, K., Sugimoto, K., Du, Y., Pulianmackal, A. J., Trivedi, Z. B., Abhayadev, P. V., Pinon, V., Meyerowitz, E. M., Scheres, B., et al. (2015). *PLETHORA* Genes Control Regeneration by a Two-Step Mechanism. *Curr. Biol.* **25**, 1017–1030.

Keller, T., Abbott, J., Moritz, T. and Doerner, P. (2006). Arabidopsis REGULATOR OF AXILLARY MERISTEMS1 controls a leaf axil stem cell niche and modulates vegetative development. *Plant Cell* **18**, 598–611.

Kleine-Vehn, J., Huang, F., Naramoto, S., Zhang, J., Michniewicz, M., Offringa, R. and Friml, J. (2009). PIN auxin efflux carrier polarity is regulated by

PINOID kinase-mediated recruitment into GNOM-independent trafficking in Arabidopsis. *Plant Cell* **21**, 3839–3849.

Koukalova, B., Fojtova, M., Lim, K. Y., Fulnecek, J., Leitch, A. R. and Kovarik, A. (2005). Dedifferentiation of tobacco cells is associated with ribosomal RNA gene hypomethylation, increased transcription, and chromatin alterations. *Plant Physiol.* **139**, 275–286.

Lafos, M., Kroll, P., Hohenstatt, M. L., Thorpe, F. L., Clarenz, O. and Schubert, D. (2011). Dynamic regulation of H3K27 trimethylation during Arabidopsis differentiation. *PLoS Genet.* **7**, e1002040.

Landrein, B., Kiss, A., Sassi, M., Chauvet, A., Das, P., Cortizo, M., Laufs, P., Takeda, S., Aida, M., Traas, J., et al. (2015). Mechanical stress contributes to the expression of the *STM* homeobox gene in Arabidopsis shoot meristems. *eLife* **4**, e07811.

Lavenus, J., Goh, T., Roberts, I., Guyomarc'h, S., Lucas, M., De Smet, I., Fukaki, H., Beeckman, T., Bennett, M. and Laplaze, L. (2013). Lateral root development in Arabidopsis: fifty shades of auxin. *Trends Plant Sci.* **18**, 450–458.

Li, W., Liu, H., Cheng, Z. J., Su, Y. H., Han, H. N., Zhang, Y. and Zhang, X. S. (2011). DNA methylation and histone modifications regulate de novo shoot regeneration in Arabidopsis by modulating *WUSCHEL* expression and auxin signaling. *PLoS Genet.* **7**, e1002243.

Malamy, J. E. and Benfey, P. N. (1997). Organization and cell differentiation in lateral roots of Arabidopsis thaliana. *Development* **124**, 33–44.

Marhavý, P., Bielach, A., Abas, L., Abuzeineh, A., Duclercq, J., Tanaka, H., Pařezová, M., Petrášek, J., Friml, J., Kleine-Vehn, J., et al. (2011). Cytokinin modulates endocytic trafficking of PIN1 auxin efflux carrier to control plant organogenesis. *Dev. Cell* **21**, 796–804.

Marhavý, P., Duclercq, J., Weller, B., Feraru, E., Bielach, A., Offringa, R., Friml, J., Schwechheimer, C., Murphy, A. and Benková, E. (2014). Cytokinin

controls polarity of PIN1-dependent auxin transport during lateral root organogenesis. *Curr. Biol.* **24**, 1031–1037.

Mayer, K. F., Schoof, H., Haecker, A., Lenhard, M., Jürgens, G., and Laux T. (1998). Role of *WUSCHEL* in regulating stem cell fate in the Arabidopsis shoot meristem. *Cell* **95**, 805-815

Motte, H., Verstraeten, I., Werbrouck, S. and Geelen, D. (2011). *CUC2* as an early marker for regeneration competence in Arabidopsis root explants. *J. Plant Physiol.* **168**, 1598–1601.

Motte, H., Vereecke, D., Geelen, D. and Werbrouck, S. (2014). The molecular path to in vitro shoot regeneration. *Biotechnol. Adv.* **32**, 107–121.

Nemhauser, J. L., Hong, F. and Chory, J. (2006). Different plant hormones regulate similar processes through largely nonoverlapping transcriptional responses. *Cell* **126**, 467–475.

Perilli, S., Di Mambro, R. and Sabatini, S. (2012). Growth and development of the root apical meristem. *Curr. Opin. Plant Biol.* **15**, 17–23.

Pi, L., Aichinger, E., van der Graaff, E., Llavata-Peris, C. I., Weijers, D., Hennig, L., Groot, E. and Laux, T. (2015). Organizer-Derived WOX5 Signal Maintains Root Columella Stem Cells through Chromatin-Mediated Repression of *CDF4* Expression. *Dev. Cell* **33**, 576–588.

Pulianmackal, A. J., Kareem, A. V. K., Durgaprasad, K., Trivedi, Z. B. and Prasad, K. (2014). Competence and regulatory interactions during regeneration in plants. *Front. Plant Sci.* **5**, 142.

Reddy, G. V. and Meyerowitz, E. M. (2005). Stem-cell homeostasis and growth dynamics can be uncoupled in the Arabidopsis shoot apex. *Science* **310**, 663–667.

Reinhardt, D., Frenz, M., Mandel, T. and Kuhlemeier, C. (2003). Microsurgical and laser ablation analysis of interactions between the zones and layers of the tomato shoot apical meristem. *Development* **130**, 4073–4083.

Roodbarkelari, F., Du, F., Truernit, E. and Laux, T. (2015). ZLL/AGO10 maintains shoot meristem stem cells during Arabidopsis embryogenesis by down-regulating ARF2-mediated auxin response. *BMC Biol.* **13**, 74.

Sarkar, A. K., Luijten, M., Miyashima, S., Lenhard, M., Hashimoto, T., Nakajima, K., Scheres, B., Heidstra, R. and Laux, T. (2007). Conserved factors regulate signalling in Arabidopsis thaliana shoot and root stem cell organizers. *Nature* **446**, 811–814.

Schaller, G. E., Bishopp, A. and Kieber, J. J. (2015). The yin-yang of hormones: cytokinin and auxin interactions in plant development. *Plant Cell* **27**, 44–63.

Scheres, B. (2007). Stem-cell niches: nursery rhymes across kingdoms. *Nat. Rev. Mol. Cell Biol.* **8**, 345–354.

Scofield, S., Dewitte, W., Nieuwland, J. and Murray, J. A. H. (2013). The Arabidopsis homeobox gene *SHOOT MERISTEMLESS* has cellular and meristem-organisational roles with differential requirements for cytokinin and CYCD3 activity. *Plant J.* **75**, 53–66.

Sebastian, J., Ryu, K. H., Zhou, J., Tarkowská, D., Tarkowski, P., Cho, Y.-H., Yoo, S.-D., Kim, E.-S. and Lee, J.-Y. (2015). PHABULOSA controls the quiescent center-independent root meristem activities in *Arabidopsis thaliana*. *PLoS Genet.* **11**, e1004973.

Seifert, M., Cortijo, S., Colomé-Tatché, M., Johannes, F., Roudier, F. and Colot, V. (2012). MeDIP-HMM: genome-wide identification of distinct DNA methylation states from high-density tiling arrays. *Bioinformatics* **28**, 2930–2939.

Sena, G., Wang, X., Liu, H.-Y., Hofhuis, H. and Birnbaum, K. D. (2009). Organ regeneration does not require a functional stem cell niche in plants. *Nature* **457**, 1150–1153.

Sena, G. (2014). Stem cells and regeneration in plants. *Nephron Exp. Nephrol.* **126**, 35.

Shemer, O., Landau, U., Candela, H., Zemach, A. and Eshed Williams, L. (2015). Competency for shoot regeneration from Arabidopsis root explants is regulated by DNA methylation. *Plant Sci.* **238**, 251–261.

Skoog, F. and Miller, C. O. (1957). Chemical regulation of growth and organ formation in plant tissues cultured *in vitro. Symp. Soc. Exp. Biol.* **11**, 118–130.

Smith, Z. R. and Long, J. A. (2010). Control of Arabidopsis apical-basal embryo polarity by antagonistic transcription factors. *Nature* **464**, 423–426.

Stuurman, J., Jäggi, F. and Kuhlemeier, C. (2002). Shoot meristem maintenance is controlled by a *GRAS*-gene mediated signal from differentiating cells. *Genes Dev.* **16**, 2213–2218.

Su, Y. H., Zhao, X. Y., Liu, Y. B., Zhang, C. L., O'Neill, S. D. and Zhang, X. S. (2009). Auxin-induced *WUS* expression is essential for embryonic stem cell renewal during somatic embryogenesis in Arabidopsis. *Plant J.* **59**, 448–460.

Su, Y. H., Liu, Y. B., Bai, B. and Zhang, X. S. (2015). Establishment of embryonic shoot-root axis is involved in auxin and cytokinin response during Arabidopsis somatic embryogenesis. *Front. Plant Sci.* **5**, 792.

Sugimoto, K., Jiao, Y. and Meyerowitz, E. M. (2010). Arabidopsis regeneration from multiple tissues occurs via a root development pathway. *Dev. Cell* **18**, 463–471.

Sugimoto, K., Gordon, S. P. and Meyerowitz, E. M. (2011). Regeneration in plants and animals: dedifferentiation, transdifferentiation, or just differentiation? *Trends Cell Biol.* **21**, 212–218.

Sugiyama, M. (1999). Organogenesis in vitro. *Curr. Opin. Plant Biol.* **2**, 61–64.

Terpstra, I. and Heidstra, R. (2009). Stem cells: The root of all cells. *Semin. Cell Dev. Biol.* **20**, 1089–1096.

Truernit, E., Bauby, H., Dubreucq, B., Grandjean, O., Runions, J., Barthélémy, J. and Palauqui, J.-C. (2008). High-resolution whole-mount imaging of three-

dimensional tissue organization and gene expression enables the study of Phloem development and structure in Arabidopsis. *Plant Cell* **20**, 1494–1503.

Ulmasov, T., Murfett, J., Hagen, G. and Guilfoyle, T. J. (1997). Aux/IAA proteins repress expression of reporter genes containing natural and highly active synthetic auxin response elements. *Plant Cell* **9**, 1963–1971.

Valvekens, D., Van Montagu, M. and Van Lijsebettens, M. (1988). *Agrobacterium tumefaciens*-mediated transformation of *Arabidopsis thaliana* root explants by using kanamycin selection. *Proc. Natl. Acad. Sci. U. S. A.* **85**, 5536–5540.

Van den Berg, C., Willemsen, V., Hage, W., Weisbeek, P. and Scheres, B. (1995). Cell fate in the Arabidopsis root meristem determined by directional signalling. *Nature* **378**, 62–65.

Vandepoele, K., Raes, J., De Veylder, L., Rouzé, P., Rombauts, S. and Inzé, D. (2002). Genome-wide analysis of core cell cycle genes in Arabidopsis. *Plant Cell* **14**, 903–916.

Xu, L. and Huang, H. (2014). Genetic and epigenetic controls of plant regeneration. *Curr. Top. Dev. Biol.* **108**, 1–33.

Xu, J., Hofhuis, H., Heidstra, R., Sauer, M., Friml, J. and Scheres, B. (2006). A molecular framework for plant regeneration. *Science* **311**, 385–388.

Yadav, R. K., Tavakkoli, M. and Reddy, G. V. (2010). WUSCHEL mediates stem cell homeostasis by regulating stem cell number and patterns of cell division and differentiation of stem cell progenitors. *Development* **137**, 3581–3589.

Zhang, J., Gao, G., Chen, J.-J., Taylor, G., Cui, K.-M. and He, X.-Q. (2011). Molecular features of secondary vascular tissue regeneration after bark girdling in *Populus*. *New Phytol.* **192**, 869–884.

Zhang, W., Swarup, R., Bennett, M., Schaller, G. E. and Kieber, J. J. (2013). Cytokinin induces cell division in the quiescent center of the Arabidopsis root apical meristem. *Curr. Biol.* **23**, 1979–1989.

Zhou, Y., Liu, X., Engstrom, E. M., Nimchuk, Z. L., Pruneda-Paz, J. L., Tarr, P. T., Yan, A., Kay, S. A. and Meyerowitz, E. M. (2015). Control of plant stem cell function by conserved interacting transcriptional regulators. *Nature* **517**, 377–380.

Zürcher, E., Tavor-Deslex, D., Lituiev, D., Enkerli, K., Tarr, P. T. and Müller, B. (2013). A robust and sensitive synthetic sensor to monitor the transcriptional output of the cytokinin signaling network in planta. *Plant Physiol.* **161**, 1066–1075.

Figures

Figure 1: Conversion of lateral root primordia into shoot meristems.

A, Differential lateral organ development. Whole primary roots were excised from 6-d plantlets and incubated on cytokinin (2-iP) medium for 6 d. 1, arrested lateral root primordia (LRPs); 2, LRP converted into shoot meristem (SM); 3, lateral root (LR). B-D, Root segment induction. Plantlets were germinated and grown on medium containing a polar auxin transport inhibitor (NPA) for 6 d, primed on NAA medium for 42 h (B), and root segments were transferred on 2-iP medium for 6 d (C and D). Depending on the position of the sections, a root fragment produced simultaneously

arrested LRPs, converted SMs and LRs (C, white mark delimited segments on B) or solely converted SMs (D, blue mark segments on B). Domains were sufficiently reproducible for the exclusive production of synchronized shoots in large amounts. E, Primary root segment after 42 h NAA, but without prior NPA application. F, The same root segment after an additional 5-d incubation on 2-iP medium. Scale bar: 2 mm. *In vitro* response was analyzed in explants prepared from L*er*-Col-0 hybrid (A-D) or Col-0 plants (E-F).

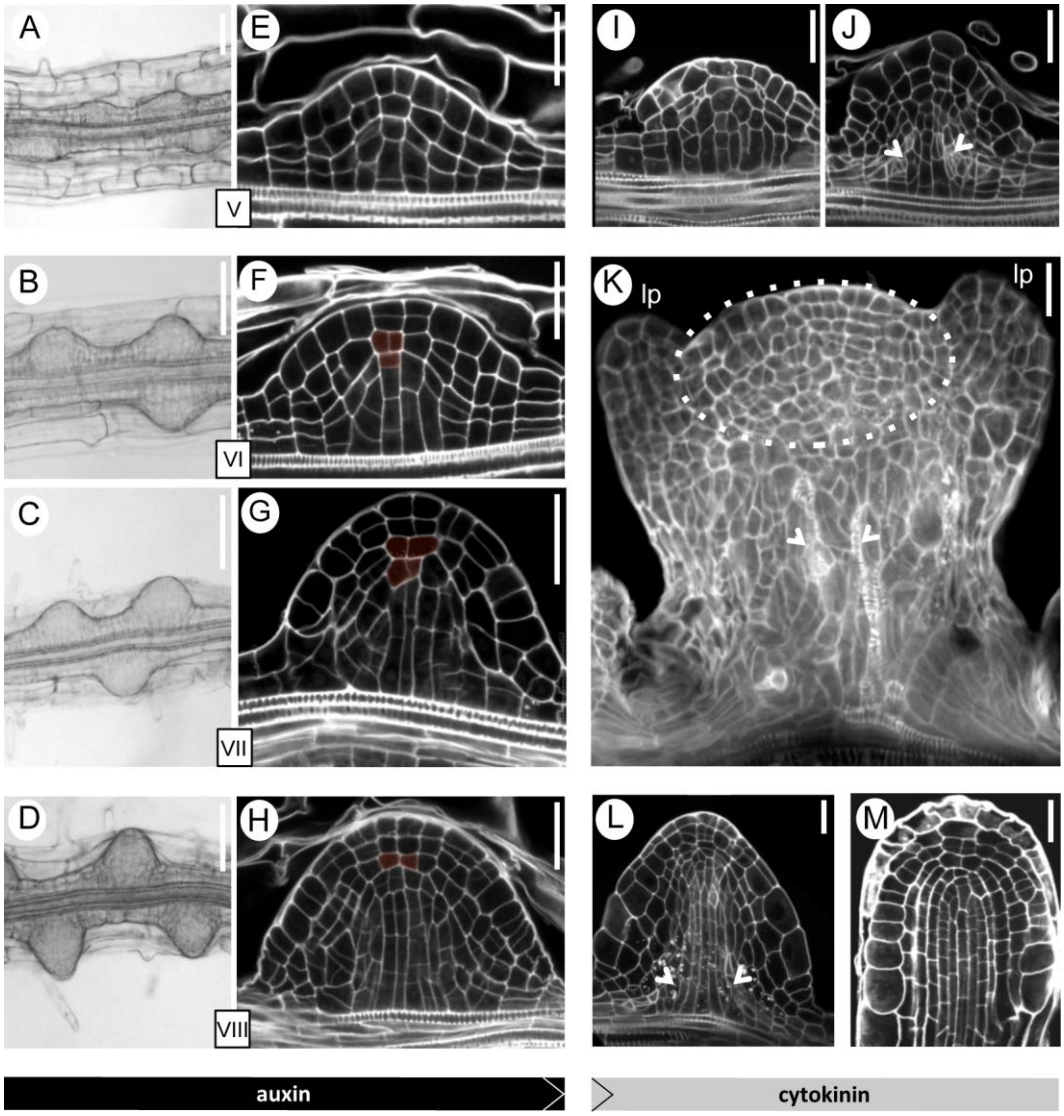

Figure 2: Organ fate depending on the developmental stage of the root primordium at cytokinin treatment.

A-D, Stages of lateral root primordium development. Nomarski images of Col-0 primary root explants exposed to NAA for 42 h, 6 d after germination. LRP developmental stages indicated in square boxes were defined by Malamy and Benfey (1997). E-M, Lateral root primordia following exposure to auxin and cytokinin. Wild-type Col-0 explants were fixed, PI-stained, and visualized as reconstructed sagittal planes after 42-h NAA-priming (E-H) and after subsequent 2-iP treatment (I-M). Explants were treated with 2-iP for two (I, L), four (J) or five days (K, M). Cells highlighted in red mark the cluster prefiguring the quiescent center (F, G, H). Single arrowheads mark vascular tissues. In Panel K: lp, leaf primordium; SM enclosed in dashed oval. Scale bars: 25 µm.

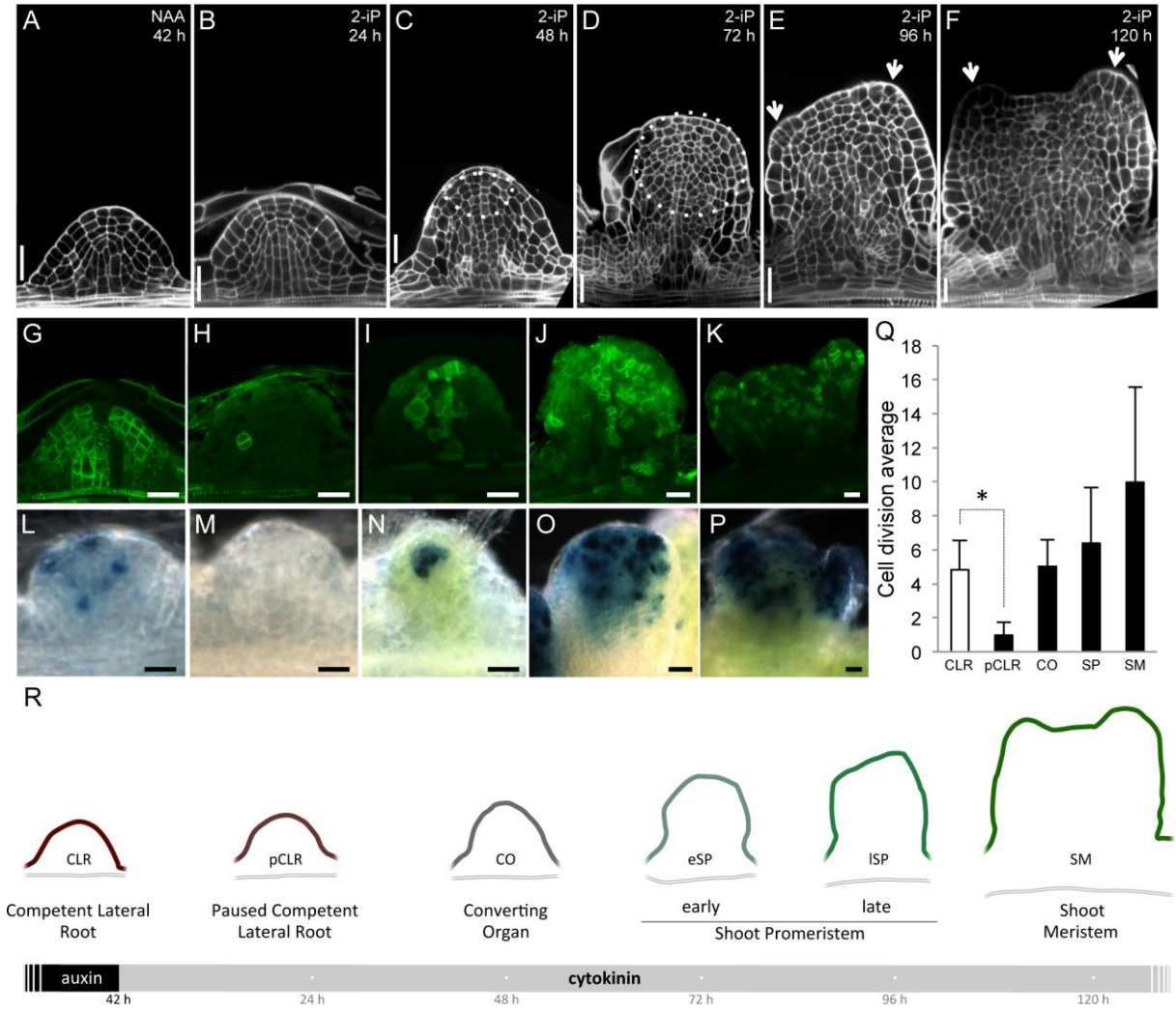

Figure 3: Sequential cellular events involved in root-to-shoot direct conversion.

A, Competent lateral root after NAA priming (CLR, *n*=13). B-F, Lateral organ on 2-iP medium. B, Paused competent lateral root (pCLR, *n*=6); C, converting organ (CO, *n*=9); D, Early shoot promeristem (eSP, *n*=12); E, Late shoot promeristem (lSP, *n*=13); F, Shoot meristem (SM, *n*=10). Dashed circles: regions with actively dividing cells. Arrows: leaf primordia. All imaged lateral organs were wild-type (Col-0) stained with propidium iodide. The most representative structures are shown for each time point. G-K, *pKNOLLE::KNOLLE-GFP*. L-P, *pCYCB1;1::DB-GUS*. Q, Mitotic activity quantification based on GUS-stained cell count (*: p<0.0001, Student's t-test). Scale bars: 25 µm. R, Schematic representation of root-to-shoot conversion.

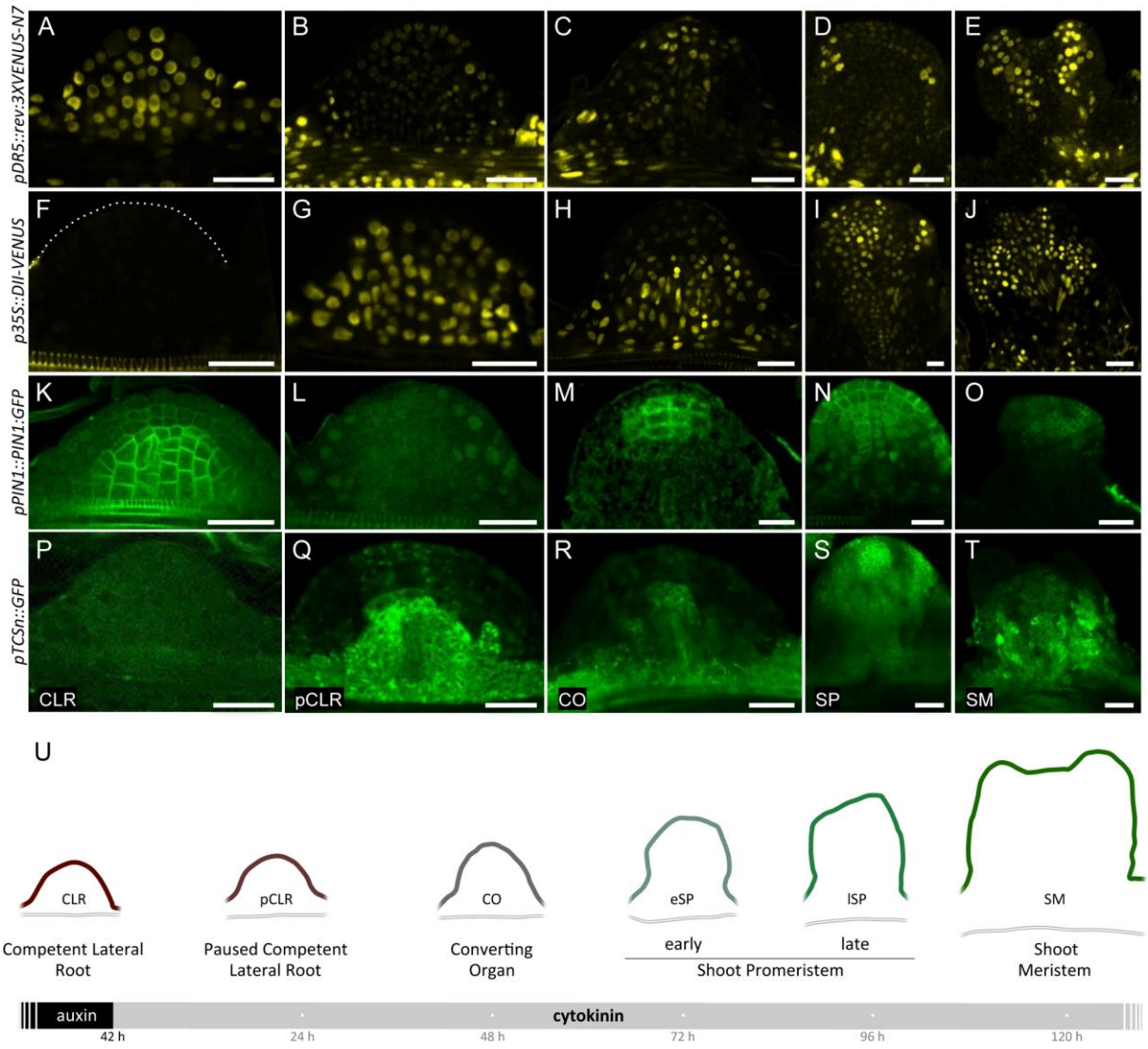

Figure 4: Hormonal responses during conversion.

A-E, Auxin *pDR5* transcriptional activity driving nuclear VENUS expression. F-J, Auxin DII-VENUS protein sensor. K-O, PIN1-GFP localization. P-T, Cytokinin *pTCSn* activity driving cytoplasmic GFP expression. A, F, K and P: competent lateral root (CLR); B, G, L and Q: paused competent lateral root (pCLR); C, H, M and R: converting organ (CO); D, I, N and S: shoot promeristem (SP); E, J, O and T: shoot meristem (SM). Scale bars: 50 µm. U, Schematic representation of root-to-shoot conversion.

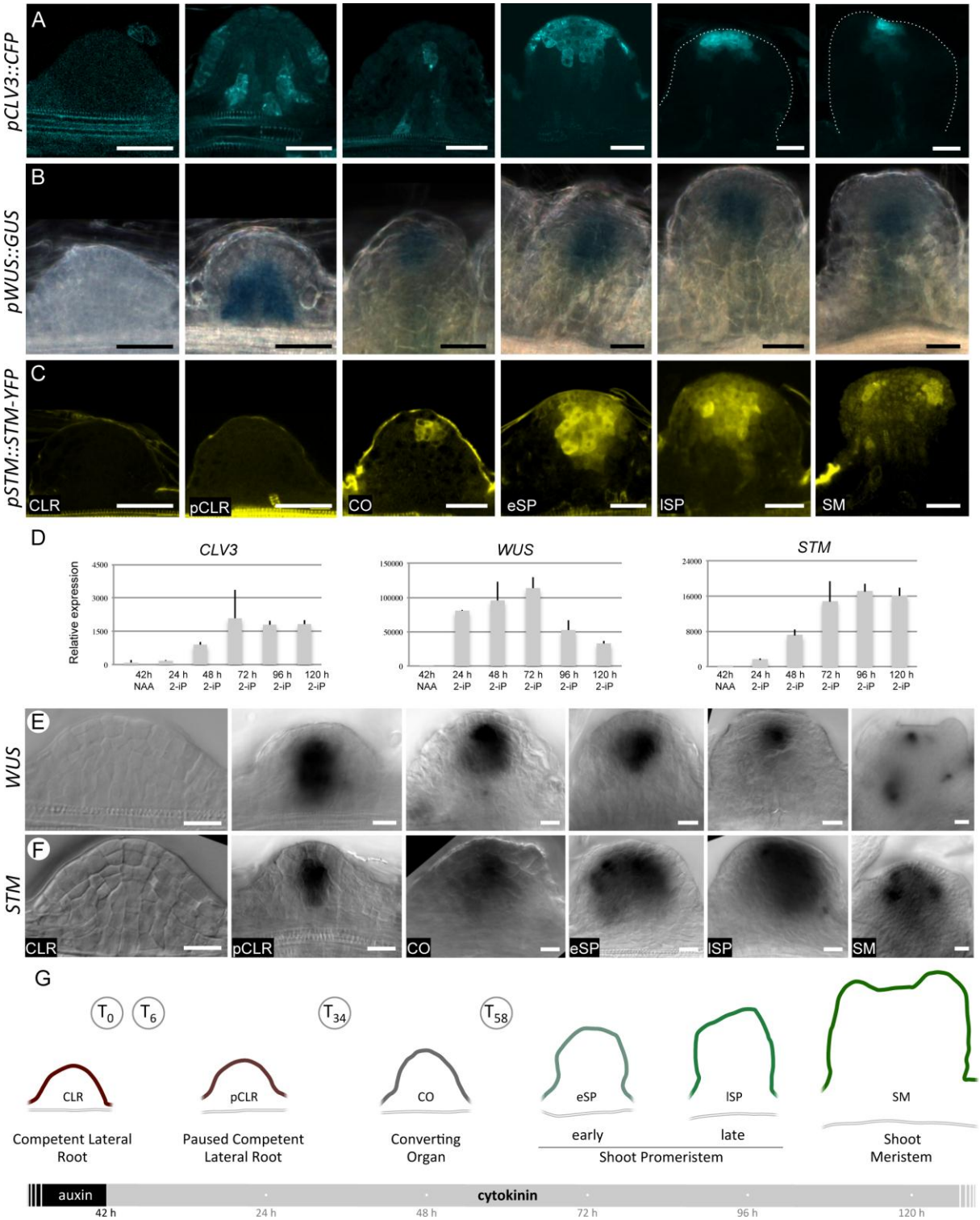

Figure 5: Expression of genes involved in shoot development during conversion.

Reporter lines: A, *pCLV3::CFP*; B, *pWUS::GUS*; C, *pSTM::STM:YFP*. Scale bars: 50 µm. D, RT-qPCR analysis gene expression in Col-0 explants. E and F, Whole mount *in situ* localization of *WUS* and *STM* transcripts. Lateral root were visualized with Nomarski microscopy (DIC). Scale bars: 20 µm. G, Schematic representation of root-to-shoot conversion. Time points expressed as hours of 2-iP treatment indicate samples collected for transcriptome and methylome analysis.

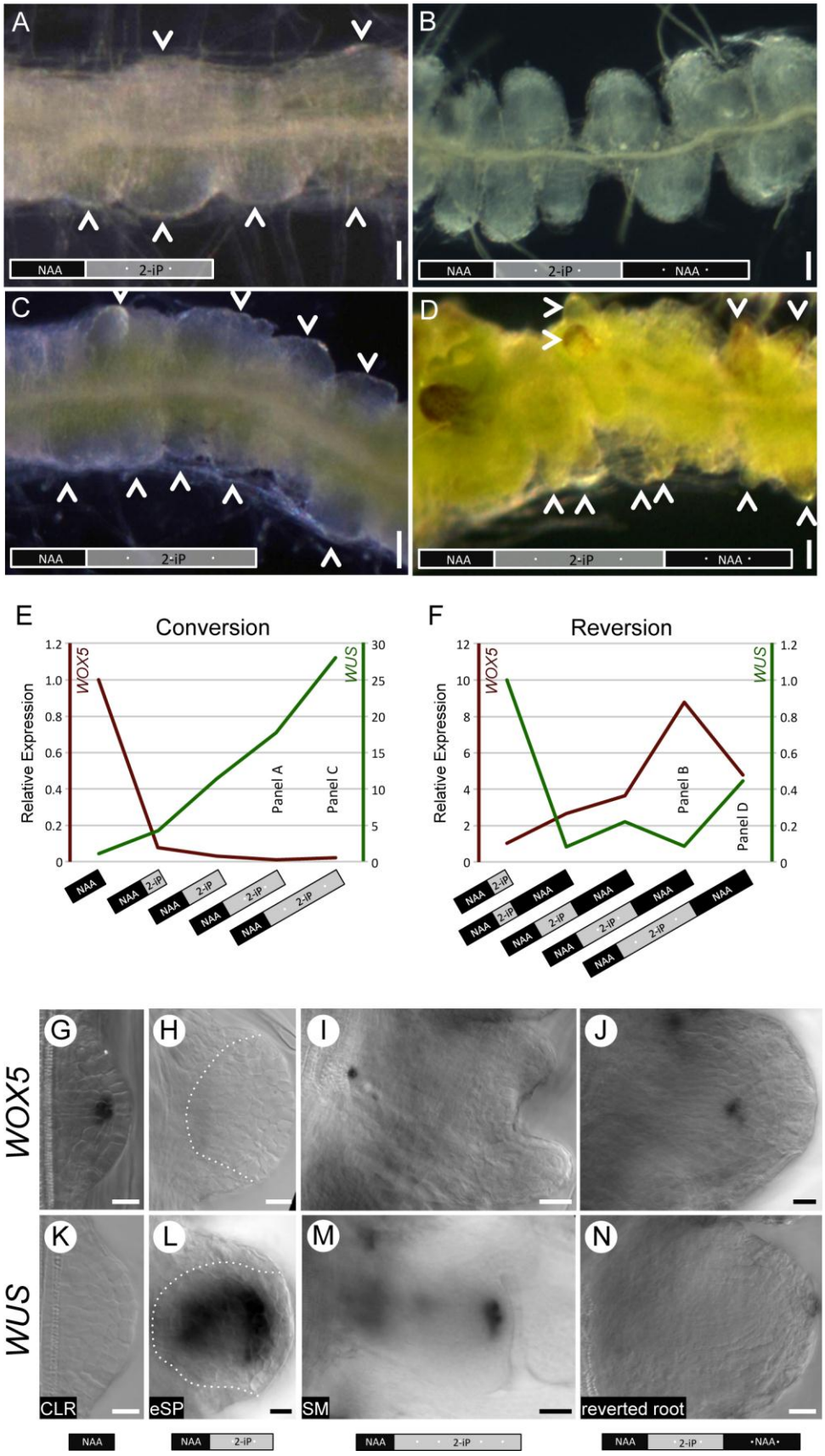

Figure 6: Shoot-to-root reversion.

A-D, Root segments after successive NAA and 2-iP treatments. Boxes are sized proportionally to the duration of hormone exposure: 42 h NAA priming (black), 1- to 6-d 2-iP (grey), and 3-d NAA (black); white dots outline 24 h periods. Arrowheads mark early shoot promeristems (A), late shoot promeristems (C), or leaf primordia (D). Scale bars: 0.1 mm. E and F, Relative expression of *WOX5* and *WUS*. Expression is measured by RT-qPCR, relative to transcript levels at the end of the initial NAA priming in E, and of a 1-d 2-iP treatment, after NAA priming, in F. *WOX5*, left axis, maroon; *WUS*, right axis, green. G-N, Whole mount *in situ* hybridization with the indicated probe. Lateral organs were analyzed after NAA priming (G, K), 2-iP treatment (H, L, I, M), or successive 2-iP and NAA treatments (J, N). Dotted line highlights the limit of the shoot promeristematic region. Conversion stages are as defined in Figure 3R. Lateral organs were visualized with Nomarski microscopy (DIC). Scale bars: 20 µm.

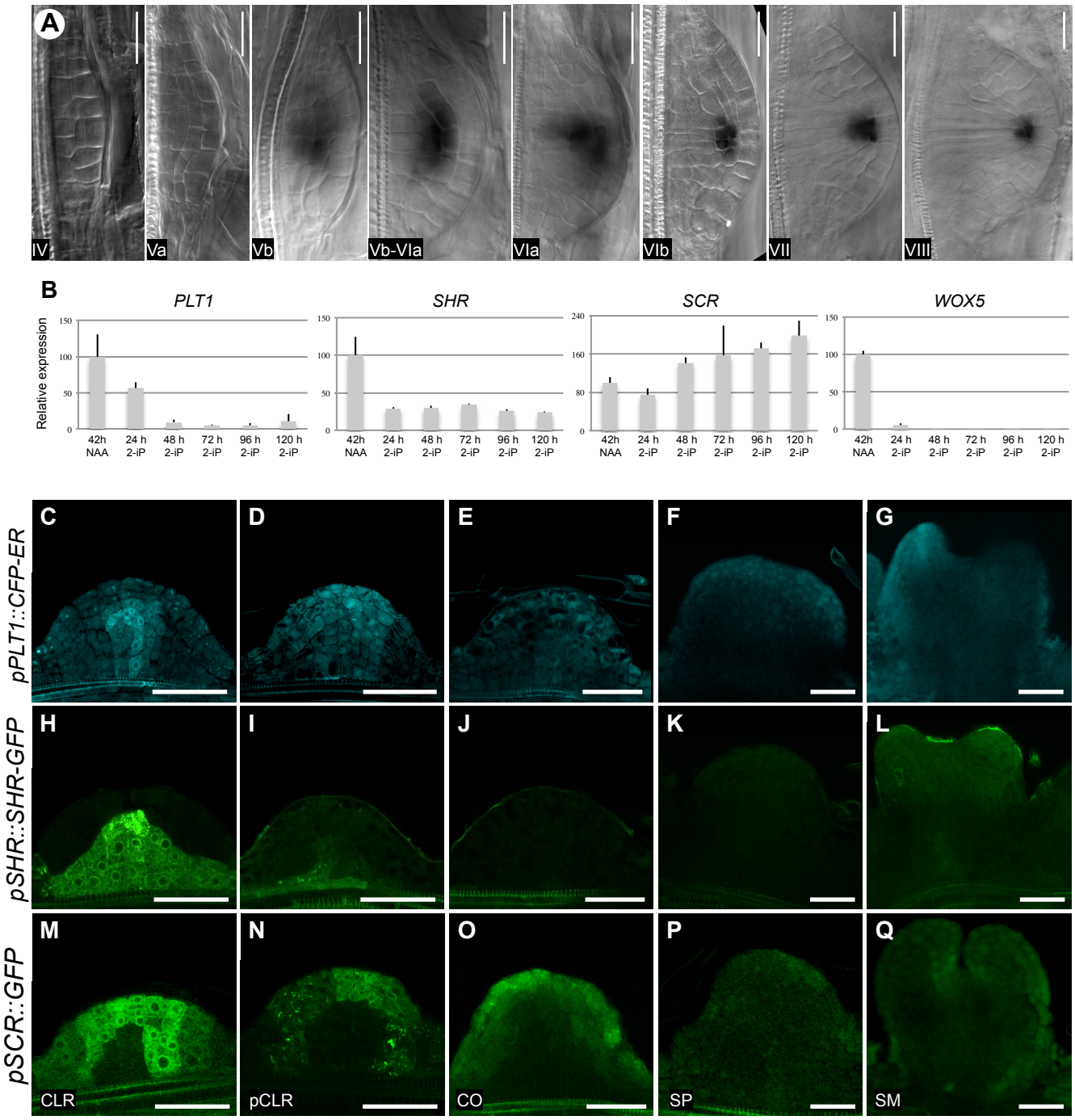

Figure S1: Expression of root identity genes during conversion.
A, Whole mount *in situ* localization of the *WOX5* transcript during lateral root development. Developmental stages indicated in the lower left corner of each picture are defined by Malamy and Benfey (1997). Lateral root were visualized with Nomarski microscopy (DIC). Scale bars: 20 µm. B, RT-qPCR analysis of *PLT1*, *SHR, SCR* and *WOX5* expression across the conversion in Col-0 explants. C, H and M: competent lateral root (CLR). *pPLT1::CFP-ER* marked CLR provascular domain, SHR protein was observed in the stele, and *SCR* was transcribed in the cell layers prefiguring the root cap, endodermis, pericycle, cortex and QC. D, I and N: paused competent lateral root primordium (pCLR). *PLT1* and *SCR* were transcribed at this stage, but *SHR* expression was rapidly turned off. E, J and O: converting organ (CO). Only transcription of *SCR* was observed. F, K and P: shoot promeristem (SP). Only transcription of *SCR* was observed. G, L and Q: shoot meristem (SM). The expression of *SCR* in the SAM can be detected. Conversion stages are as defined in Figure 2R. Reporter lines are indicated to the left of panels A to O. Scale bars: 50 µm.

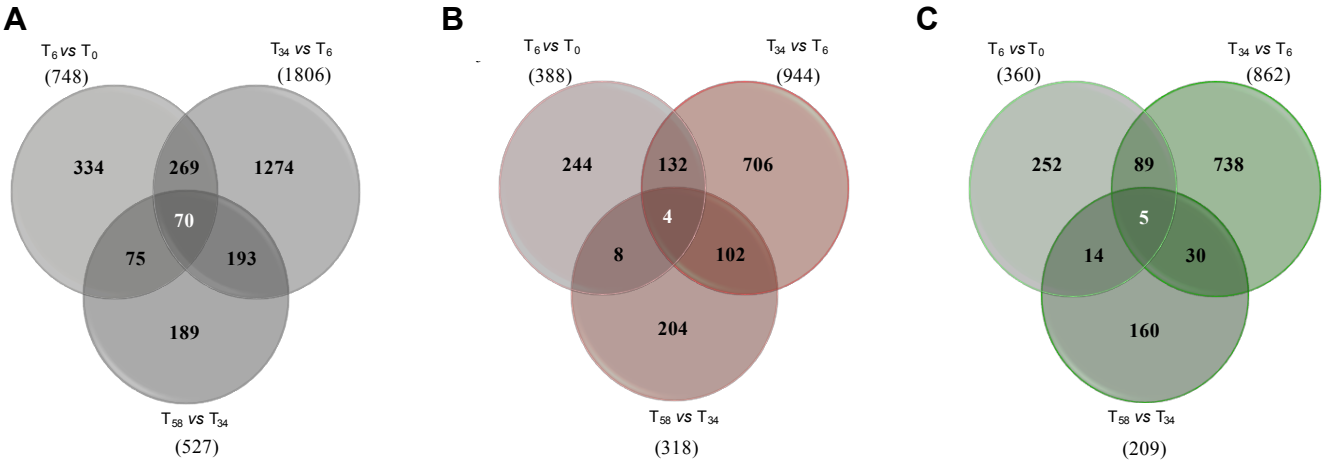

D

Comparisons	T6 vs T0		T34 vs T6		T58 vs T34	
DEG	All	Specific	All	Specific	All	Specific
Up-regulated	388	244	944	706	318	204
Down-regulated	360	252	862	738	209	160
Total	**748**	**334**	**1806**	**1274**	**527**	**189**

Figure S2: Distribution of differentially expressed genes.
A, Venn diagrams of the total; B, up-regulated and C, down-regulated genes DEGs identified in the T_6 *vs.* T_0, T_{34} *vs.* T_6, T_{58} *vs.* T_{34} comparisons. Numbers in parenthesis correspond to the total number of DEGs. Differentially expressed genes counted (Table S1) were selected by statistical analysis based on the Bonferroni method using a p-value cut-off of 0.05. D, Summary table.

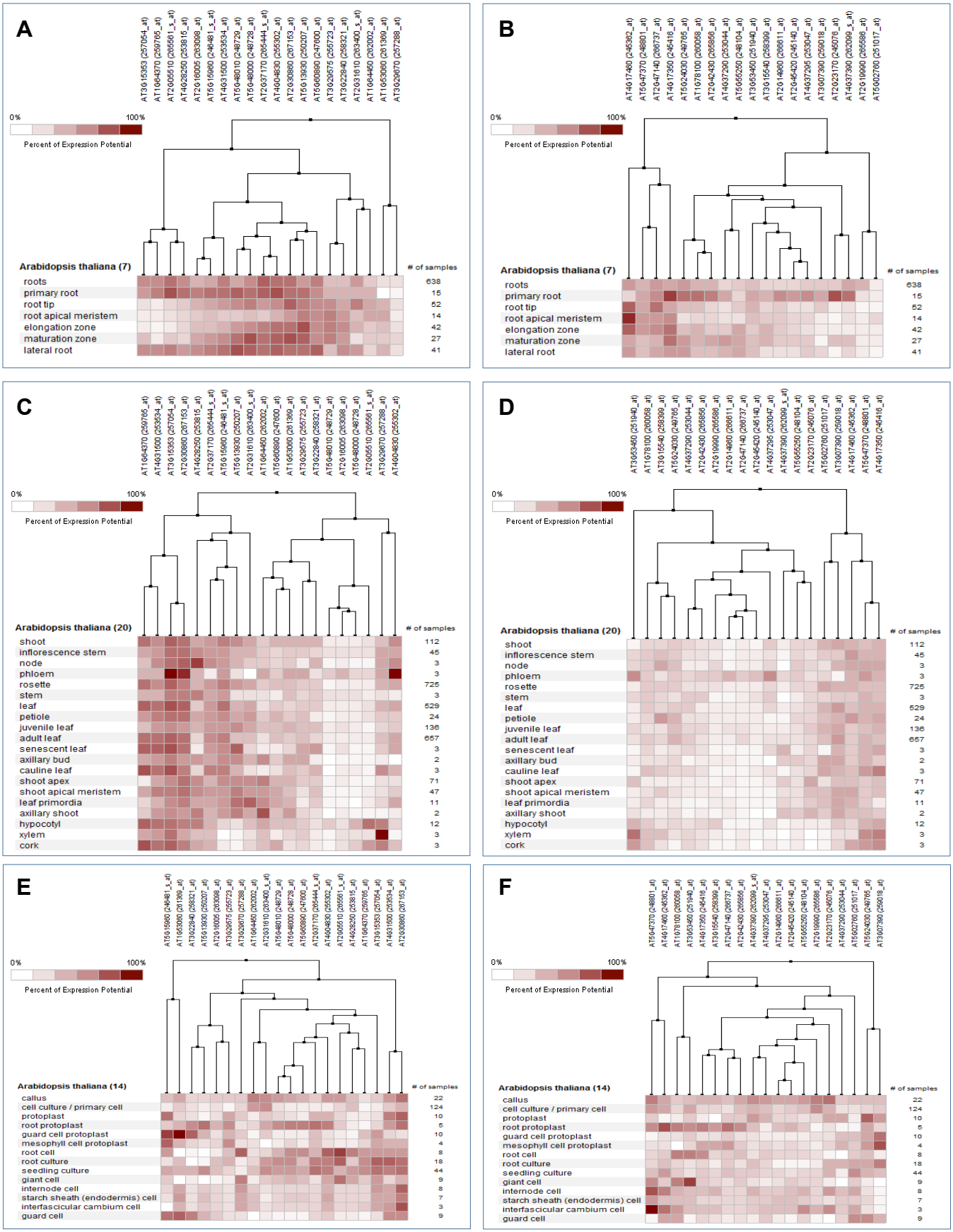

Figure S3: Comparison of our most DEGs with transcriptomic data sets.
Hierarchical clustering of the top 20 most up- (A, C, E, G, I, K, M, O, Q) or down-regulated (B, D, F, H, J, L, N, P, R) of T_6 *vs.* T_0 (A-F), T_{34} *vs.* T_6 (G-L) and T_{58} *vs.* T_{34} (M-R) comparisons with 7, 20 and 14 anatomical parts corresponding to root (A, B, G, H, M, N) shoot (C, D, I, J, O, P) and cell culture/primary cell (E, F, K, L, Q, R) transcriptomic data sets, respectively. A, Up-related DEGs from the T_6 *vs.* T_0 comparison correspond mostly to genes induced in 7 anatomical parts of the root and C, partially to genes induced in 20 anatomical parts of the shoot selection. I and J *vs.* O and P, The amount of genes induced in these later shoot selection increases in T_{34} *vs.* T_6 comparison gene set to become the main anatomical selection in which most of the genes up-regulated set from the T_{58} *vs.* T_{34} comparison are regulated.

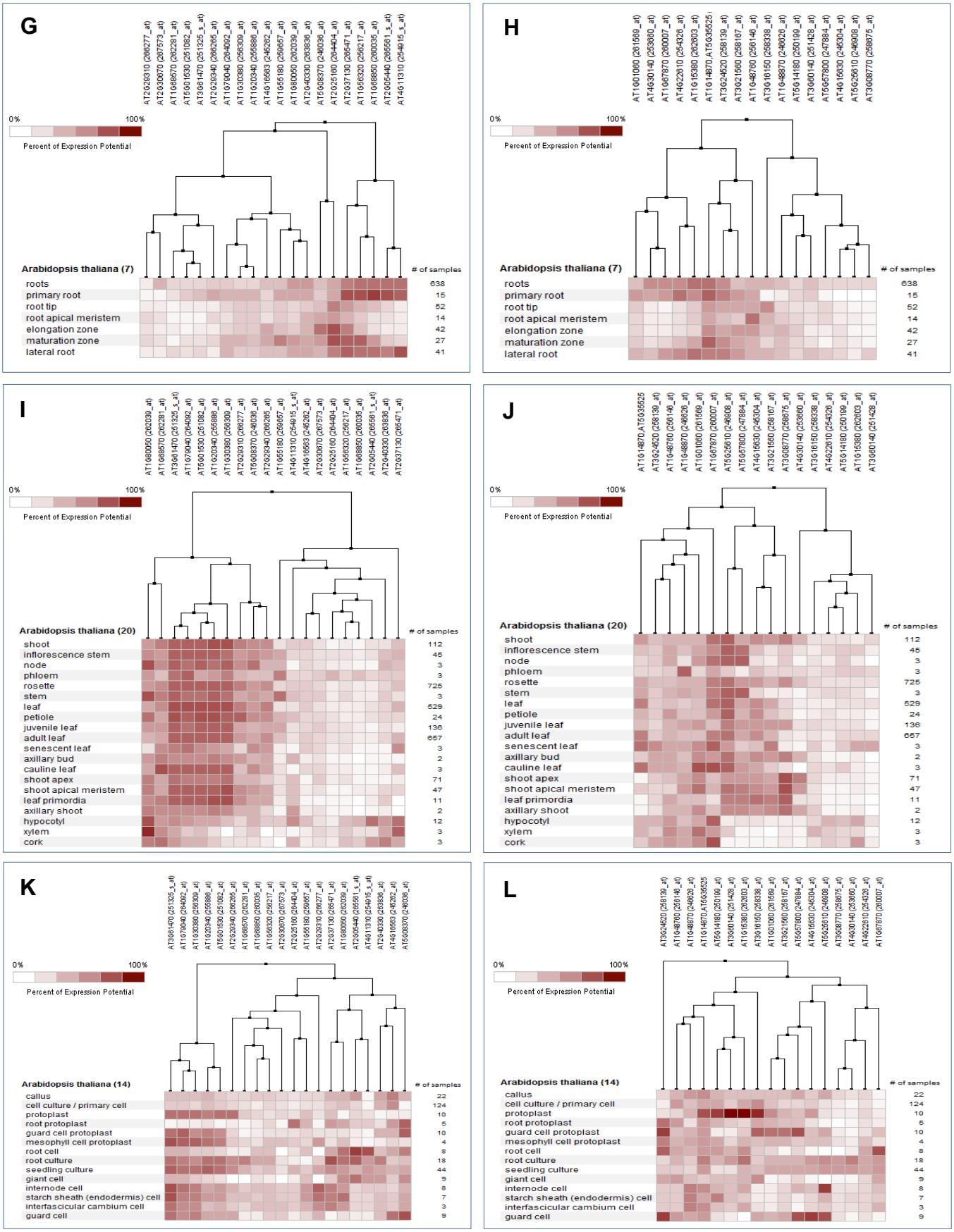

Figure S3: Comparison of our most DEGs with transcriptomic data sets.
Hierarchical clustering of the top 20 most up- (A, C, E, G, I, K, M, O, Q) or down-regulated (B, D, F, H, J, L, N, P, R) of T_6 *vs.* T_0 (A-F), T_{34} *vs.* T_6 (G-L) and T_{58} *vs.* T_{34} (M-R) comparisons with 7, 20 and 14 anatomical parts corresponding to root (A, B, G, H, M, N) shoot (C, D, I, J, O, P) and cell culture/primary cell (E, F, K, L, Q, R) transcriptomic data sets, respectively. A, Up-related DEGs from the T_6 *vs.* T_0 comparison correspond mostly to genes induced in 7 anatomical parts of the root and C, partially to genes induced in 20 anatomical parts of the shoot selection. I and J *vs.* O and P, The amount of genes induced in these later shoot selection increases in T_{34} *vs.* T_6 comparison gene set to become the main anatomical selection in which most of the genes up-regulated set from the T_{58} *vs.* T_{34} comparison are regulated.

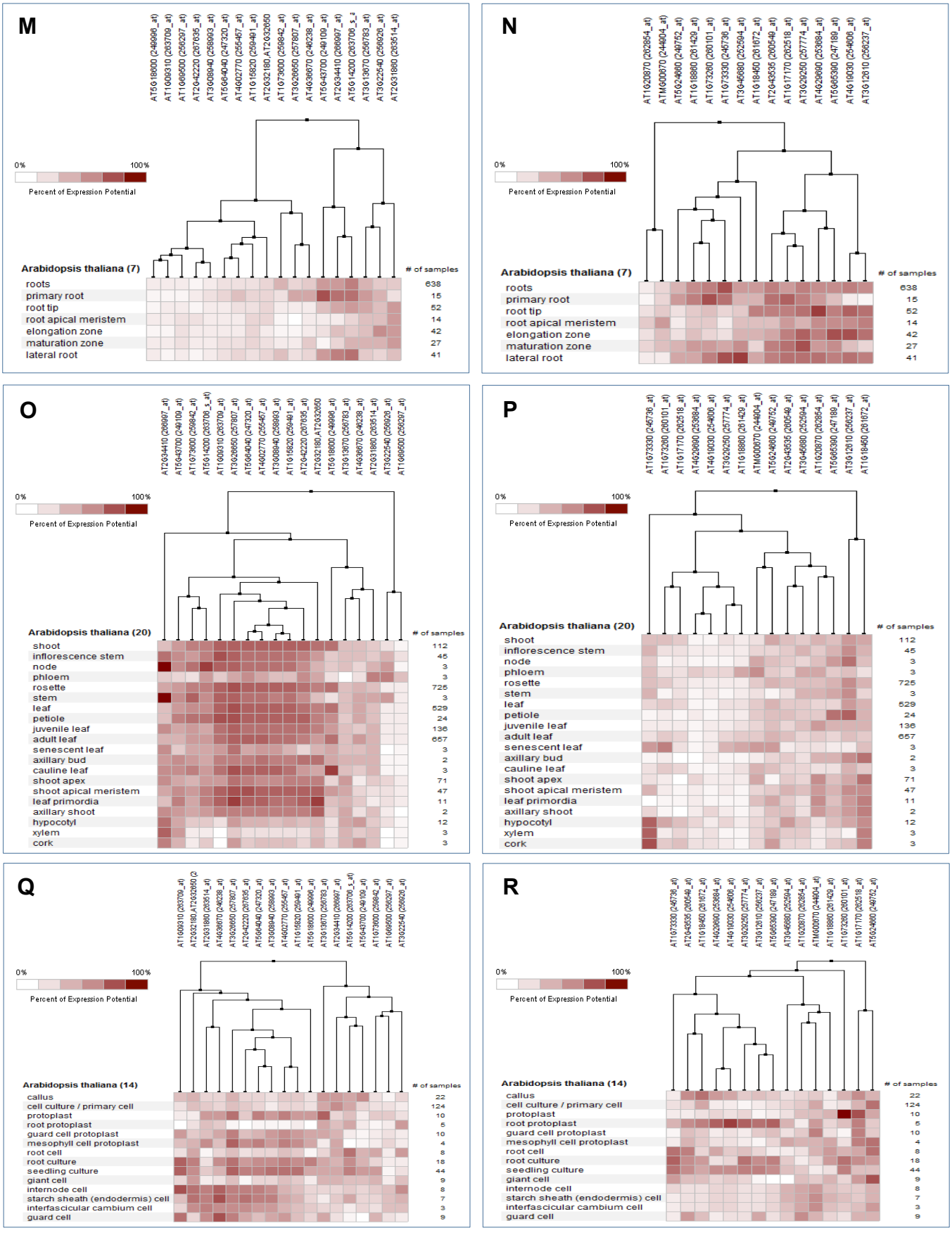

Figure S3: Comparison of our most DEGs with transcriptomic data sets.
Hierarchical clustering of the top 20 most up- (A, C, E, G, I, K, M, O, Q) or down-regulated (B, D, F, H, J, L, N, P, R) of T_6 *vs.* T_0 (A-F), T_{34} *vs.* T_6 (G-L) and T_{58} *vs.* T_{34} (M-R) comparisons with 7, 20 and 14 anatomical parts corresponding to root (A, B, G, H, M, N) shoot (C, D, I, J, O, P) and cell culture/primary cell (E, F, K, L, Q, R) transcriptomic data sets, respectively. A, Up-related DEGs from the T_6 *vs.* T_0 comparison correspond mostly to genes induced in 7 anatomical parts of the root and C, partially to genes induced in 20 anatomical parts of the shoot selection. I and J *vs.* O and P, The amount of genes induced in these later shoot selection increases in T_{34} *vs.* T_6 comparison gene set to become the main anatomical selection in which most of the genes up-regulated set from the T_{58} *vs.* T_{34} comparison are regulated.

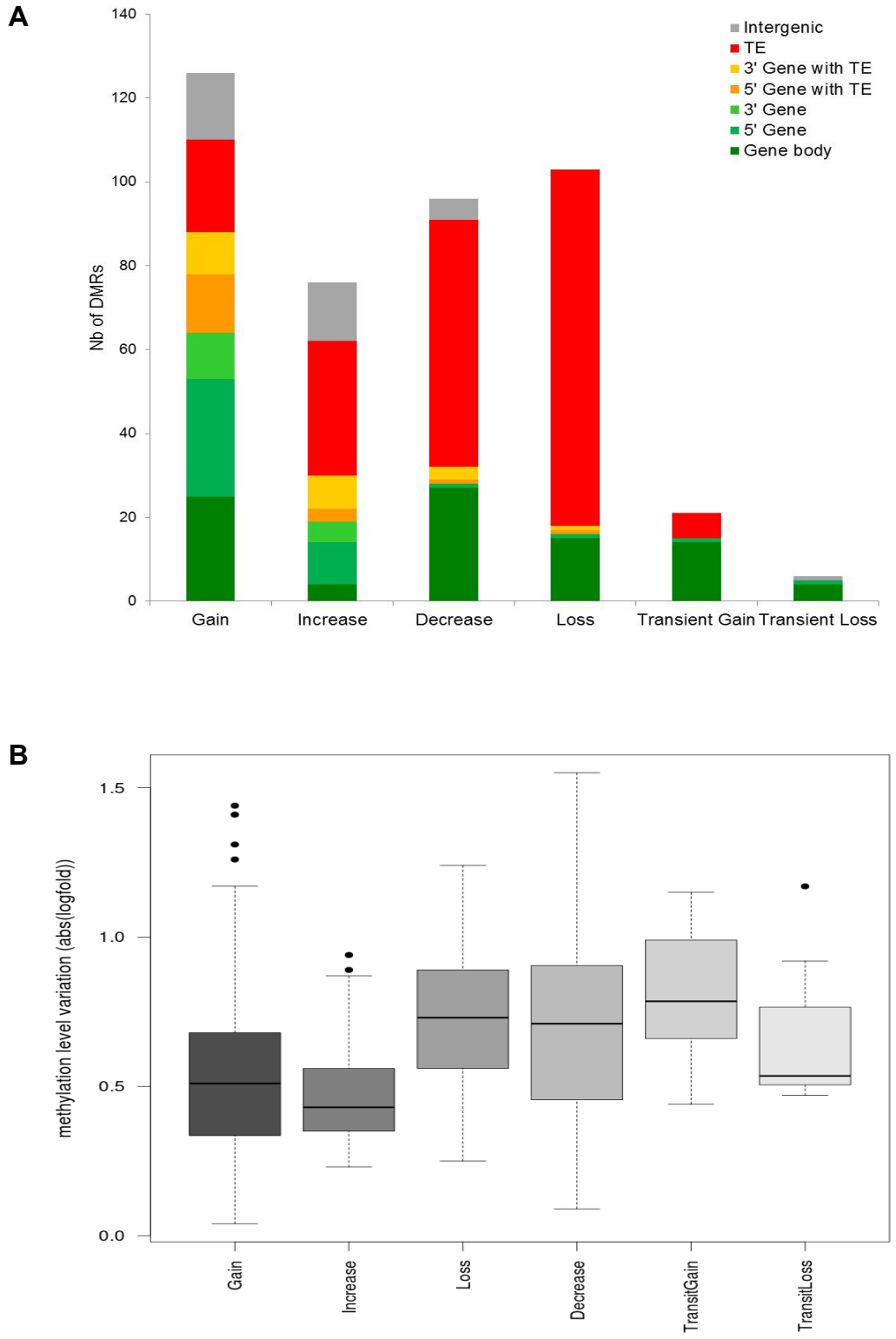

Figure S4: A limited number of low amplitude DMRs are detected across the conversion sequence.

A, Distribution of DMRs according to patterns of DNA methylation variation. Gain, continuous methylation increase, from unmethylated state at T_0 to higher methylation level at T_{58}. Loss, continuous methylation decrease, down to unmethylated at T_{58}. Increase and Decrease, positive and negative changes between intermediate methylation levels during conversion, respectively. Transient Gain and Transient Loss, higher and lower level of methylation in T_6 and T_{34} in comparison to T_0 and T_{58}, respectively. B, Average fold-change in DNA methylation levels according to patterns of DNA methylation variation.

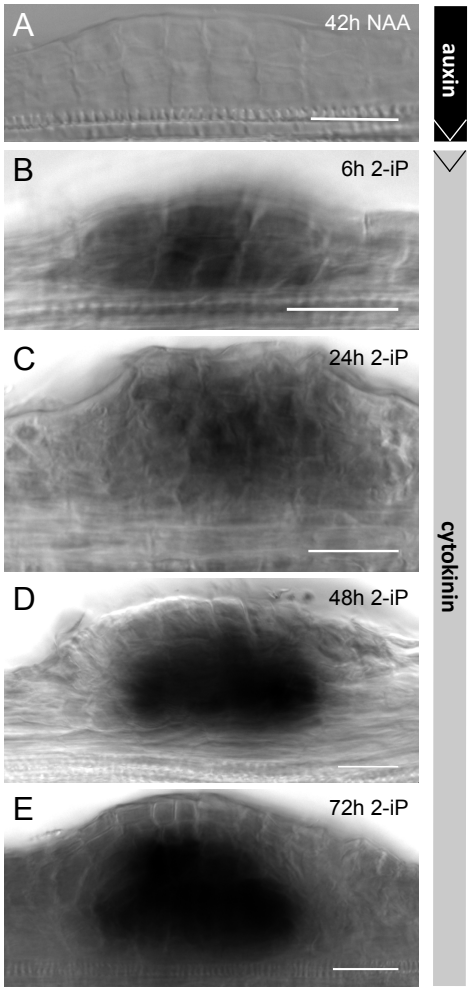

Figure S5: Expression of *WUS* in lateral root primordia induced with exogenous cytokinin at stage V.
Whole mount root segments were hybridized *in situ* with the *WUS* antisense probe after auxin (NAA) priming (A), and subsequent cytokinin (2iP) induction (B-E). Lateral organs were visualized with Nomarski microscopy (DIC). Scale bars: 20 µm.

Table S1: Differentially expressed genes (DEGs) between consecutive time points in the conversion sequence (cf : Table S1.xls)

Click here to Download Table S1

Table S2: Comparisons with published microarray data. Synthesis of the number of genes in commun between our study and query lists of genes involved in metabolism and dowstream signaling of auxin and cytokinin (Nemhauser et al., 2006; Brenner and Schmülling, 2015), in cell cycle (Vandepoele et al., 2002; Chatfield et al., 2013), in regeneration of shoots, calli or roots in tissue culture from Arabidopsis (Che et al., 2006) and in regeneration of shoots obtained in tissue culture from Arabidopsis mutant affected in DNA methylation (Li et al., 2011 ; see Supplemental Experimental Procedures for details). Percents in black correspond to set of genes found in commun studies or query lists significantly enriched at the significant threshold of hypergeometric and Bonferonni test p-value<0.05. preCIM : preculture on Callus-Inducing Medium, SIM : Shoot-Inducing Medium, CIM : Callus-Inducing Medium, RIM : Root-Inducing Medium. *: DEG that have been subtracted from EUGENE predictions and genes encoding microRNAs or predicted to encode HypmiRNAs.

DEGs in this study*			*T6 (vs T0)*			*T34 (vs T6)*			*T58 (vs T34)*		
			up	down	Total	up	down	Total	up	down	Total
			378	359	738	935	849	1784	305	200	505
Brenner and Schmülling (2015)	Cytokinin	up	6%	0%	3%	2%	0%	1%	1%	7%	3%
		down	0%	1%	0%	0%	0%	0%	0%	0%	0%
Nemhauser et al. (2006)			9%	4%	7%	6%	5%	5%	4%	11%	7%
Nemhauser et al. (2006)	Auxin		12%	21%	17%	8%	6%	7%	9%	13%	10%
Vandepoele et al. (2002) Chatfield et al. (2013)	Cell cycle		1%	3%	2%	0%	1%	1%	1%	0%	0%
Che et al. (2006)	preCIM	up	23%	43%	33%	12%	32%	21%	5%	8%	6%
		down	29%	17%	23%	24%	6%	15%	4%	10%	6%
	SIM		10%	1%	5%	1%	0%	0%	10%	6%	8%
	CIM		1%	2%	1%	1%	1%	1%	1%	1%	1%
	RIM		5%	3%	4%	7%	2%	4%	4%	3%	4%
Li et al. (2011)	M0/S0		7%	7%	7%	11%	3%	7%	21%	3%	14%
	M0 in S6/S0		3%	1%	2%	8%	1%	5%	17%	2%	11%

Table S3: Biological pathways significantly over-represented among deregulated genes. Significant pathways are in bold. ns: not significant.

	MAPMAN Classification	Frequency	T_6 *vs.* T_0 ± *bootstrap StdDev*	p-value	Frequency	T_{34} *vs.* T_6 ± *bootstrap StdDev*	p-value	Frequency	T_{58} *vs.* T_{34} ± *bootstrap StdDev*	p-value
Up –regulated genes	amino acid metabolism	**3.02**	***0.949***	**2.328e-03**	**3.17**	***0.629***	**9.105e-07**	ns	ns	ns
	cell	ns	ns	ns	**0.56**	***0.156***	**7.173e-03**	ns	ns	ns
	cell wall	ns	ns	ns	**2.42**	***0.367***	**5.380e-07**	ns	ns	ns
	development	**1.88**	***0.458***	**5.288e-03**	**1.5**	***0.249***	**5.530e-03**	ns	ns	ns
	DNA	**0.19**	***0.065***	**1.293e-09**	**0.11**	***0.035***	**1.489e-27**	**0.2**	***0.085***	**7.267e-08**
	gluconeogenesis / glyoxylate cycle	ns	ns	ns	**8.29**	***4.266***	**4.636e-03**	ns	ns	ns
	glycolysis	**3.23**	***0.744***	**3.813e-06**	ns	ns	ns	ns	ns	ns
	hormone metabolism	ns	ns	ns	**2.32**	***0.457***	**2.658e-06**	ns	ns	ns
	metal handling	ns	ns	ns	**3.46**	***1.304***	**1.684e-03**	ns	ns	ns
	micro RNA, natural antisense etc	ns	ns	ns	**0.07**	***0.057***	**2.809e-05**	ns	ns	ns
	minor CHO metabolism	ns	ns	ns	**3.76**	***1.05***	**3.434e-05**	ns	ns	ns
	miscaellous	**2.42**	***0.327***	**4.149e-08**	**2.39**	***0.191***	**4.854e-17**	**1.75**	***0.339***	**2.022e-03**
	N-metabolism	**10.09**	***5.15***	**2.962e-03**	**6.91**	***2.858***	**6.022e-04**	ns	ns	ns
	not assigned	**0.67**	***0.057***	**3.438e-07**	**0.65**	***0.035***	**2.227e-16**	**0.72**	***0.077***	**6.575e-05**
	nucleotide metabolism	**3.4**	***1.127***	**3.675e-03**	ns	ns	ns	ns	ns	ns
	protein	**0.37**	***0.081***	**1.191e-08**	**0.54**	***0.056***	**2.637e-10**	ns	ns	ns
	photosynthesis	ns	ns	ns	**5.58**	***0.986***	**2.818e-15**	**17.71**	***2.792***	**2.987e-32**
	redox	ns	ns	ns	**2.39**	***0.641***	**1.533e-03**	ns	ns	ns
	S-assimilation	**26.92**	***13.842***	**1.084e-05**	ns	ns	ns	ns	ns	ns
	secondary metabolism	**4.92**	***0.855***	**6.805e-11**	**3.39**	***0.538***	**5.097e-12**	**2.41**	***0.794***	**6.026e-03**
	signalling	**0.44**	***0.188***	**6.760e-03**	ns	ns	ns	ns	ns	ns
	stress	**1.78**	***0.33***	**2.085e-03**	**1.43**	***0.203***	**2.819e-03**	ns	ns	ns
	tetrapyrrole synthesis	ns	ns	ns	**5.24**	***2.003***	**2.948e-04**	17.89	*5.554*	**1.358e-08**
	transport	**2.48**	***0.438***	**5.095e-06**	**1.93**	***0.253***	**1.556e-06**	ns	ns	ns
Down-regulated genes	DNA	**0,5**	***0,13***	**4,26E-04**	**0,22**	***0,047***	**3,22E-18**	**0,1**	***0,055***	**3,05E-07**
	fermentation	ns	ns	ns	ns	ns	ns	**22,96**	***14,315***	**3,25E-03**
	hormone metabolism	**3,78**	***0,83***	**9,80E-08**	ns	ns	ns	**4,75**	***1,211***	**2,72E-07**
	lipid metabolism	**2,38**	***0,677***	**4,60E-03**	ns	ns	ns	ns	ns	ns
	miscaellous	**2,22**	***0,322***	**2,38E-06**	ns	ns	ns	**2,93**	***0,539***	**1,53E-07**
	not assigned	**0,68**	***0,067***	**1,60E-06**	**0,63**	***0,036***	**9,16E-17**	**0,59**	***0,081***	**3,32E-06**
	nucleotide metabolism	ns	ns	ns	**3,48**	***0,913***	**1,26E-05**	ns	ns	ns
	protein	**0,51**	***0,093***	**1,88E-05**	**2**	***0,106***	**4,97E-29**	ns	ns	ns
	RNA	**1,37**	***0,2***	**6,29E-03**	**1,48**	***0,127***	**5,22E-06**	ns	ns	ns

Table S4: Most differentially expressed genes during conversion (cf : Table S4.xls)

Click here to Download Table S4

Table S5: Loci with coinciding DNA methylation and transcript level changes. Variation in methylation and expression levels are represented for the few DMRs corresponding to a gene showing a change in expression during the conversion process. Relative levels of methylation at the different time points are represented by a heatmap, from low (green) to high (red) and variations in expression of the corresponding gene are represented by arrows.

Methylation						Expression				
Domain name	methylation change	T_0	T_6	T_{34}	T_{58}	$T_0 \rightarrow T_6$	$T_6 \rightarrow T_{34}$	$T_{34} \rightarrow T_{58}$	Annotation	
Chr3:19229787..19230313	gain	0,40	0,47	0,78	1,53	↗	↗	→	AT3G51820	ATG4/CHLG/G4 (CHLOROPHYLL SYNTHASE)
Chr2:7926498..7927189	gain	0,16	0,56	0,48	1,24	↘	↗	→	AT2G18193	AAA-type ATPase family protein
Chr1:28900772..28901152	gain	-0,38	-0,28	0,20	0,46	↘	↗	↗	AT1G76930	ATEXT4 (EXTENSIN 4)
Chr3:17030490..17031209	gain	0,01	0,25	0,06	0,83	↘	→	→	AT3G46320	histone H4
Chr3:20638713..20639257	gain	-0,13	-0,27	0,14	0,53	→	→	↘	AT3G55610	P5CS2 (DELTA 1-PYRROLINE-5-CARBOXYLATE SYNTHASE 2)
Chr2:11552315..11552703	gain	-0,11	-0,22	0,32	0,44	↘	→	→	AT2G27050	EIL1 (ETHYLENE-INSENSITIVE3-LIKE 1)
Chr2:14393613..14393996	increase	1,09	1,58	1,78	1,93	↗	→	→	AT2G34060	peroxidase, putative
Chr4:17684540..17685089	decrease	1,85	1,63	1,76	1,22	↘	→	→	AT4G37640	ACA2 (CALCIUM ATPASE 2)
Chr1:12566595..12567299	loss	0,40	0,21	0,28	-0,21	↗	→	→	AT1G34400	unknown protein
Chr3:17483630..17484009	loss	0,79	0,40	0,80	0,24	↘	→	→	AT3G47420	glycerol-3-phosphate transporter, putative

Supplemental Experimental Procedures

Arabidopsis growth medium composition

Arabidopsis solid growth medium consisted of MS salts with vitamins (Duchefa, M0222), supplemented with 0.5 $g.L^{-1}$ 2-(N-morpholino) ethane sulfonic acid (pH5.7; Sigma, M8250), 1 % (w/v) sucrose (Sigma, S9378). The gelling agent was 0.6 % (w/v) Agarose (Euromedex, D5) for Col-0 and 0.7% (w/v) Plant Agar (Duchefa, P1001) for L*er*. In explants sampled for RT-qPCR, transcriptomic and methylome studies, LR initiation was further synchronized by germinating and growing plantlets in the presence of the auxin transport inhibitor 1-N-naphthylphthalamic acid (NPA) prior to NAA priming. NPA first prevents the formation of auxin maxima and thus inhibits LR initiation. NAA then massively induces LR initiation along the primary root (Himanen et al., 2002). For these experiments, Col-0 plantlets were germinated and grown in the presence of 1.25 µM 1-N-Naphthylphthalamic acid (NPA) (Duchefa, N0926) for 6 d prior to NAA treatment. To induce lateral root formation, plantlets were transferred and grown for 42 hours on an auxin medium, similar to the previous one, but without NPA, and with 3.3 µM and 10 µM 1-naphthaleneacetic acid (NAA) (Duchefa, N0903) for Col-0 and L*er*, respectively. To induce shoot meristem formation, primary root segments were excised and transferred on a cytokinin medium, similar to the previous one but where auxin was replaced with 8.16 µM and 24.6 µM N6-[2-isopentenyl]adenine (2-iP) (Duchefa, D0906) for Col-0 and L*er*, respectively, and sucrose was replaced with 2% D-(+)-Glucose (Sigma, G8270) for all genotypes. The Col-0 x L*er* hybrid line was always treated as L*er*. In explants prepared for morphological and marker line analysis, LR initiation was induced with NAA priming for 42 h, but without NPA treatment during germination and growth on the first medium. Contrarily to the NPA treatment, this unsynchronized protocol avoids LRP fusion and was chosen as more convenient to follow the development of individual LRPs.

Phytohormones were dissolved in dimethylsulfoxide (DMSO; Sigma, D8418). Sugars and hormones were added to the media after autoclaving.

Arabidopsis reporter lines	Background	Reference
pWUS::GUS	Col-0xL*er*	(Gross-Hardt et al., 2002)
pPLT1::CFP	Col-0	(Aida et al., 2004)
pSHR::SHR-GFP	Col-0	(Helariutta et al., 2000)
pSCR::mGFP5-ER	Col-0	(Wysocka-Diller et al., 2000)
pCLV3::CFP-ER	L*er*	(Tucker et al., 2008)
pKNOLLE::KNOLLE-GFP	L*er*	(Boutté et al., 2010)
pPIN1:PIN1-GFP	L*er*	(Vernoux et al., 2000)
pCYCB1;1::DB-GUS	Col-0	(Colón-Carmona et al., 1999)
pTCSn ::GFP	Col-0	Gift from B. Müller
pPIN1::PIN1 :GFP/pSTM::STM :YFP	L*er*	NASC N66314
pDR5::rev:3XVENUS-N7/pCUC2::RFP	Col-0	Gift from P. Laufs
p35S::DII-VENUS	Col-0	(Brunoud et al., 2012)

Quantification of the conversion and reversion *in vitro* responses

Conversion. The distribution of converted organs was assessed relative to the LRP stages of development (Malamy and Benfey, 1997) at the onset of cytokinin treatment. A total of 210 Col-0 roots segments were analyzed carrying 4453 LRPs classified in three classes when transferred on 2-iP medium: stages V and younger ($n_{LRP\leq V}$ = 432, 7 converted in SMs, 0.7% of converted LRPs); stages VI and VII ($n_{LRP\ VIorVII}$ = 1716, 967 SMs; 90.2%); stages VIII and emerged ($n_{LRP\geq VIII}$ = 2305, 98 SMs; 9.1%). Conversion was assessed for each individual LR after 6 days of 2-iP treatment, by comparing images acquired at the beginning and at the end of the treatment.

Rates measured in a separate experiment showed that Landsberg *erecta* (L*er*) LRPs have a similar ability to convert according to their developmental stages: $n_{LRP\leq V}$ = 55, 6 SMs, 3.0%; $n_{LRP\ VIorVII}$ = 485, 175 SMs, 89.3%; $n_{LRP\geq VIII}$ = 162, 15 SMs, 7.7%. The conversion from an LR into an established SM is slower in L*er* than in Col-0, five days instead of four in our hands, which may be explained by the different gelling agent and hormone concentrations that were optimized empirically for both ecotypes.

For clarity, the lateral organs were preferentially labeled according to their developmental time, determined based to their structure, rather that their incubation time on 2-iP medium that varied slightly between ecotypes and transgenic markers lines.

Reversion. The distribution of reverted LRPs was assessed in excised root segments primed with NAA for 42h. A total of 73 Col-0 root segments carrying 8546 lateral roots at different stages were transferred on 2-iP medium for 3 d, then split in two batches: 3986 LRs (33 root segments) remained on the 2-iP medium for 3 more days, of which 1286 switched into shoot meristem development (conversion); 4560 LRs (40 root segments) were transferred back on NAA medium for 3 d, of which only 139 shoot promeristems did not switch back into LRPs (reversion).

Propidium iodide staining, confocal microscopy and image analysis

The protocol was adapted from (Truernit et al., 2008). Explants were fixed and stained with propidium iodide. The developing lateral organs were imaged as stacks of confocal optical sections and their organization was analyzed in the sagittal plane reconstructed for each object. Briefly, the explants were fixed in a 75% ethanol / 25% acetic anhydride solution for 2 d. Samples were rehydrated by successive immersion in 50%, 30% and 10% ethanol, and washed 3 times in distilled water. Amyloplasts were dissolved with amylase (0.2 mg/ml) for 3 h at 37 °C. Fixed explants were washed 3 times in distilled water, incubated in 1% periodic acid for 20 min, rinsed again with water, and stained overnight in Schiff reagent with propidium iodide (PI) (100 mM sodium metabisulphite, 0.15 N HCl, freshly added PI at a final concentration of 0.1 mg/µl). Samples on microscope slides were covered with a chloral hydrate solution (4 g chloral hydrate, 1 mL glycerol, 2 mL water) after 3 washes in water. Explants were imaged with a Leica SP5 spectral confocal laser scanning microscope (Leica Microsystems). Excitation wavelength for PI–stained samples was 488 nm, emission signal was collected from 520 to 720 nm. Acquired Z stacked images (lif format) were converted (tif format) with ImageJ (V1.46, 64 bits). See Table below for voxel size. Stacks were reoriented according to the main axis of the primary root to define the transverse and sagittal planes passing through the center of the LRP by 3D multi-planar reconstruction with the OsiriX software (V.5.6, 32 bits). LRP developmental stages were identified based on the number of epidermal cells and the organization of the cells in the stele, as observed in the reconstructed sagittal plane.

Voxel sizes in images of propidium iodide-stained explants

	Panel	Width	Height	Depth
Figure 2	E	0.2225987	0.2225987	0.4196171
	F	0.2225986	0.2225986	0.4196171
	G	0.1082093	0.1082093	0.293732
	H	0.158513	0.158513	0.2098085
	I	0.2225987	0.2225987	0.4196171
	J	0.2225987	0.2225987	0.7133491
	K	0.3029291	0.3029291	1.0070810
	L	0.2225987	0.2225987	0.7133491
	M	0.2225986	0.2225986	
Figure 3	A	0.1224285	0.1224285	0.293732
	B	0.1650829	0.1650829	0.7133491
	C	0.2225986	0.2225986	0.7133491
	D	0.2225986	0.2225986	0.7133491
	E	0.2225986	0.2225986	0.4196171
	F	0.4451973	0.4451973	0.7133491

GUS staining and quantification

Tissues were fixed in ice-cold 90% acetone for 10 min on ice, rinsed with water for 5 min, vacuum infiltrated for 5 min with staining solution (50 mM sodium phosphate buffer pH 7, 0.2% Triton-X-100, 2 mM potassium ferrocyanide, 2 mM potassium ferricyanide, 1 mM X-gluc) and incubated at 37°C for 7 to 18 h. The reaction was stopped with 70% ethanol and conserved at 4°C until observation. The samples were mounted in 10% glycerol and photographs were taken with a Zeiss Axio zoom stereo-microscope.

To quantify the cell division average in the converting organs, the number of blue GUS-stained spots were counted in *pCYCB1;1::DB-GUS* explants to measure the number of dividing cells in a converting organ and averaged per developmental stage: CLR at stage VI or VII (NAA 42 h, n=160); pCLR (2-iP 24 and 48 h, n=57 of which 24 showed no GUS spot); CO (2-iP 72 h, n=35); SP (2-iP 96 h,

n=40); SM (2-iP 120 h, n=14).

Quantitative real-time RT-PCR analysis

Total RNA was isolated with the RNeasy Plant mini-kit (Qiagen). For RT-qPCR, 5 µg of RNAs were DNase-treated using DNaseI according to the manufacturer's instructions (Qiagen) and cDNAs were synthesized using oligo(dT) with Superscript II reverse transcriptase (Invitrogen) according to the manufacturer's instructions. Quantitative real-time RT-qPCR was performed in an Eppendorf Mastercycler realplex (Eppendorf) with MESA GREEN qPCR MasterMix Plus for SYBRAssay (Eurogentec) as per manufacturer's instructions. Data analysis, including calculation of primer pair reaction efficiencies and Ct values, was carried out by Eppendorf Manager software. The results of two technical replicates of two biological samples were normalized with 1 to 4 genes with a steady level of transcription. The first point of the kinetic is used as the 100% reference for the normalization of the relative expression. All RT-qPCR data points were obtained with 60-80 pooled explants. Each explants harbored dozens of converting/reverting primordia at synchronized developmental stages. List of primers pairs used in RT-qPCR experiments:

Gene name	5' primer	3' primer
WUS	gtgttcccatgcagagacct	tcagtacctgagcttgcatga
STM	ccaagatcatggctcatcct	cctgttggtcccatagatgc
WOX5	ggagaggcagaaacgtcgta	tgaattcaccggaaagagttg
PLT1	gccggaaacaaagacctctac	aatggctttcacgtcgtacc
SHR	gagacagcgaggaagtggtc	ccatcgaccaaacaccttct
SCR	tgaggaaaagggaagctgtg	agcgtggctcaaatcttgtt
CLV3	gtccggtccagttcaacaac	gcttctccatttgctccaac
CUC2	aaggaagagctccgaaagga	tccggtgctagctaaagtgg
Ubq5	cttgaagacggccgtaccctc	cgctgaacctttcaagatccatcg
AT5G13440	acaagccaatttttgctgagc	acaacagtccgagtgtcatggt
AT2G26060	gggatggtcaagatttggca	caaaccaacagcagtcacggt
AT429130	ggcgttttctgatagcgaaaa	atggatcaggcattggagct
HIS4	cgaagattggctcgtagagg	gctcggtgtaagtgacagca
CYCB2;4	ggatacgaggattggagcaa	ttgtgatgcaaaccaaccat
KRP2	ggtgacgatcgtgaaacaga	aagatctttctccgccacct
RGF1	gtgaaggtcttggagcaagc	tctcatttgcctccaccttc
LBD16	ccatgatcgatgtgaagctg	ggttggtactttccgagctg
LBD18	aggtccgatgctgtcgtaac	gatgccaaatgggcttgtaa
ARF16	tcaaatacgcaggaaacgaa	cgctctcacttccttgttcc
TMO5	gggttcgatggtgagatcat	acttccgctagcaaagaagc
TMO7	atgtcgggaagaagatcacg	cttgtaacaccctcgctgct
PID	tgaaaatgcttgaccatcca	actagaacttcggcggcata
IAA17	ggtatcaatggacggagcac	cccagctattcaccaaatcc
IAA19	tggatggtgtgccttatttg	cgagcatccagtctccatct
IAA28	taaagttctggtcggggatg	aaggcgtgggaggtcttta

Transcript profiling

Microarray analyses were carried out with the CATMA array containing 24,576 gene-specific tags corresponding to 22,089 genes and 633 mitochondrial and chloroplastic genome segments from *Arabidopsis thaliana* (Crowe et al., 2003; Hilson et al., 2004). To maximize specificity, the lateral organs were laser micro-dissected and pooled for transcript profile analysis at four time points: T_0, 42 h NAA-priming, competent lateral root (CLR); T_6, 6 h 2-iP treatment, paused CLR; T_{34}, 34 h 2-iP, converting organ (CO) resuming active cell division; T_{58}, 58 h 2-iP, early shoot primordium (eSP) (Fig. 5G). Total RNA was extracted from samples corresponding to the four time points in two independent biological experiments, with the Qiagen RNAeasy plant minikit according the manufacturer's instructions. For T_6 vs. T_0, T_{34} vs. T_6 and T_{58} vs. T_{34} comparisons, two technical replicates in dye-swap were performed for each of the two biological repeats. The labeling of cRNA with Cy3-dUTP or Cy5-dUTP (Perkin-Elmer- NEN Life Science Products), the hybridization to the slides, and the scanning were performed as described in Lurin et al. (2004). Specific statistics were developed to analyze CATMA hybridizations. For each array, the raw data comprises the logarithm of median feature pixel intensity (in log base 2) at wavelengths 635 nm (red) and 532 nm (green). No background was subtracted. The normalization method used is described in Lurin et al. *(*2004). To determine differentially expressed genes, we performed a pair t-test on the log ratios averaged on the dye-swap.

A trimmed variance is calculated from spots which do not display extreme variance. The raw p-value are adjusted by the Bonferroni method, which controls the Family Wise Error Rate (FWER) (with a type I error equal to 5%). We also adjusted the raw p-values to control a FDR using Benjamini-Yetkutieli at level 1%. Nonetheless, in the CATMA analysis pipeline, FWER proved to be the best solution to balance the estimated number of false positives and false negatives (Ge et al., 2003). As described in Gagnot et al. (2008), when the Bonferroni P value was lower than 0.05, the gene was considered differentially expressed. Hereafter, a transcript profile change at a given time point refers to a pairwise comparison with the previous time point. Accordingly, 748 genes were differentially expressed (DEGs) at T_6, 1806 at T_{34} and 527 at T_{58} (Table S1, Fig. S2).

Profiles were confirmed by real time RT-qPCR analysis for sets of genes involved in root meristem initiation or maintenance, cell cycle, and auxin metabolism (*RGF1*: AT5G60810, LBD16: AT2G42430, *LBD18*: AT2G45420, *IAA17*: AT1G04250, *IAA19*: AT3G15540, *IAA28*: AT5G25890, *TMO5*: AT3G25710, *TMO7*: AT1G74500, *PID*: AT2G34650, *KRP2*: AT3G50630, *CYCB2.4*: AT1G76310, *ARF16*: AT4G30080). Each gene profile was classified according to the statistically differential change(s), up or down, measured between the successive time points. Lists of set of genes specifically regulated across the conversion sequence are available in Table S1.

Biological pathways enrichment

Analyzed DEG sets correspond to genes significantly up- or down-regulated between two consecutive time points (Table S1). Biological pathways significantly over-represented (p-value < 0,01; Table S3) were identified with the classification superviewer tool of the university of Toronto website (http://bar.utoronto.ca/ntools/cgi-bin/ntools_classification_superviewer.cgi) using MAPMAN classification as a source (Provart and Zhu, 2003).

Comparative analysis of experimental data sets

The differentially expressed genes (DEGs) identified in our study (Table S1) were classified according to auxin or cytokinin metabolism and downstream signaling (in comparison to data sets published in Nemhauser et al., 2006), induced or repressed by cytokinin treatment (in at least three of four data sources as described in Brenner and Schmülling, 2015), involved in cell cycle (Vandepoele et al., 2002; Chatfield et al., 2013), or whether independent studies highlighted the same genes (Che et al., 2006; Li et al., 2011). Note that transcriptome data sets were produced with different microarray platforms. In our comparative analyses, genes tracked with Affymetrix chips were grouped according to the MAPMAN pathway classification, based on the Ath_Affy1_TAIR10_August 2012 Arabidopsis genome annotation. The genes tracked with the CATMA microarray were defined according to the EuGène prediction (Sclep et al., 2007). Hypergeometric tests were realized to determine if DEGs identified in this study were significantly over-represented in gene sets found in others. The comparable gene pool is defined as the 20,693 genes represented on both the ATH1 Affymetrix chips and the CATMA arrays (Table S2). To control for false positive results, raw p-values were adjusted with the Bonferroni correction. H_0, meaning that the overlap between our DEG lists and other gene sets is a random event, was rejected for adjusted p-value < 5% (Tables S1 and S2). Genes identically and specifically regulated between two consecutive time points were classified with the Venny software tool (http://bioinfogp.cnb.csic.es/tools/venny/). The list of genes in the intersections can be extracted from Table S1.

We examined whether DEGs identified in this study may be regulated by MET1-dependent DNA methylation by crossing our data with the results of Li et al. (2011) (Table S2). Li and coworkers showed that 768 genes were differentially regulated when comparing *met1-1* mutant (M0) *vs.* wild-type calli (S0), following a 20-day-culture on CIM medium (M0/S0 in Table S2). Among these, 308 genes were also differentially expressed in wild-type explants cultivated for 20 days on CIM (S0) and those transferred for 6 more days on SIM (S6) (M0 in S6/S0 in Table S2), suggesting that they might be induced on SIM and be regulated by MET1-dependent DNA methylation. A significant number of DEGs mostly induced at T_{34} and T_{58} were found to be over-represented in the 308 candidate genes pointing to the putative involvement of MET1-dependent transcriptional regulation during the conversion process.

Clustering

Hierarchical clustering analyses were performed via the Genevestigator online web tools (https://www.genevestigator.com/gv/), with the 20-most DEGs identified in this transcriptome study (Table S4), measured as Euclidian distance, and based on *Anatomy* and *Perturbation* data selections.

The *Anatomy* selection corresponds to 829, 2,394 and 281 hybridization results including 7, 20 and 14 anatomical parts from root, shoot and callus/cell culture/primary cell (only for wild-type), respectively (Fig. S3). The *Perturbation* selection corresponds to all wild-type genetic background experiments (5,825 hybridization results) available in Genevestigator. The same conclusions were drawn when matching the 200-most DEGs with anatomical parts (extracted from Table S1), indicating that similarity is not skewed by the size of the DEG sets (data not shown).

***In situ* hybridization**

Whole-mount *in situ* hybridization was performed using a protocol described by Morin et al. (in press). Labeled RNA probes were produced by *in vitro* transcription from a PCR amplified fragment of *STM* (700 bp), *WOX5* (527 bp) and *WUS* (1003 bp), using a DIG-RNA labeling kit (Roche, cat. no. 11175025910). For antisense probes (as), T7 promoter sequence was added to 3' primers. A *WOX5* sense probe (s) was produced as a negative control, in this case T7 promoter sequence was added to a 5' primer of *WOX5*. *STM* and *WUS* RNA probes are hydrolyzed into fragments with an average size of 400–500 nt before hybridization.

STM as, 5'-tgtaatacgactcactatagggctcaaagcatggtggaggagg-3'
WOX5 as, 5'-tgtaatacgactcactatagggcagatctaatggcggtggatg-3'
WUS as, 5'-tgtaatacgactcactatagggcctagttcagacgtagctcaaga-3'
WOX5 s, 5'-tgtaatacgactcactatagggcacggtggagcagttgaagat-3'

The colorimetric detection was performed with "BCIP/NBT Color Development Substrate" (Promega, cat. no. S3771). Images were taken through optical longitudinal section of explants visualized by Nomarski microscopy (DIC) with an Axio Imager 2 ZEISS microscope.

Supplemental References

Aida, M., Beis, D., Heidstra, R., Willemsen, V., Blilou, I., Galinha, C., Nussaume, L., Noh, Y.-S., Amasino, R. and Scheres, B. (2004). The *PLETHORA* genes mediate patterning of the Arabidopsis root stem cell niche. *Cell* **119**, 109–120.

Boutté, Y., Frescatada-Rosa, M., Men, S., Chow, C.-M., Ebine, K., Gustavsson, A., Johansson, L., Ueda, T., Moore, I., Jürgens, G., et al. (2010). Endocytosis restricts Arabidopsis KNOLLE syntaxin to the cell division plane during late cytokinesis. *EMBO J.* **29**, 546–558.

Brenner, W. G. and Schmülling, T. (2015). Summarizing and exploring data of a decade of cytokinin-related transcriptomics. *Front. Plant Sci.* **6**, 29.

Brunoud, G., Wells, D. M., Oliva, M., Larrieu, A., Mirabet, V., Burrow, A. H., Beeckman, T., Kepinski, S., Traas, J., Bennett, M. J., et al. (2012). A novel sensor to map auxin response and distribution at high spatio-temporal resolution. *Nature* **482**, 103–106.

Chatfield, S. P., Capron, R., Severino, A., Penttila, P.-A., Alfred, S., Nahal, H. and Provart, N. J. (2013). Incipient stem cell niche conversion in tissue culture: using a systems approach to probe early events in *WUSCHEL*-dependent conversion of lateral root primordia into shoot meristems. *Plant J.* **73**, 798–813.

Che, P., Lall, S., Nettleton, D. and Howell, S. H. (2006). Gene expression programs during shoot, root, and callus development in Arabidopsis tissue culture. *Plant Physiol.* **141**, 620–637.

Colón-Carmona, A., You, R., Haimovitch-Gal, T. and Doerner, P. (1999). Technical advance: spatio-temporal analysis of mitotic activity with a labile cyclin-GUS fusion protein. *Plant J.* **20**, 503–508.

Crowe, M.L., Serizet, C., Thareau, V., Aubourg, S., Rouzé, P., Beynon, J.L., Hilson, P., Weisbeek, P., Van Hummelen, P., Reymond, P., et al. (2003). CATMA - A complete Arabidopsis GST database. *Nucleic Acids Res.* **31**, 156–158

Gagnot, S., Tamby, J.P., Martin-Magniette, M.L., Bitton, F., Taconnat, L., Balzergue, S., Aubourg, S., Renou, J.P., Lecharny, A., Brunaud, V. (2008). CATdb: a public access to Arabidopsis transcriptome data from the URGV-CATMA platform. *Nucleic Acids Res.* **36**, D986–990.

Ge, Y., Dudoit, S., Speed, T.P. (2003). Resampling-based multiple testing for microarray data analysis. *TEST* **12**, 1–44.

Gross-Hardt, R., Lenhard, M. and Laux, T. (2002). WUSCHEL signaling functions in interregional communication during Arabidopsis ovule development. *Genes Dev.* **16**, 1129–1138.

Helariutta, Y., Fukaki, H., Wysocka-Diller, J., Nakajima, K., Jung, J., Sena, G., Hauser, M. T. and Benfey, P. N. (2000). The *SHORT-ROOT* gene controls radial patterning of the Arabidopsis root through radial signaling. *Cell* **101**, 555–567.

Hilson, P., Allemeersch, J., Altmann, T., Aubourg, S., Avon, A., Beynon, J., Bhalerao, R., Bitton, F., Caboche, M., Cannoot, B., et al. (2004). Versatile Gene-Specific Sequence Tags for *Arabidopsis* Functional Genomics: transcript profiling and reverse genetics applications. *Genome Res.* **14**, 2176–2189.

Himanen, K., Boucheron, E., Vanneste, S., de Almeida Engler, J., Inzé, D. and Beeckman, T. (2002). Auxin-mediated cell cycle activation during early lateral root initiation. *Plant Cell* **14**, 2339–2351.

Li, W., Liu, H., Cheng, Z. J., Su, Y. H., Han, H. N., Zhang, Y. and Zhang, X. S. (2011). DNA methylation and histone modifications regulate de novo shoot regeneration in Arabidopsis by modulating *WUSCHEL* expression and auxin signaling. *PLoS Genet.* **7**, e1002243.

Lurin, C., Andrés, C., Aubourg, S., Bellaoui, M., Bitton, F., Bruyère, C., Caboche, M., Debast, C., Gualberto, J., Hoffmann, B. et al. (2004). Genome-wide analysis of Arabidopsis pentatricopeptide repeat proteins reveals their essential role in organelle biogenesis. *Plant Cell* **16**, 2089–2103.

Malamy, J. E. and Benfey, P. N. (1997). Organization and cell differentiation in lateral roots of Arabidopsis thaliana. *Development* **124**, 33–44.

Nemhauser, J. L., Hong, F. and Chory, J. (2006). Different plant hormones regulate similar processes through largely nonoverlapping transcriptional responses. *Cell* **126**, 467–475.

Provart, N. J. and Zhu, T. (2003). A Browser-based Functional Classification SuperViewer for Arabidopsis Genomics. *Curr. Comput. Mol. Biol.* 271–272.

Sclep, G., Allemeersch, J., Liechti, R., De Meyer, B., Beynon, J., Bhalerao, R., Moreau, Y., Nietfeld, W., Renou, J. P., Reymond, P., Kuiper, M. T. and Hilson P. (2007) CATMA, a comprehensive genome-scale resource for silencing and transcript profiling of Arabidopsis genes. *BMC Bioinformatics* **8**, 400.

Truernit, E., Bauby, H., Dubreucq, B., Grandjean, O., Runions, J., Barthélémy, J. and Palauqui, J.-C. (2008). High-resolution whole-mount imaging of three-dimensional tissue organization and gene expression enables the study of Phloem development and structure in Arabidopsis. *Plant Cell* **20**, 1494–1503.

Tucker, M. R., Hinze, A., Tucker, E. J., Takada, S., Jürgens, G. and Laux, T. (2008). Vascular signalling mediated by ZWILLE potentiates WUSCHEL function during shoot meristem stem cell development in the Arabidopsis embryo. *Development* **135**, 2839–2843.

Vandepoele, K., Raes, J., De Veylder, L., Rouzé, P., Rombauts, S. and Inzé, D. (2002). Genome-wide analysis of core cell cycle genes in Arabidopsis. *Plant Cell* **14**, 903–916.

Vernoux, T., Kronenberger, J., Grandjean, O., Laufs, P. and Traas, J. (2000). PIN-FORMED 1 regulates cell fate at the periphery of the shoot apical meristem. *Development* **127**, 5157–5165.

Wysocka-Diller, J. W., Helariutta, Y., Fukaki, H., Malamy, J. E. and Benfey, P. N. (2000). Molecular analysis of SCARECROW function reveals a radial patterning mechanism common to root and shoot. *Development* **127**, 595–603.

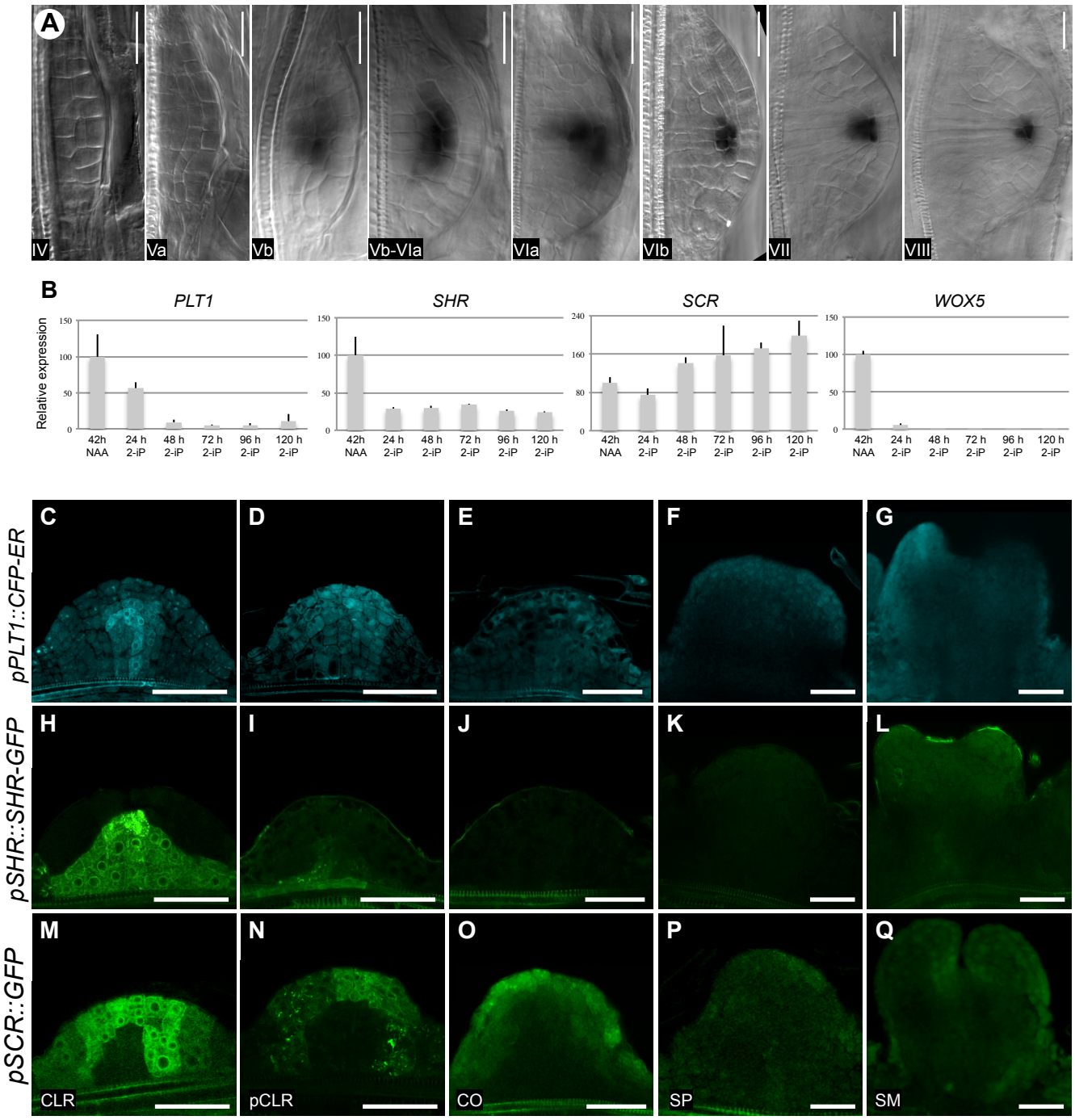

Figure S1: Expression of root identity genes during conversion.
A, Whole mount *in situ* localization of the *WOX5* transcript during lateral root development. Developmental stages indicated in the lower left corner of each picture are defined by Malamy and Benfey (1997). Lateral root were visualized with Nomarski microscopy (DIC). Scale bars: 20 µm. B, RT-qPCR analysis of *PLT1*, *SHR, SCR* and *WOX5* expression across the conversion in Col-0 explants. C, H and M: competent lateral root (CLR). *pPLT1::CFP-ER* marked CLR provascular domain, SHR protein was observed in the stele, and *SCR* was transcribed in the cell layers prefiguring the root cap, endodermis, pericycle, cortex and QC. D, I and N: paused competent lateral root primordium (pCLR). *PLT1* and *SCR* were transcribed at this stage, but *SHR* expression was rapidly turned off. E, J and O: converting organ (CO). Only transcription of *SCR* was observed. F, K and P: shoot promeristem (SP). Only transcription of *SCR* was observed. G, L and Q: shoot meristem (SM). The expression of *SCR* in the SAM can be detected. Conversion stages are as defined in Figure 2R. Reporter lines are indicated to the left of panels A to O. Scale bars: 50 µm.

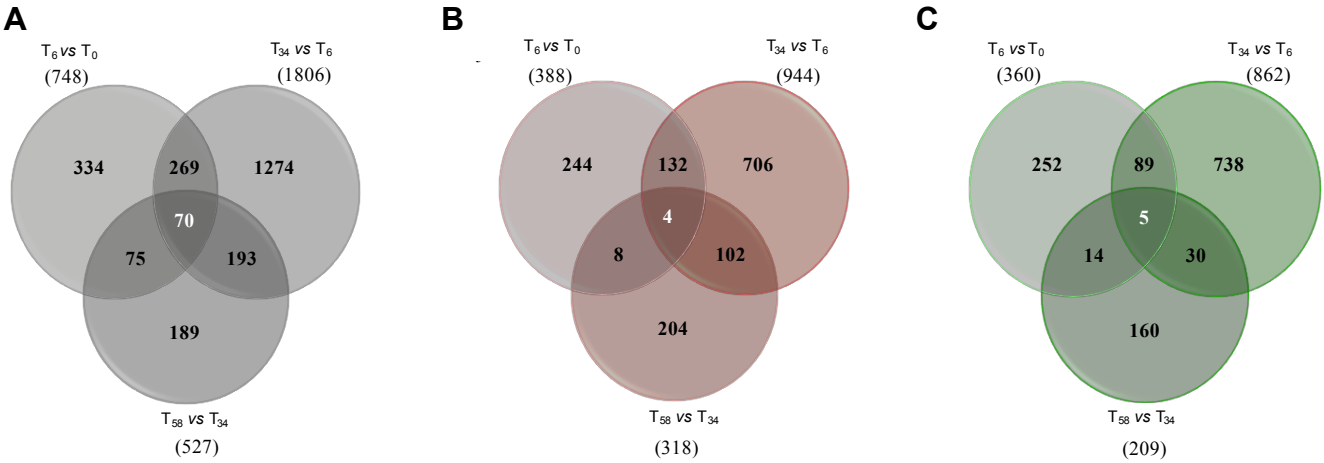

D

Comparisons	T6 vs T0		T34 vs T6		T58 vs T34	
DEG	All	Specific	All	Specific	All	Specific
Up-regulated	388	244	944	706	318	204
Down-regulated	360	252	862	738	209	160
Total	**748**	**334**	**1806**	**1274**	**527**	**189**

Figure S2: Distribution of differentially expressed genes.
A, Venn diagrams of the total; B, up-regulated and C, down-regulated genes DEGs identified in the T_6 *vs.* T_0, T_{34} *vs.* T_6, T_{58} *vs.* T_{34} comparisons. Numbers in parenthesis correspond to the total number of DEGs. Differentially expressed genes counted (Table S1) were selected by statistical analysis based on the Bonferroni method using a p-value cut-off of 0.05. D, Summary table.

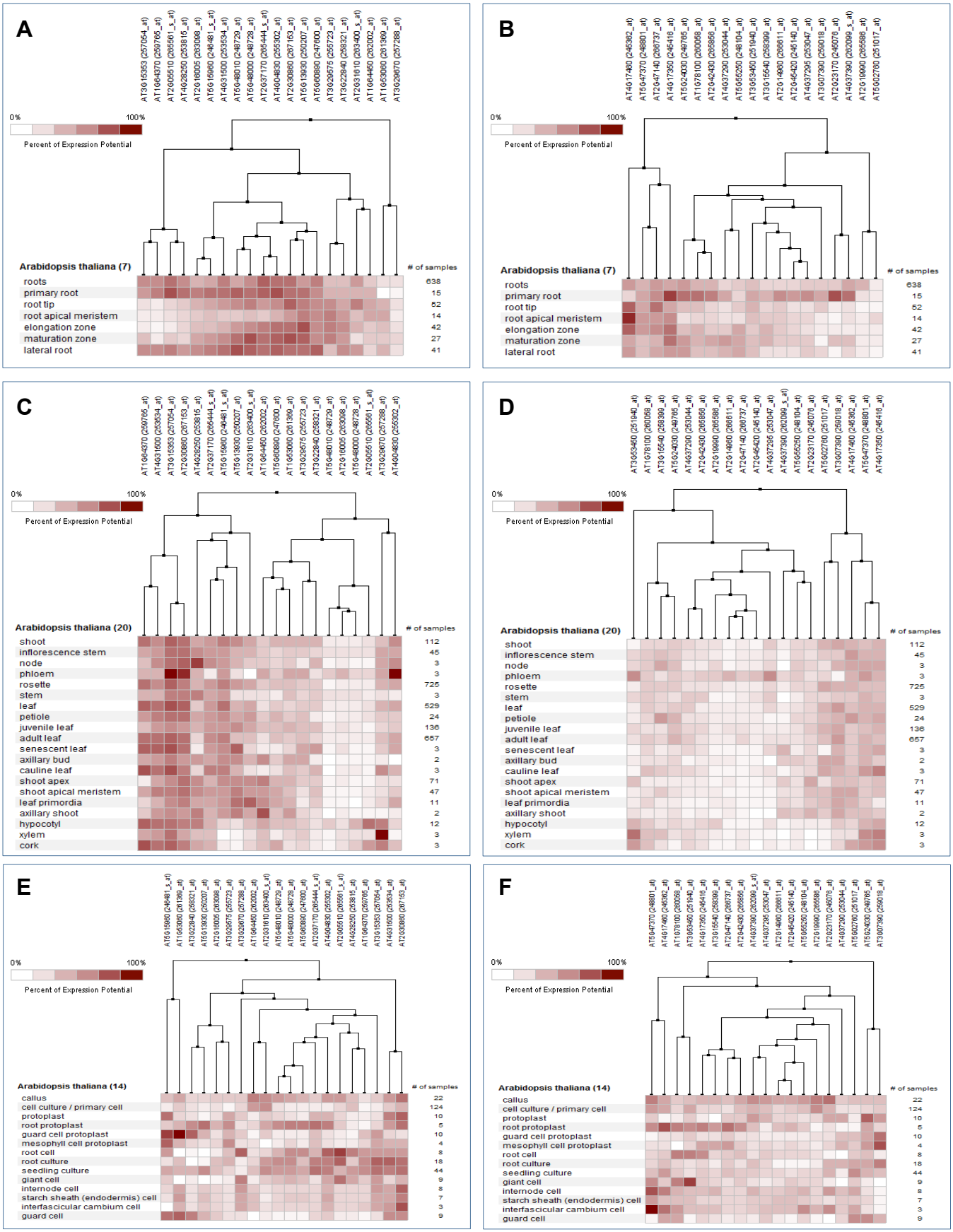

Figure S3: Comparison of our most DEGs with transcriptomic data sets.
Hierarchical clustering of the top 20 most up- (A, C, E, G, I, K, M, O, Q) or down-regulated (B, D, F, H, J, L, N, P, R) of T_6 *vs.* T_0 (A-F), T_{34} *vs.* T_6 (G-L) and T_{58} *vs.* T_{34} (M-R) comparisons with 7, 20 and 14 anatomical parts corresponding to root (A, B, G, H, M, N) shoot (C, D, I, J, O, P) and cell culture/primary cell (E, F, K, L, Q, R) transcriptomic data sets, respectively. A, Up-related DEGs from the T_6 *vs.* T_0 comparison correspond mostly to genes induced in 7 anatomical parts of the root and C, partially to genes induced in 20 anatomical parts of the shoot selection. I and J *vs.* O and P, The amount of genes induced in these later shoot selection increases in T_{34} *vs.* T_6 comparison gene set to become the main anatomical selection in which most of the genes up-regulated set from the T_{58} *vs.* T_{34} comparison are regulated.

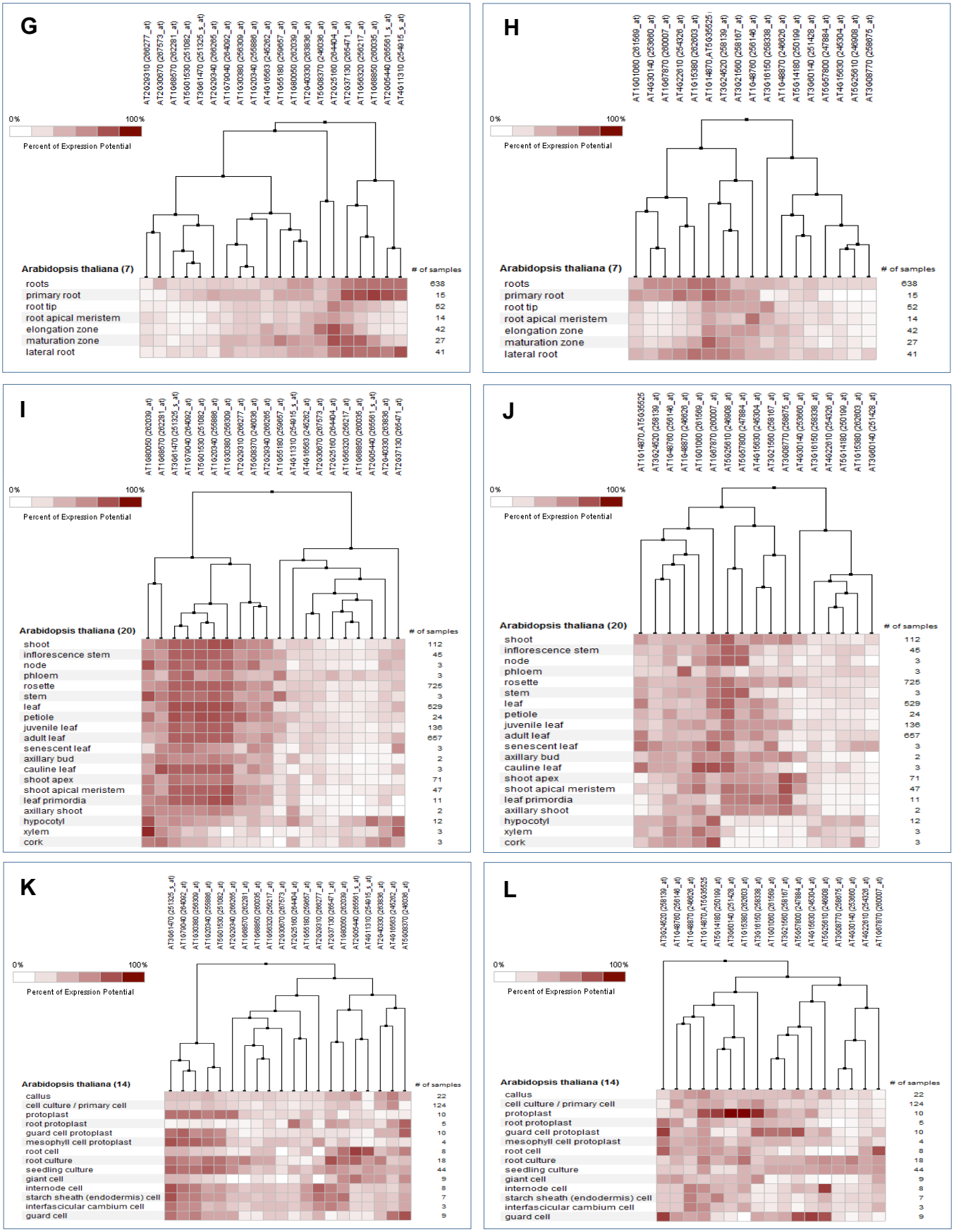

Figure S3: Comparison of our most DEGs with transcriptomic data sets.
Hierarchical clustering of the top 20 most up- (A, C, E, G, I, K, M, O, Q) or down-regulated (B, D, F, H, J, L, N, P, R) of T_6 *vs.* T_0 (A-F), T_{34} *vs.* T_6 (G-L) and T_{58} *vs.* T_{34} (M-R) comparisons with 7, 20 and 14 anatomical parts corresponding to root (A, B, G, H, M, N) shoot (C, D, I, J, O, P) and cell culture/primary cell (E, F, K, L, Q, R) transcriptomic data sets, respectively. A, Up-related DEGs from the T_6 *vs.* T_0 comparison correspond mostly to genes induced in 7 anatomical parts of the root and C, partially to genes induced in 20 anatomical parts of the shoot selection. I and J *vs.* O and P, The amount of genes induced in these later shoot selection increases in T_{34} *vs.* T_6 comparison gene set to become the main anatomical selection in which most of the genes up-regulated set from the T_{58} *vs.* T_{34} comparison are regulated.

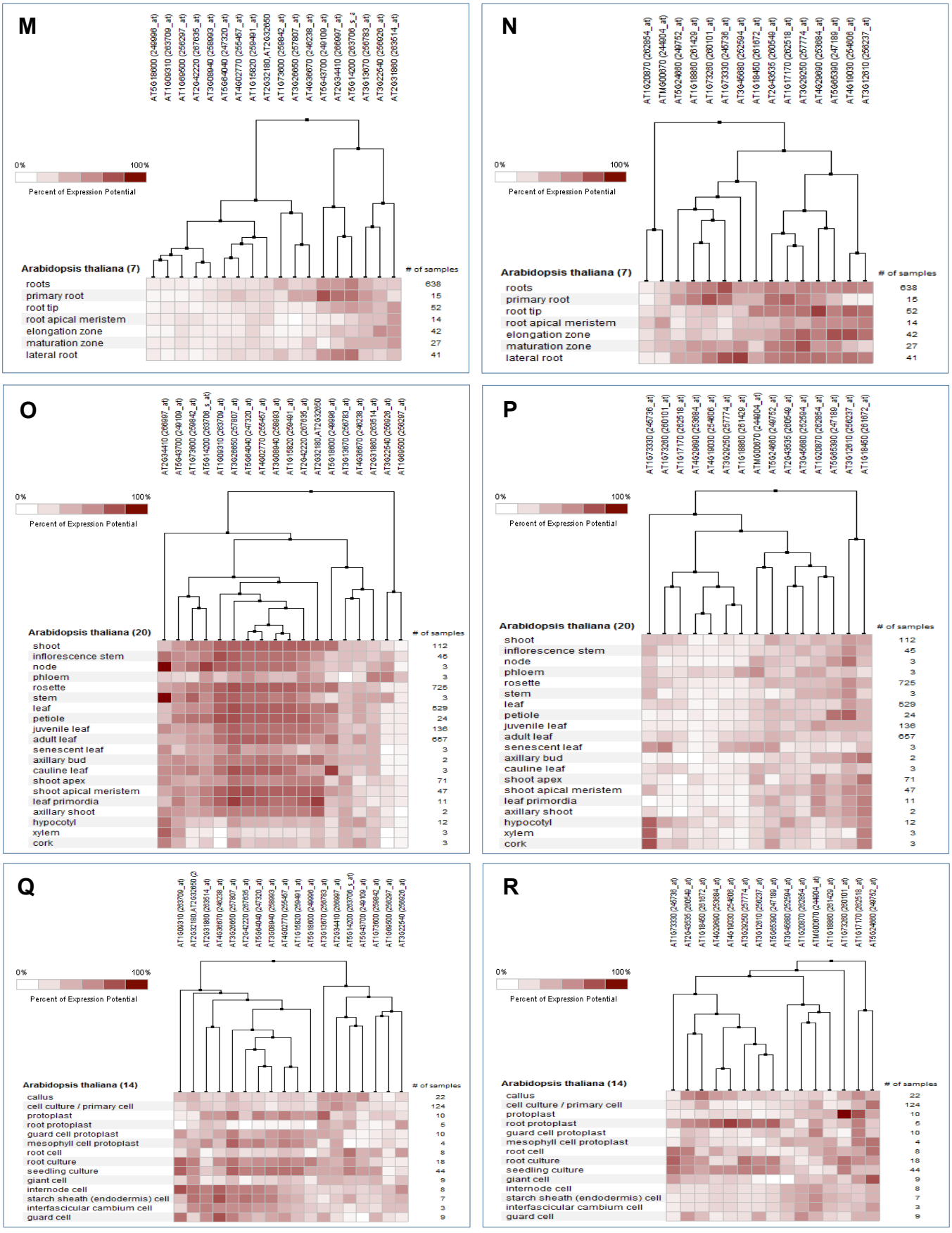

Figure S3: Comparison of our most DEGs with transcriptomic data sets.
Hierarchical clustering of the top 20 most up- (A, C, E, G, I, K, M, O, Q) or down-regulated (B, D, F, H, J, L, N, P, R) of T_6 *vs.* T_0 (A-F), T_{34} *vs.* T_6 (G-L) and T_{58} *vs.* T_{34} (M-R) comparisons with 7, 20 and 14 anatomical parts corresponding to root (A, B, G, H, M, N) shoot (C, D, I, J, O, P) and cell culture/primary cell (E, F, K, L, Q, R) transcriptomic data sets, respectively. A, Up-related DEGs from the T_6 *vs.* T_0 comparison correspond mostly to genes induced in 7 anatomical parts of the root and C, partially to genes induced in 20 anatomical parts of the shoot selection. I and J *vs.* O and P, The amount of genes induced in these later shoot selection increases in T_{34} *vs.* T_6 comparison gene set to become the main anatomical selection in which most of the genes up-regulated set from the T_{58} *vs.* T_{34} comparison are regulated.

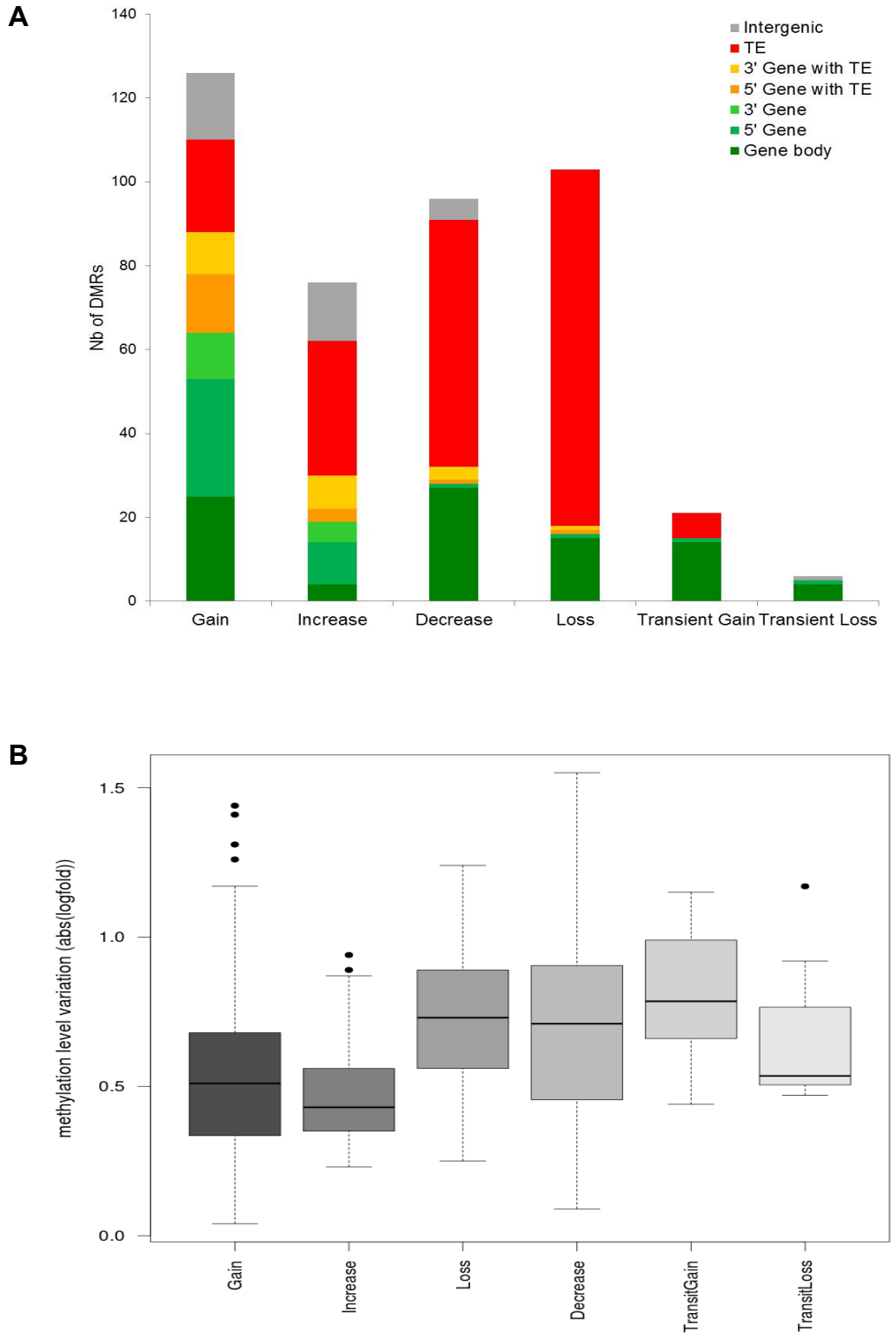

Figure S4: A limited number of low amplitude DMRs are detected across the conversion sequence.

A, Distribution of DMRs according to patterns of DNA methylation variation. Gain, continuous methylation increase, from unmethylated state at T_0 to higher methylation level at T_{58}. Loss, continuous methylation decrease, down to unmethylated at T_{58}. Increase and Decrease, positive and negative changes between intermediate methylation levels during conversion, respectively. Transient Gain and Transient Loss, higher and lower level of methylation in T_6 and T_{34} in comparison to T_0 and T_{58}, respectively. B, Average fold-change in DNA methylation levels according to patterns of DNA methylation variation.

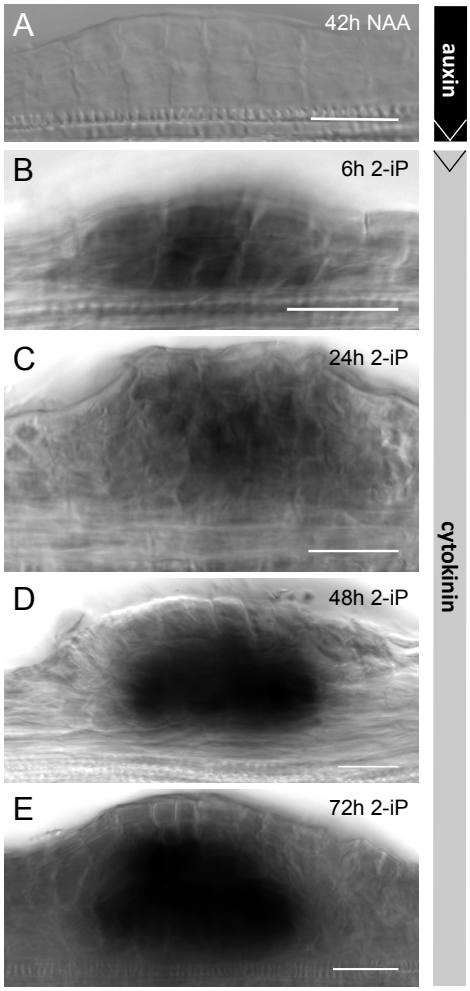

Figure S5: Expression of *WUS* in lateral root primordia induced with exogenous cytokinin at stage V.
Whole mount root segments were hybridized *in situ* with the *WUS* antisense probe after auxin (NAA) priming (A), and subsequent cytokinin (2iP) induction (B-E). Lateral organs were visualized with Nomarski microscopy (DIC). Scale bars: 20 µm.

Table S1: Differentially expressed genes (DEGs) between consecutive time points in the conversion sequence (cf : Table S1.xls)

Click here to Download Table S1

Table S2: Comparisons with published microarray data. Synthesis of the number of genes in commun between our study and query lists of genes involved in metabolism and dowstream signaling of auxin and cytokinin (Nemhauser et al., 2006; Brenner and Schmülling, 2015), in cell cycle (Vandepoele et al., 2002; Chatfield et al., 2013), in regeneration of shoots, calli or roots in tissue culture from Arabidopsis (Che et al., 2006) and in regeneration of shoots obtained in tissue culture from Arabidopsis mutant affected in DNA methylation (Li et al., 2011 ; see Supplemental Experimental Procedures for details). Percents in black correspond to set of genes found in commun studies or query lists significantly enriched at the significant threshold of hypergeometric and Bonferonni test p-value<0.05. preCIM : preculture on Callus-Inducing Medium, SIM : Shoot-Inducing Medium, CIM : Callus-Inducing Medium, RIM : Root-Inducing Medium. *: DEG that have been subtracted from EUGENE predictions and genes encoding microRNAs or predicted to encode HypmiRNAs.

DEGs in this study*			*T6 (vs T0)*			*T34 (vs T6)*			*T58 (vs T34)*		
			up	down	Total	up	down	Total	up	down	Total
			378	359	738	935	849	1784	305	200	505
Brenner and Schmülling (2015)	Cytokinin	up	6%	0%	3%	2%	0%	1%	1%	7%	3%
		down	0%	1%	0%	0%	0%	0%	0%	0%	0%
Nemhauser et al. (2006)			9%	4%	7%	6%	5%	5%	4%	11%	7%
Nemhauser et al. (2006)	Auxin		12%	21%	17%	8%	6%	7%	9%	13%	10%
Vandepoele et al. (2002) Chatfield et al. (2013)	Cell cycle		1%	3%	2%	0%	1%	1%	1%	0%	0%
Che et al. (2006)	preCIM	up	23%	43%	33%	12%	32%	21%	5%	8%	6%
		down	29%	17%	23%	24%	6%	15%	4%	10%	6%
	SIM		10%	1%	5%	1%	0%	0%	10%	6%	8%
	CIM		1%	2%	1%	1%	1%	1%	1%	1%	1%
	RIM		5%	3%	4%	7%	2%	4%	4%	3%	4%
Li et al. (2011)	M0/S0		7%	7%	7%	11%	3%	7%	21%	3%	14%
	M0 in S6/S0		3%	1%	2%	8%	1%	5%	17%	2%	11%

Table S3: Biological pathways significantly over-represented among deregulated genes. Significant pathways are in bold. ns: not significant.

	MAPMAN Classification	Frequency	T_6 *vs.* T_0 ± *bootstrap StdDev*	p-value	Frequency	T_{34} *vs.* T_6 ± *bootstrap StdDev*	p-value	Frequency	T_{58} *vs.* T_{34} ± *bootstrap StdDev*	p-value
Up –regulated genes	amino acid metabolism	**3.02**	***0.949***	**2.328e-03**	**3.17**	***0.629***	**9.105e-07**	ns	ns	ns
	cell	ns	ns	ns	**0.56**	***0.156***	**7.173e-03**	ns	ns	ns
	cell wall	ns	ns	ns	**2.42**	***0.367***	**5.380e-07**	ns	ns	ns
	development	**1.88**	***0.458***	**5.288e-03**	**1.5**	***0.249***	**5.530e-03**	ns	ns	ns
	DNA	**0.19**	***0.065***	**1.293e-09**	**0.11**	***0.035***	**1.489e-27**	**0.2**	***0.085***	**7.267e-08**
	gluconeogenesis / glyoxylate cycle	ns	ns	ns	**8.29**	***4.266***	**4.636e-03**	ns	ns	ns
	glycolysis	**3.23**	***0.744***	**3.813e-06**	ns	ns	ns	ns	ns	ns
	hormone metabolism	ns	ns	ns	**2.32**	***0.457***	**2.658e-06**	ns	ns	ns
	metal handling	ns	ns	ns	**3.46**	***1.304***	**1.684e-03**	ns	ns	ns
	micro RNA, natural antisense etc	ns	ns	ns	**0.07**	***0.057***	**2.809e-05**	ns	ns	ns
	minor CHO metabolism	ns	ns	ns	**3.76**	***1.05***	**3.434e-05**	ns	ns	ns
	miscaellous	**2.42**	***0.327***	**4.149e-08**	**2.39**	***0.191***	**4.854e-17**	**1.75**	***0.339***	**2.022e-03**
	N-metabolism	**10.09**	***5.15***	**2.962e-03**	**6.91**	***2.858***	**6.022e-04**	ns	ns	ns
	not assigned	**0.67**	***0.057***	**3.438e-07**	**0.65**	***0.035***	**2.227e-16**	**0.72**	***0.077***	**6.575e-05**
	nucleotide metabolism	**3.4**	***1.127***	**3.675e-03**	ns	ns	ns	ns	ns	ns
	protein	**0.37**	***0.081***	**1.191e-08**	**0.54**	***0.056***	**2.637e-10**	ns	ns	ns
	photosynthesis	ns	ns	ns	**5.58**	***0.986***	**2.818e-15**	**17.71**	***2.792***	**2.987e-32**
	redox	ns	ns	ns	**2.39**	***0.641***	**1.533e-03**	ns	ns	ns
	S-assimilation	**26.92**	***13.842***	**1.084e-05**	ns	ns	ns	ns	ns	ns
	secondary metabolism	**4.92**	***0.855***	**6.805e-11**	**3.39**	***0.538***	**5.097e-12**	**2.41**	***0.794***	**6.026e-03**
	signalling	**0.44**	***0.188***	**6.760e-03**	ns	ns	ns	ns	ns	ns
	stress	**1.78**	***0.33***	**2.085e-03**	**1.43**	***0.203***	**2.819e-03**	ns	ns	ns
	tetrapyrrole synthesis	ns	ns	ns	**5.24**	***2.003***	**2.948e-04**	17.89	*5.554*	**1.358e-08**
	transport	**2.48**	***0.438***	**5.095e-06**	**1.93**	***0.253***	**1.556e-06**	ns	ns	ns
Down-regulated genes	DNA	**0,5**	***0,13***	**4,26E-04**	**0,22**	***0,047***	**3,22E-18**	**0,1**	***0,055***	**3,05E-07**
	fermentation	ns	ns	ns	ns	ns	ns	**22,96**	***14,315***	**3,25E-03**
	hormone metabolism	**3,78**	***0,83***	**9,80E-08**	ns	ns	ns	**4,75**	***1,211***	**2,72E-07**
	lipid metabolism	**2,38**	***0,677***	**4,60E-03**	ns	ns	ns	ns	ns	ns
	miscaellous	**2,22**	***0,322***	**2,38E-06**	ns	ns	ns	**2,93**	***0,539***	**1,53E-07**
	not assigned	**0,68**	***0,067***	**1,60E-06**	**0,63**	***0,036***	**9,16E-17**	**0,59**	***0,081***	**3,32E-06**
	nucleotide metabolism	ns	ns	ns	**3,48**	***0,913***	**1,26E-05**	ns	ns	ns
	protein	**0,51**	***0,093***	**1,88E-05**	**2**	***0,106***	**4,97E-29**	ns	ns	ns
	RNA	**1,37**	***0,2***	**6,29E-03**	**1,48**	***0,127***	**5,22E-06**	ns	ns	ns

Table S4: Most differentially expressed genes during conversion (cf : Table S4.xls)

Click here to Download Table S4

Table S5: Loci with coinciding DNA methylation and transcript level changes. Variation in methylation and expression levels are represented for the few DMRs corresponding to a gene showing a change in expression during the conversion process. Relative levels of methylation at the different time points are represented by a heatmap, from low (green) to high (red) and variations in expression of the corresponding gene are represented by arrows.

Methylation						Expression				
Domain name	methylation change	T_0	T_6	T_{34}	T_{58}	$T_0 \rightarrow T_6$	$T_6 \rightarrow T_{34}$	$T_{34} \rightarrow T_{58}$	Annotation	
Chr3:19229787..19230313	gain	0,40	0,47	0,78	1,53	↗	↗	→	AT3G51820	ATG4/CHLG/G4 (CHLOROPHYLL SYNTHASE)
Chr2:7926498..7927189	gain	0,16	0,56	0,48	1,24	↘	↗	→	AT2G18193	AAA-type ATPase family protein
Chr1:28900772..28901152	gain	-0,38	-0,28	0,20	0,46	↘	↗	↗	AT1G76930	ATEXT4 (EXTENSIN 4)
Chr3:17030490..17031209	gain	0,01	0,25	0,06	0,83	↘	→	→	AT3G46320	histone H4
Chr3:20638713..20639257	gain	-0,13	-0,27	0,14	0,53	→	→	↘	AT3G55610	P5CS2 (DELTA 1-PYRROLINE-5-CARBOXYLATE SYNTHASE 2)
Chr2:11552315..11552703	gain	-0,11	-0,22	0,32	0,44	↘	→	→	AT2G27050	EIL1 (ETHYLENE-INSENSITIVE3-LIKE 1)
Chr2:14393613..14393996	increase	1,09	1,58	1,78	1,93	↗	→	→	AT2G34060	peroxidase, putative
Chr4:17684540..17685089	decrease	1,85	1,63	1,76	1,22	↘	→	→	AT4G37640	ACA2 (CALCIUM ATPASE 2)
Chr1:12566595..12567299	loss	0,40	0,21	0,28	-0,21	↗	→	→	AT1G34400	unknown protein
Chr3:17483630..17484009	loss	0,79	0,40	0,80	0,24	↘	→	→	AT3G47420	glycerol-3-phosphate transporter, putative

Supplemental Experimental Procedures

Arabidopsis growth medium composition

Arabidopsis solid growth medium consisted of MS salts with vitamins (Duchefa, M0222), supplemented with 0.5 $g.L^{-1}$ 2-(N-morpholino) ethane sulfonic acid (pH5.7; Sigma, M8250), 1 % (w/v) sucrose (Sigma, S9378). The gelling agent was 0.6 % (w/v) Agarose (Euromedex, D5) for Col-0 and 0.7% (w/v) Plant Agar (Duchefa, P1001) for L*er*. In explants sampled for RT-qPCR, transcriptomic and methylome studies, LR initiation was further synchronized by germinating and growing plantlets in the presence of the auxin transport inhibitor 1-N-naphthylphthalamic acid (NPA) prior to NAA priming. NPA first prevents the formation of auxin maxima and thus inhibits LR initiation. NAA then massively induces LR initiation along the primary root (Himanen et al., 2002). For these experiments, Col-0 plantlets were germinated and grown in the presence of 1.25 µM 1-N-Naphthylphthalamic acid (NPA) (Duchefa, N0926) for 6 d prior to NAA treatment. To induce lateral root formation, plantlets were transferred and grown for 42 hours on an auxin medium, similar to the previous one, but without NPA, and with 3.3 µM and 10 µM 1-naphthaleneacetic acid (NAA) (Duchefa, N0903) for Col-0 and L*er*, respectively. To induce shoot meristem formation, primary root segments were excised and transferred on a cytokinin medium, similar to the previous one but where auxin was replaced with 8.16 µM and 24.6 µM N6-[2-isopentenyl]adenine (2-iP) (Duchefa, D0906) for Col-0 and L*er*, respectively, and sucrose was replaced with 2% D-(+)-Glucose (Sigma, G8270) for all genotypes. The Col-0 x L*er* hybrid line was always treated as L*er*. In explants prepared for morphological and marker line analysis, LR initiation was induced with NAA priming for 42 h, but without NPA treatment during germination and growth on the first medium. Contrarily to the NPA treatment, this unsynchronized protocol avoids LRP fusion and was chosen as more convenient to follow the development of individual LRPs.

Phytohormones were dissolved in dimethylsulfoxide (DMSO; Sigma, D8418). Sugars and hormones were added to the media after autoclaving.

Arabidopsis reporter lines	Background	Reference
pWUS::GUS	Col-0xL*er*	(Gross-Hardt et al., 2002)
pPLT1::CFP	Col-0	(Aida et al., 2004)
pSHR::SHR-GFP	Col-0	(Helariutta et al., 2000)
pSCR::mGFP5-ER	Col-0	(Wysocka-Diller et al., 2000)
pCLV3::CFP-ER	L*er*	(Tucker et al., 2008)
pKNOLLE::KNOLLE-GFP	L*er*	(Boutté et al., 2010)
pPIN1:PIN1-GFP	L*er*	(Vernoux et al., 2000)
pCYCB1;1::DB-GUS	Col-0	(Colón-Carmona et al., 1999)
pTCSn ::GFP	Col-0	Gift from B. Müller
pPIN1::PIN1 :GFP/pSTM::STM :YFP	L*er*	NASC N66314
pDR5::rev:3XVENUS-N7/pCUC2::RFP	Col-0	Gift from P. Laufs
p35S::DII-VENUS	Col-0	(Brunoud et al., 2012)

Quantification of the conversion and reversion *in vitro* responses

Conversion. The distribution of converted organs was assessed relative to the LRP stages of development (Malamy and Benfey, 1997) at the onset of cytokinin treatment. A total of 210 Col-0 roots segments were analyzed carrying 4453 LRPs classified in three classes when transferred on 2-iP medium: stages V and younger ($n_{LRP\leq V}$ = 432, 7 converted in SMs, 0.7% of converted LRPs); stages VI and VII ($n_{LRP\ VIorVII}$ = 1716, 967 SMs; 90.2%); stages VIII and emerged ($n_{LRP\geq VIII}$ = 2305, 98 SMs; 9.1%). Conversion was assessed for each individual LR after 6 days of 2-iP treatment, by comparing images acquired at the beginning and at the end of the treatment.

Rates measured in a separate experiment showed that Landsberg *erecta* (L*er*) LRPs have a similar ability to convert according to their developmental stages: $n_{LRP\leq V}$ = 55, 6 SMs, 3.0%; $n_{LRP\ VIorVII}$ = 485, 175 SMs, 89.3%; $n_{LRP\geq VIII}$ = 162, 15 SMs, 7.7%. The conversion from an LR into an established SM is slower in L*er* than in Col-0, five days instead of four in our hands, which may be explained by the different gelling agent and hormone concentrations that were optimized empirically for both ecotypes.

For clarity, the lateral organs were preferentially labeled according to their developmental time, determined based to their structure, rather that their incubation time on 2-iP medium that varied slightly between ecotypes and transgenic markers lines.

Reversion. The distribution of reverted LRPs was assessed in excised root segments primed with NAA for 42h. A total of 73 Col-0 root segments carrying 8546 lateral roots at different stages were transferred on 2-iP medium for 3 d, then split in two batches: 3986 LRs (33 root segments) remained on the 2-iP medium for 3 more days, of which 1286 switched into shoot meristem development (conversion); 4560 LRs (40 root segments) were transferred back on NAA medium for 3 d, of which only 139 shoot promeristems did not switch back into LRPs (reversion).

Propidium iodide staining, confocal microscopy and image analysis

The protocol was adapted from (Truernit et al., 2008). Explants were fixed and stained with propidium iodide. The developing lateral organs were imaged as stacks of confocal optical sections and their organization was analyzed in the sagittal plane reconstructed for each object. Briefly, the explants were fixed in a 75% ethanol / 25% acetic anhydride solution for 2 d. Samples were rehydrated by successive immersion in 50%, 30% and 10% ethanol, and washed 3 times in distilled water. Amyloplasts were dissolved with amylase (0.2 mg/ml) for 3 h at 37 °C. Fixed explants were washed 3 times in distilled water, incubated in 1% periodic acid for 20 min, rinsed again with water, and stained overnight in Schiff reagent with propidium iodide (PI) (100 mM sodium metabisulphite, 0.15 N HCl, freshly added PI at a final concentration of 0.1 mg/µl). Samples on microscope slides were covered with a chloral hydrate solution (4 g chloral hydrate, 1 mL glycerol, 2 mL water) after 3 washes in water. Explants were imaged with a Leica SP5 spectral confocal laser scanning microscope (Leica Microsystems). Excitation wavelength for PI–stained samples was 488 nm, emission signal was collected from 520 to 720 nm. Acquired Z stacked images (lif format) were converted (tif format) with ImageJ (V1.46, 64 bits). See Table below for voxel size. Stacks were reoriented according to the main axis of the primary root to define the transverse and sagittal planes passing through the center of the LRP by 3D multi-planar reconstruction with the OsiriX software (V.5.6, 32 bits). LRP developmental stages were identified based on the number of epidermal cells and the organization of the cells in the stele, as observed in the reconstructed sagittal plane.

Voxel sizes in images of propidium iodide-stained explants

	Panel	Width	Height	Depth
Figure 2	E	0.2225987	0.2225987	0.4196171
	F	0.2225986	0.2225986	0.4196171
	G	0.1082093	0.1082093	0.293732
	H	0.158513	0.158513	0.2098085
	I	0.2225987	0.2225987	0.4196171
	J	0.2225987	0.2225987	0.7133491
	K	0.3029291	0.3029291	1.0070810
	L	0.2225987	0.2225987	0.7133491
	M	0.2225986	0.2225986	
Figure 3	A	0.1224285	0.1224285	0.293732
	B	0.1650829	0.1650829	0.7133491
	C	0.2225986	0.2225986	0.7133491
	D	0.2225986	0.2225986	0.7133491
	E	0.2225986	0.2225986	0.4196171
	F	0.4451973	0.4451973	0.7133491

GUS staining and quantification

Tissues were fixed in ice-cold 90% acetone for 10 min on ice, rinsed with water for 5 min, vacuum infiltrated for 5 min with staining solution (50 mM sodium phosphate buffer pH 7, 0.2% Triton-X-100, 2 mM potassium ferrocyanide, 2 mM potassium ferricyanide, 1 mM X-gluc) and incubated at 37°C for 7 to 18 h. The reaction was stopped with 70% ethanol and conserved at 4°C until observation. The samples were mounted in 10% glycerol and photographs were taken with a Zeiss Axio zoom stereo-microscope.

To quantify the cell division average in the converting organs, the number of blue GUS-stained spots were counted in *pCYCB1;1::DB-GUS* explants to measure the number of dividing cells in a converting organ and averaged per developmental stage: CLR at stage VI or VII (NAA 42 h, n=160); pCLR (2-iP 24 and 48 h, n=57 of which 24 showed no GUS spot); CO (2-iP 72 h, n=35); SP (2-iP 96 h,

n=40); SM (2-iP 120 h, n=14).

Quantitative real-time RT-PCR analysis

Total RNA was isolated with the RNeasy Plant mini-kit (Qiagen). For RT-qPCR, 5 µg of RNAs were DNase-treated using DNaseI according to the manufacturer's instructions (Qiagen) and cDNAs were synthesized using oligo(dT) with Superscript II reverse transcriptase (Invitrogen) according to the manufacturer's instructions. Quantitative real-time RT-qPCR was performed in an Eppendorf Mastercycler realplex (Eppendorf) with MESA GREEN qPCR MasterMix Plus for SYBRAssay (Eurogentec) as per manufacturer's instructions. Data analysis, including calculation of primer pair reaction efficiencies and Ct values, was carried out by Eppendorf Manager software. The results of two technical replicates of two biological samples were normalized with 1 to 4 genes with a steady level of transcription. The first point of the kinetic is used as the 100% reference for the normalization of the relative expression. All RT-qPCR data points were obtained with 60-80 pooled explants. Each explants harbored dozens of converting/reverting primordia at synchronized developmental stages. List of primers pairs used in RT-qPCR experiments:

Gene name	5' primer	3' primer
WUS	gtgttcccatgcagagacct	tcagtacctgagcttgcatga
STM	ccaagatcatggctcatcct	cctgttggtcccatagatgc
WOX5	ggagaggcagaaacgtcgta	tgaattcaccggaaagagttg
PLT1	gccggaaacaaagacctctac	aatggctttcacgtcgtacc
SHR	gagacagcgaggaagtggtc	ccatcgaccaaacaccttct
SCR	tgaggaaaagggaagctgtg	agcgtggctcaaatcttgtt
CLV3	gtccggtccagttcaacaac	gcttctccatttgctccaac
CUC2	aaggaagagctccgaaagga	tccggtgctagctaaagtgg
Ubq5	cttgaagacggccgtaccctc	cgctgaacctttcaagatccatcg
AT5G13440	acaagccaatttttgctgagc	acaacagtccgagtgtcatggt
AT2G26060	gggatggtcaagatttggca	caaaccaacagcagtcacggt
AT429130	ggcgttttctgatagcgaaaa	atggatcaggcattggagct
HIS4	cgaagattggctcgtagagg	gctcggtgtaagtgacagca
CYCB2;4	ggatacgaggattggagcaa	ttgtgatgcaaaccaaccat
KRP2	ggtgacgatcgtgaaacaga	aagatctttctccgccacct
RGF1	gtgaaggtcttggagcaagc	tctcatttgcctccaccttc
LBD16	ccatgatcgatgtgaagctg	ggttggtactttccgagctg
LBD18	aggtccgatgctgtcgtaac	gatgccaaatgggcttgtaa
ARF16	tcaaatacgcaggaaacgaa	cgctctcacttccttgttcc
TMO5	gggttcgatggtgagatcat	acttccgctagcaaagaagc
TMO7	atgtcgggaagaagatcacg	cttgtaacaccctcgctgct
PID	tgaaaatgcttgaccatcca	actagaacttcggcggcata
IAA17	ggtatcaatggacggagcac	cccagctattcaccaaatcc
IAA19	tggatggtgtgccttatttg	cgagcatccagtctccatct
IAA28	taaagttctggtcggggatg	aaggcgtgggaggtcttta

Transcript profiling

Microarray analyses were carried out with the CATMA array containing 24,576 gene-specific tags corresponding to 22,089 genes and 633 mitochondrial and chloroplastic genome segments from *Arabidopsis thaliana* (Crowe et al., 2003; Hilson et al., 2004). To maximize specificity, the lateral organs were laser micro-dissected and pooled for transcript profile analysis at four time points: T_0, 42 h NAA-priming, competent lateral root (CLR); T_6, 6 h 2-iP treatment, paused CLR; T_{34}, 34 h 2-iP, converting organ (CO) resuming active cell division; T_{58}, 58 h 2-iP, early shoot primordium (eSP) (Fig. 5G). Total RNA was extracted from samples corresponding to the four time points in two independent biological experiments, with the Qiagen RNAeasy plant minikit according the manufacturer's instructions. For T_6 vs. T_0, T_{34} vs. T_6 and T_{58} vs. T_{34} comparisons, two technical replicates in dye-swap were performed for each of the two biological repeats. The labeling of cRNA with Cy3-dUTP or Cy5-dUTP (Perkin-Elmer- NEN Life Science Products), the hybridization to the slides, and the scanning were performed as described in Lurin et al. (2004). Specific statistics were developed to analyze CATMA hybridizations. For each array, the raw data comprises the logarithm of median feature pixel intensity (in log base 2) at wavelengths 635 nm (red) and 532 nm (green). No background was subtracted. The normalization method used is described in Lurin et al. *(*2004). To determine differentially expressed genes, we performed a pair t-test on the log ratios averaged on the dye-swap.

A trimmed variance is calculated from spots which do not display extreme variance. The raw p-value are adjusted by the Bonferroni method, which controls the Family Wise Error Rate (FWER) (with a type I error equal to 5%). We also adjusted the raw p-values to control a FDR using Benjamini-Yetkutieli at level 1%. Nonetheless, in the CATMA analysis pipeline, FWER proved to be the best solution to balance the estimated number of false positives and false negatives (Ge et al., 2003). As described in Gagnot et al. (2008), when the Bonferroni P value was lower than 0.05, the gene was considered differentially expressed. Hereafter, a transcript profile change at a given time point refers to a pairwise comparison with the previous time point. Accordingly, 748 genes were differentially expressed (DEGs) at T_6, 1806 at T_{34} and 527 at T_{58} (Table S1, Fig. S2).

Profiles were confirmed by real time RT-qPCR analysis for sets of genes involved in root meristem initiation or maintenance, cell cycle, and auxin metabolism (*RGF1*: AT5G60810, LBD16: AT2G42430, *LBD18*: AT2G45420, *IAA17*: AT1G04250, *IAA19*: AT3G15540, *IAA28*: AT5G25890, *TMO5*: AT3G25710, *TMO7*: AT1G74500, *PID*: AT2G34650, *KRP2*: AT3G50630, *CYCB2.4*: AT1G76310, *ARF16*: AT4G30080). Each gene profile was classified according to the statistically differential change(s), up or down, measured between the successive time points. Lists of set of genes specifically regulated across the conversion sequence are available in Table S1.

Biological pathways enrichment

Analyzed DEG sets correspond to genes significantly up- or down-regulated between two consecutive time points (Table S1). Biological pathways significantly over-represented (p-value < 0,01; Table S3) were identified with the classification superviewer tool of the university of Toronto website (http://bar.utoronto.ca/ntools/cgi-bin/ntools_classification_superviewer.cgi) using MAPMAN classification as a source (Provart and Zhu, 2003).

Comparative analysis of experimental data sets

The differentially expressed genes (DEGs) identified in our study (Table S1) were classified according to auxin or cytokinin metabolism and downstream signaling (in comparison to data sets published in Nemhauser et al., 2006), induced or repressed by cytokinin treatment (in at least three of four data sources as described in Brenner and Schmülling, 2015), involved in cell cycle (Vandepoele et al., 2002; Chatfield et al., 2013), or whether independent studies highlighted the same genes (Che et al., 2006; Li et al., 2011). Note that transcriptome data sets were produced with different microarray platforms. In our comparative analyses, genes tracked with Affymetrix chips were grouped according to the MAPMAN pathway classification, based on the Ath_Affy1_TAIR10_August 2012 Arabidopsis genome annotation. The genes tracked with the CATMA microarray were defined according to the EuGène prediction (Sclep et al., 2007). Hypergeometric tests were realized to determine if DEGs identified in this study were significantly over-represented in gene sets found in others. The comparable gene pool is defined as the 20,693 genes represented on both the ATH1 Affymetrix chips and the CATMA arrays (Table S2). To control for false positive results, raw p-values were adjusted with the Bonferroni correction. H_0, meaning that the overlap between our DEG lists and other gene sets is a random event, was rejected for adjusted p-value < 5% (Tables S1 and S2). Genes identically and specifically regulated between two consecutive time points were classified with the Venny software tool (http://bioinfogp.cnb.csic.es/tools/venny/). The list of genes in the intersections can be extracted from Table S1.

We examined whether DEGs identified in this study may be regulated by MET1-dependent DNA methylation by crossing our data with the results of Li et al. (2011) (Table S2). Li and coworkers showed that 768 genes were differentially regulated when comparing *met1-1* mutant (M0) *vs.* wild-type calli (S0), following a 20-day-culture on CIM medium (M0/S0 in Table S2). Among these, 308 genes were also differentially expressed in wild-type explants cultivated for 20 days on CIM (S0) and those transferred for 6 more days on SIM (S6) (M0 in S6/S0 in Table S2), suggesting that they might be induced on SIM and be regulated by MET1-dependent DNA methylation. A significant number of DEGs mostly induced at T_{34} and T_{58} were found to be over-represented in the 308 candidate genes pointing to the putative involvement of MET1-dependent transcriptional regulation during the conversion process.

Clustering

Hierarchical clustering analyses were performed via the Genevestigator online web tools (https://www.genevestigator.com/gv/), with the 20-most DEGs identified in this transcriptome study (Table S4), measured as Euclidian distance, and based on *Anatomy* and *Perturbation* data selections.

The *Anatomy* selection corresponds to 829, 2,394 and 281 hybridization results including 7, 20 and 14 anatomical parts from root, shoot and callus/cell culture/primary cell (only for wild-type), respectively (Fig. S3). The *Perturbation* selection corresponds to all wild-type genetic background experiments (5,825 hybridization results) available in Genevestigator. The same conclusions were drawn when matching the 200-most DEGs with anatomical parts (extracted from Table S1), indicating that similarity is not skewed by the size of the DEG sets (data not shown).

***In situ* hybridization**

Whole-mount *in situ* hybridization was performed using a protocol described by H. Morin and A. Bendahmane (Institute of Plant Sciences Paris-Saclay, France). Labeled RNA probes were produced by *in vitro* transcription from a PCR amplified fragment of *STM* (700 bp), *WOX5* (527 bp) and *WUS* (1003 bp), using a DIG-RNA labeling kit (Roche, cat. no. 11175025910). For antisense probes (as), T7 promoter sequence was added to 3' primers. A *WOX5* sense probe (s) was produced as a negative control, in this case T7 promoter sequence was added to a 5' primer of *WOX5*. *STM* and *WUS* RNA probes are hydrolyzed into fragments with an average size of 400–500 nt before hybridization.

STM as, 5'-tgtaatacgactcactatagggctcaaagcatggtggaggagg-3'
WOX5 as, 5'-tgtaatacgactcactatagggcagatctaatggcggtggatg-3'
WUS as, 5'-tgtaatacgactcactatagggcctagttcagacgtagctcaaga-3'
WOX5 s, 5'-tgtaatacgactcactatagggcacggtggagcagttgaagat-3'

The colorimetric detection was performed with "BCIP/NBT Color Development Substrate" (Promega, cat. no. S3771). Images were taken through optical longitudinal section of explants visualized by Nomarski microscopy (DIC) with an Axio Imager 2 ZEISS microscope.

Supplemental References

Aida, M., Beis, D., Heidstra, R., Willemsen, V., Blilou, I., Galinha, C., Nussaume, L., Noh, Y.-S., Amasino, R. and Scheres, B. (2004). The *PLETHORA* genes mediate patterning of the Arabidopsis root stem cell niche. *Cell* **119**, 109–120.

Boutté, Y., Frescatada-Rosa, M., Men, S., Chow, C.-M., Ebine, K., Gustavsson, A., Johansson, L., Ueda, T., Moore, I., Jürgens, G., et al. (2010). Endocytosis restricts Arabidopsis KNOLLE syntaxin to the cell division plane during late cytokinesis. *EMBO J.* **29**, 546–558.

Brenner, W. G. and Schmülling, T. (2015). Summarizing and exploring data of a decade of cytokinin-related transcriptomics. *Front. Plant Sci.* **6**, 29.

Brunoud, G., Wells, D. M., Oliva, M., Larrieu, A., Mirabet, V., Burrow, A. H., Beeckman, T., Kepinski, S., Traas, J., Bennett, M. J., et al. (2012). A novel sensor to map auxin response and distribution at high spatio-temporal resolution. *Nature* **482**, 103–106.

Chatfield, S. P., Capron, R., Severino, A., Penttila, P.-A., Alfred, S., Nahal, H. and Provart, N. J. (2013). Incipient stem cell niche conversion in tissue culture: using a systems approach to probe early events in *WUSCHEL*-dependent conversion of lateral root primordia into shoot meristems. *Plant J.* **73**, 798–813.

Che, P., Lall, S., Nettleton, D. and Howell, S. H. (2006). Gene expression programs during shoot, root, and callus development in Arabidopsis tissue culture. *Plant Physiol.* **141**, 620–637.

Colón-Carmona, A., You, R., Haimovitch-Gal, T. and Doerner, P. (1999). Technical advance: spatio-temporal analysis of mitotic activity with a labile cyclin-GUS fusion protein. *Plant J.* **20**, 503–508.

Crowe, M.L., Serizet, C., Thareau, V., Aubourg, S., Rouzé, P., Beynon, J.L., Hilson, P., Weisbeek, P., Van Hummelen, P., Reymond, P., et al. (2003). CATMA - A complete Arabidopsis GST database. *Nucleic Acids Res.* **31**, 156–158

Gagnot, S., Tamby, J.P., Martin-Magniette, M.L., Bitton, F., Taconnat, L., Balzergue, S., Aubourg, S., Renou, J.P., Lecharny, A., Brunaud, V. (2008). CATdb: a public access to Arabidopsis transcriptome data from the URGV-CATMA platform. *Nucleic Acids Res.* **36**, D986–990.

Ge, Y., Dudoit, S., Speed, T.P. (2003). Resampling-based multiple testing for microarray data analysis. *TEST* **12**, 1–44.

Gross-Hardt, R., Lenhard, M. and Laux, T. (2002). WUSCHEL signaling functions in interregional communication during Arabidopsis ovule development. *Genes Dev.* **16**, 1129–1138.

Helariutta, Y., Fukaki, H., Wysocka-Diller, J., Nakajima, K., Jung, J., Sena, G., Hauser, M. T. and Benfey, P. N. (2000). The *SHORT-ROOT* gene controls radial patterning of the Arabidopsis root through radial signaling. *Cell* **101**, 555–567.

Hilson, P., Allemeersch, J., Altmann, T., Aubourg, S., Avon, A., Beynon, J., Bhalerao, R., Bitton, F., Caboche, M., Cannoot, B., et al. (2004). Versatile Gene-Specific Sequence Tags for *Arabidopsis* Functional Genomics: transcript profiling and reverse genetics applications. *Genome Res.* **14**, 2176–2189.

Himanen, K., Boucheron, E., Vanneste, S., de Almeida Engler, J., Inzé, D. and Beeckman, T. (2002). Auxin-mediated cell cycle activation during early lateral root initiation. *Plant Cell* **14**, 2339–2351.

Li, W., Liu, H., Cheng, Z. J., Su, Y. H., Han, H. N., Zhang, Y. and Zhang, X. S. (2011). DNA methylation and histone modifications regulate de novo shoot regeneration in Arabidopsis by modulating *WUSCHEL* expression and auxin signaling. *PLoS Genet.* **7**, e1002243.

Lurin, C., Andrés, C., Aubourg, S., Bellaoui, M., Bitton, F., Bruyère, C., Caboche, M., Debast, C., Gualberto, J., Hoffmann, B. et al. (2004). Genome-wide analysis of Arabidopsis pentatricopeptide repeat proteins reveals their essential role in organelle biogenesis. *Plant Cell* **16**, 2089–2103.

Malamy, J. E. and Benfey, P. N. (1997). Organization and cell differentiation in lateral roots of Arabidopsis thaliana. *Development* **124**, 33–44.

Nemhauser, J. L., Hong, F. and Chory, J. (2006). Different plant hormones regulate similar processes through largely nonoverlapping transcriptional responses. *Cell* **126**, 467–475.

Provart, N. J. and Zhu, T. (2003). A Browser-based Functional Classification SuperViewer for Arabidopsis Genomics. *Curr. Comput. Mol. Biol.* 271–272.

Sclep, G., Allemeersch, J., Liechti, R., De Meyer, B., Beynon, J., Bhalerao, R., Moreau, Y., Nietfeld, W., Renou, J. P., Reymond, P., Kuiper, M. T. and Hilson P. (2007) CATMA, a comprehensive genome-scale resource for silencing and transcript profiling of Arabidopsis genes. *BMC Bioinformatics* **8**, 400.

Truernit, E., Bauby, H., Dubreucq, B., Grandjean, O., Runions, J., Barthélémy, J. and Palauqui, J.-C. (2008). High-resolution whole-mount imaging of three-dimensional tissue organization and gene expression enables the study of Phloem development and structure in Arabidopsis. *Plant Cell* **20**, 1494–1503.

Tucker, M. R., Hinze, A., Tucker, E. J., Takada, S., Jürgens, G. and Laux, T. (2008). Vascular signalling mediated by ZWILLE potentiates WUSCHEL function during shoot meristem stem cell development in the Arabidopsis embryo. *Development* **135**, 2839–2843.

Vandepoele, K., Raes, J., De Veylder, L., Rouzé, P., Rombauts, S. and Inzé, D. (2002). Genome-wide analysis of core cell cycle genes in Arabidopsis. *Plant Cell* **14**, 903–916.

Vernoux, T., Kronenberger, J., Grandjean, O., Laufs, P. and Traas, J. (2000). PIN-FORMED 1 regulates cell fate at the periphery of the shoot apical meristem. *Development* **127**, 5157–5165.

Wysocka-Diller, J. W., Helariutta, Y., Fukaki, H., Malamy, J. E. and Benfey, P. N. (2000). Molecular analysis of SCARECROW function reveals a radial patterning mechanism common to root and shoot. *Development* **127**, 595–603.